UNIVERSITY OF CALIFORNIA, MERCED

The Effect of Contextually Specific, Action-Based Timing Behavior on Human Brain Responses

A dissertation submitted in partial satisfaction of the requirements for the degree Doctor of Philosophy

In

Psychological Sciences

by

Ali Rahimpour Jounghani

Committee in charge:

Professor Heather Bortfeld, chair
Professor Elif Isbell
Professor Ramesh Balasubramaniam
Professor Rose Scott

2022

The Dissertation of Ali Rahimpour Jounghani is approved, and it is acceptable in quality and form for publication on microfilm and electronically:

Ramesh Balasubramaniam

Rose Scott

Elif Isbell

Heather Bortfeld, Chair

University of California, Merced

2022

Dedication

In loving memory of my father,

Manouchehr Rahimpour Jounghani

Tables of Contents

Lists of Abbreviations ..... **viii**
Lists of Symbols ..... **x**
Lists of Tables ..... **xi**
Lists of Figures ..... **xii**
Acknowledgements ..... **xviii**
Curriculum Vita, Publications, and Field of Study ..... **xix**
Abstract ..... **xxiv**
Chapter 1: Introduction **1**
Timing Scales 1
Timing With Millisecond Resolution 1
Timing Interval Properties 2
Implications of Timing Behavior 2
Timing and External Sensory Input 4
Timing Parameters Available for Manipulation 4
Neural Representation of Timing Action 5
Aims 6
References 8
Chapter 2 ..... **14**
Abstract 14
Introduction 15
Materials and Methods 18
Participants 18
Task Procedure 18
Statistical Analysis 19
fNIRS Instrument and Analysis 22
Results 23
Behavior 23
Cortical Hemodynamics 37
Discussion 40
Conclusion 42
References 43
Chapter 3 ..... **47**

Abstract.....47
Introduction.....48
Neural Activation.....49
Current Study.....50
Materials and Methods.....52
Participants.....52
Stimuli and Task.....52
EEG Data Recording.....53
Data Analyses.....54
Results.....59
Behavioral results.....59
Neural results.....63
Discussion.....78
Conclusion.....80
References.....81
Chapter 4.....**87**
Abstract.....87
Introduction.....88
Brain Activity.....89
Materials and Methods.....90
Participants.....90
Experiment.....91
Task.....91
Behavioral Analysis.....91
EEG Approach.....91
fNIRS Approach.....93
Region of Interest.....94
Behavioral Results.....94
Mean Accuracy Asynchrony.....94
IRI.....96
Brain Activation Comparison.....98
Synchronized Pacing.....99
Synchronized Continuation.....100

Syncopated Pacing 102
Syncopated Continuation 104
Discussion 106
Conclusion 107
References 108
Chapter 5 113
Summary 113
Developmental Implication 114
Limitations and Future Works 116
References 117

Lists of Abbreviations

Abbreviation	Full Form
AR-IRLS	Auto-Regressive Iteratively Reweighted Least Square
BIC	Bayesian Information Criterion
BOLD	Blood Oxygen Level Dependent
CBPT	Cluster Based Permutation Test
CNS	Central Nervous System
deoxy-Hb	Deoxygenated Hemoglobin
DC	Direct Current
DID	Difference in Difference
DIPFIT	Dipole Fitting
DLPFC	Dorsal Lateral Pre-Frontal Cortex
EEG	Electroencephalogram
ELU	Exponential Linear Unit
ERP	Event Related Potential
FDR	False Discovery Rate
fMRI	Functional Magnetic Resonance Imaging
fNIRS	Functional Near-Infrared Spectroscopy
fps	frame per second
GLM	General Linear Modeling
HRF	Hemodynamic Response Function
HSD	Tukey's Honestly Significant Difference
ICA	Independent Component Analysis
IFG	Inferior Frontal Gyrus
IPL	Inferior Parietal Lobule
IRI	Inter-response Interval
ITPC	Inter-Trial Phase Coherence
LRP	Lateralized Readiness Potential
MLR	Multiple Linear Modeling
MNI	Montreal Neurological Institute and Hospital
MTG	Medial Temporal Gyrus
NMA	Negative Mean Asynchrony
obs	Observation
OLS	Ordinary Least Square
Oxy-Hb	Oxygenated Hemoglobin
PCA	Principle Component Analysis
PET	Positron Emission Tomography
PGCM	Piecewise Growth Curve Modeling
PMC	Premotor Cortex
PTG	Parietal Temporal Gyrus
ROI	Region of Interest
S1/M1	Sensorimotor Cortex

SD	Standard Deviation
SE	Standard Error
sLORETA	standardized Low-Resolution Electromagnetic Tomographic Analysis
SMA	Supplementary Motor Area
SMS	Sensorimotor Synchronization
SNR	Signal Noise Ratio
SSEP	Steady State Evoked Potential
STG	Superior Temporal Gyrus
TTG	Transverse Temporal Gyrus

Lists of Symbols

Symbol	Definition
μ	Micro
Δ	Delta
β	Regression Coefficient
ε	Error
η	Sample size
$k\Omega$	Kiloohm
C	Channel
D	Spatial filter
Hb	Hemoglobin
k	Number of independent variables
N	Number of samples
Q1	25^{th} Percentile
Q3	75^{th} Percentile
S	Second
T	Time
Tap	Tapping
Y	Regression Output

Lists of Tables

Table Number: Caption	**Page**
Table 1. Basic DID models of mean asynchrony for study design causality	**29**
Table 2. Basic DID models of IRI for study design causality	**36**
Table 3. Details of EEGNet architecture for single trial EEG classification adapted from (ref)	**58**
Table 4. Brain regions showing oxy-Hb hemodynamic significant effects in syncopated continuation condition in fNIRS alternating designs	**102**
Table 5. Brain regions showing oxy-Hb hemodynamic significant effects in syncopated pacing condition in fNIRS alternating designs	**104**
Table 6. Brain regions showing oxy-Hb hemodynamic significant effects in syncopated continuation condition in fNIRS alternating designs	**105**

Lists of Figures

Figure Number: Caption	Page
Figure 1. Schematic diagrams stimulus design A) blocked and B) alternating study designs. Participants perform repetitive finger tapping in the presence and then absence of an auditory metronome tone. The task consisted of 20 tapping trials. Each trial began with a pacing phase (15 cycles of tapping with the tone) followed by a continuation phase (12 tapping cycles continued in the same manner established during pacing but without the tone). Tapping patterns were performed in two different coordination modes: synchronized tapping (blue color) or syncopated tapping (red). Ten trials of tapping in each coordination mode were performed corresponding to block or alternating study design. During each trial, participants fixated a crosshair (+).	**19**
Figure 2. fNIRS probes and channel placement adapted from (Rahimpour et al., 2020). Depiction of the geometrical layout of sources (S, red) and detectors (D, blue) concerning the international 10-10 EEG system (A) and the corresponding sensitivity maps (B) of the probe in a 3D head model. A and P indicate anterior and posterior, respectively.	**22**
Figure 3. Mean asynchronies of each timing condition for the block design (black) and alternating design (red). Error bars show standard deviation (SD). Dashed brackets indicate statistically significant comparisons between two study designs and solid brackets represent significant contrast effect between timing conditions.	**25**
Figure 4. Values of mean asynchrony from block design to alternating design for each timing condition: synchronization (blue); syncopation (green); pacing (solid line); continuation (dashed line). Error bar indicates standard error (SE).	**26**
Figure 5. (A) Estimated asynchrony trend during maintenance (pacing followed by continuation) and (B) second derivatives of the corresponding trends locating the turning points (blue square marks) in: blocked synchronization (b_s as solid black line); blocked syncopation (b_sn as dashed black line); alternating synchronization (a_s as solid red line); and alternating syncopation (a_sn as dashed red line). Gold vertical solid line represents continuation phase onset.	**27**
Figure 6. (A) Estimated asynchrony trend for the maintenance paradigm (pacing followed by continuation) averaged for timing coordination, and (B) second derivatives of the corresponding trends locating the turning points (x-marks) in the block design (black line) and alternating design (red line). The gold vertical solid line represents continuation phase onset.	**28**
Figure 7. Graphic illustration of the DID estimator. Values of mean asynchrony averaged by timing coordination modes from pacing to continuation for each study design: block (black) and alternating (red).	**30**
Figure 8. Averaged IRIs with SDs for each condition for block (black) and alternating designs (red). Dashed brackets indicate statistically significant	**32**

comparisons between the two study designs and solid brackets represent significant contrast effects between timing conditions.	
Figure 9. Mean values of IRIs from block and alternating designs for each condition: synchronization (blue); syncopation (green); pacing (solid line); continuation (dashed line). Error bar indicates standard error (SE).	**33**
Figure 10. (A) Estimated IRI trend of maintenance paradigm (pacing followed by continuation), and (B) second derivatives of the corresponding trends locating the turning points (blue square marks) in synchronization + block design (b_s as solid black line); syncopation + block design (b_sn as dashed black line); synchronization + alternating design (a_s as solid red line); and syncopation + alternating design (a_sn as dashed red line). Gold vertical solid line represents continuation phase onset.	**34**
Figure 11. (A) Estimated IRI trend for maintenance paradigm (pacing followed by continuation) across coordination mode by design type, and (B) second derivatives of the corresponding trends locating the turning points for the block design (black line) and alternating design (red line). Gold vertical solid line represents continuation phase onset.	**35**
Figure 12. Graphic illustration of the DID estimator. The values of IRIs averaged across coordination mode with pacing to continuation phase for each study design: block (black line); alternating (red line).	**36**
Figure 13. Channel maps of the main effect ($q<0.5$) of synchronized pacing condition on [Oxy-Hb] hemodynamic activation obtained by (A) Block design and (B) Alternating design. Color bars represent the t-value range.	**37**
Figure 14. Channel maps of the main effect ($q<0.5$) in synchronized continuation condition obtained by (A) block design and (B) alternating design. Color bars represent the t-value range.	**38**
Figure 15. [Oxy-Hb] channel maps of the main effect ($q<0.5$) in syncopated pacing condition obtained by (A) block design and (B) alternating design. Color bars represent the t-value range.	**39**
Figure 16. [Oxy-Hb] channel maps of the main effect ($q<0.5$) in the syncopated continuation condition obtained by (A) block design and (B) alternating design. Color bars represent the t-value range.	**40**
Figure 17. Schematic of the experimental paradigm adapted from Rahimpour et al (2020) to perform repetitive right finger tapping in the presence of the auditory metronome in the alternating study design. Blue and orange colors indicate synchronized and syncopated tapping, respectively.	**52**
Figure 18. Channel locations according to the 10-20 international electrode system.	**54**
Figure 19. Structure of the EEGNet architecture adopted from (ref). Lines denote the convolutional kernel connection between inputs and feature maps. Full details about the network architecture can be found in Table 3.	**57**
Figure 20. (A) Mean asynchronies of each timing condition. Error bars show standard deviation (SD). Solid brackets indicate statistically significant comparisons between timing conditions. (B) Values of mean asynchrony from each timing condition: synchronization (red); syncopation (black); Error bar	**61**

indicates standard error (SE). (C- Top) Estimated asynchrony trend during maintenance (pacing followed by continuation). (C-Bottom) Second derivatives of the corresponding trends locating the turning points (blue square marks) in: synchronization (red line); syncopation (black line); Gold vertical solid line represents continuation phase onset.	
Figure 21. (A) IRIs of each timing condition. Error bars show standard deviation (SD). Solid brackets indicate statistically significant comparisons between timing conditions. (B) IRI values from each timing condition: synchronization (red); syncopation (black); Error bar indicates standard error (SE). (C- Top) Estimated IRI trend during maintenance (pacing followed by continuation). (C-Bottom) Second derivatives of the corresponding trends locating the turning points (blue square marks) in: synchronization (red line); syncopation (black line); Gold vertical solid line represents continuation phase onset.	**62**
Figure 22. A) Confusion matrix showing the classification results for the stimulus-locked trials of the pacing and continuation in synchronization mode. Color shadings and number in the matrix denote the frequency at which the read data "true" label was classified into one of the two possible predicted classes. B) Visualization maps showing the relevance of all timepoints and electrodes for classification between two classes of pacing trials and continuation stimulus-locked trials in synchronization mode. Values close to 1 indicate that the specific feature at the specific timepoints contributes most to classification accuracy. The x-axis denotes the time in ms after auditory stimulus presentation. The y-axis indicates the different electrode sites.	**65**
Figure 23. Stimulus-locked ERPs at the electrode sites contributing most to classification (between pacing and continuation phase) accuracy of synchronization mode in the deep learning model. The x-axis the time in ms after auditory stimulus-locked presentation. The black and red curves indicate the averaged ERP values of pacing and continuation phases, respectively. The shading indicates the SE across the time. The y-axis indicates the voltage in μV (note that the scaling of the y-axis differs between the plots. The yellow shading shows the time interval that was found to contribute strongly to classification performance in the deep learning network.	**66**
Figure 24. A) Confusion matrix showing the classification results for the pacing and continuation in the syncopation coordination mode. Color shadings and number in the matrix denote the frequency at which the read data "true" label was classified into one of the two possible predicted classes. B) Visualization maps showing the relevance of all timepoints and electrodes for classification between two classes of pacing trials and continuation stimulus-locked trials in syncopation mode. Values close to 1 indicate that the specific feature at the specific timepoints contributes most to classification accuracy.	**68**

The x-axis denotes the time in ms after auditory stimulus presentation. The y-axis indicates the different electrode sites.	
Figure 25. Stimulus-locked ERPs at the electrode sites contributing most to classification (pacing-continuation phases) accuracy of syncopation mode in the deep learning model. The x-axis the time in ms after auditory stimulus-locked presentation. The black and red curves indicate the averaged ERP values of pacing and continuation phases, respectively. The shading indicates the SE across the time. The y-axis indicates the voltage in μV (note that the scaling of the y-axis differs between the plots. The yellow shading shows the time interval that was found to contribute strongly to classification performance in the deep learning network.	**69**
Figure 26. A) Confusion matrix showing the classification results for the response-locked trials of the pacing and continuation in syncopation mode. Color shadings and number in the matrix denote the frequency at which the read data "true" label was classified into one of the two possible predicted classes. B) Visualization maps showing the relevance of all timepoints and electrodes for classification between two classes of pacing trials and continuation tapping response-locked trials in syncopation mode. Values close to 1 indicate that the specific feature at the specific timepoints contributes most to classification accuracy. The x-axis denotes the time in ms after tapping response presentation. The y-axis indicates the different electrode sites.	**71**
Figure 27. Response-locked ERPs at the electrode sites contributing most to classification accuracy (syncopated-pacing and syncopated continuation) in the deep learning model. The x-axis the time in ms after auditory tapping response-locked presentation. The black and red curves indicate the averaged ERP values of pacing and continuation phases, respectively. The shading indicates the SE across the time. The y-axis indicates the voltage in μV (note that the scaling of the y-axis differs between the plots. The yellow shading shows the time interval that was found to contribute strongly to classification performance in the deep learning network.	**72**
Figure 28. Scatterplots showing individual indices of extracted auditory locked single-trial neural features corresponding to mean asynchrony in synchronized continuation condition. The plot illustrates that behavioral accuracy improves with increasing strength of amplitude of selective neural features.	**74**
Figure 29. Scatterplots showing individual indices of extracted response tapping locked single-trial neural features corresponding to mean asynchrony in syncopated pacing condition. The plot illustrates that behavioral accuracy improves with increasing strength of amplitude of selective neural features in FC1.	**75**

Figure 30. Scatterplots showing individual indices of extracted response tapping locked single-trial neural features corresponding to mean asynchrony in syncopated continuation condition. The plot illustrates that behavioral accuracy improves with decreasing strength of amplitude of selective neural features in Pz.	**76**
Figure 31. Scatterplots showing individual indices of extracted auditory locked single-trial neural features corresponding to IRI in syncopated pacing condition. The plot illustrates that behavioral accuracy improves with decreasing strength of amplitude of selective neural features in Pz.	**77**
Figure 32. Scatterplots showing individual indices of extracted response tapping locked single-trial neural features corresponding to IRI in syncopated pacing condition. The plot illustrates that IRI behavioral accuracy may improves with decreasing strength of amplitude of selective neural features on T8.	**78**
Figure 33. Channel placement and sensitivity. (A) Depiction of temporal head channel positioning relative to common scalp landmarks. Red numbers represent 10 –20 scalp landmarks. Yellow lines connecting light sources and detectors represent data channels. (B) Sensitivity map (mm^{-1}) derived from photon migration simulations of probe in a 3D head model. This figure is adapted from Chapter 2-Figure 2.	**94**
Figure 34. Mean asynchronies of each timing condition in session 1 (black) and session 2 (red). Error bars show standard deviation (SD). Dashed brackets indicate statistically significant comparisons between two study sessions.	**96**
Figure 35. Averaged IRIs with SDs for each condition for block (black) and alternating designs (red). Dashed brackets indicate statistically significant comparisons between the two study sessions.	**98**
Figure 36. (A) Channel maps of the main effect (q<0.5) of synchronized pacing condition on [Oxy-Hb] hemodynamic activation obtained by synchronized pacing condition. (B) Cluster component equivalent dipoles generated by stimulus-locked ERPs in blue and dipole centroid in red. Bottom: The averaged of IC components and cluster mean IC scalp map. Color bars in A and B represent the t-value and amplitude range, respectively.	**99**
Figure 37. (A) Channel maps of the main effect (q<0.5) of synchronized pacing condition on [Oxy-Hb] hemodynamic activation obtained by synchronized pacing condition. (B) Cluster component equivalent dipoles generated by response-locked ERPs in blue and dipole centroid in red. Bottom: The averaged of IC components and cluster mean IC scalp map. Color bars in A and B represent the t-value range and amplitude, respectively.	**100**
Figure 38. (A) Channel maps of the main effect (q<0.5) of synchronized continuation condition on [Oxy-Hb] hemodynamic activation obtained by synchronized pacing condition. (B) Cluster component equivalent dipoles	**101**

generated by stimulus-locked ERPs in blue and dipole centroid in red. Bottom: The averaged of IC components and cluster mean IC scalp map. Color bars in A and B represent the amplitude and t-value range, respectively.	
Figure 39. (A) Channel maps of the main effect (q<0.5) of synchronized continuation condition on [Oxy-Hb] hemodynamic activation obtained by synchronized pacing condition. (B) Cluster component equivalent dipoles generated by response-locked ERPs in blue and dipole centroid in red. Bottom: The averaged of IC components and cluster mean IC scalp map. Color bars in A and B represent the t-value range and amplitude, respectively.	**102**
Figure 40. (A) Channel maps of the main effect (q<0.5) on [Oxy-Hb] hemodynamic activation obtained by syncopated pacing condition. (B) Cluster component equivalent dipoles generated by stimulus-locked ERPs in blue and dipole centroid in red. Bottom: The averaged of IC components and cluster mean IC scalp map. Color bars in A and B represent the t-value and amplitude range, respectively.	**103**
Figure 41. (A) Channel maps of the main effect (q<0.5) of syncopated continuation condition on [Oxy-Hb] hemodynamic activation obtained by synchronized pacing condition. (B) Cluster component equivalent dipoles generated by response-locked ERPs in blue and dipole centroid in red. Bottom: The averaged of IC components and cluster mean IC scalp map. Color bars in A and B represent the t-value range and amplitude, respectively.	**105**

Acknowledgements

Words cannot express my gratitude to my professor and chair of my committee, professor Heather Bortfeld, for her invaluable patience and feedback. I also could not have undertaken this journey without my defense committee, who generously provided knowledge and expertise.
Lastly, I would be remiss in not mentioning my family, especially my wife, Samira. Her belief in me has kept my ‘spirits’ and motivation high during this process.

Curriculum Vita, Publications, and Field of Study

EDUCATION

Graduate Student, Psychological Sciences (August 2017- July 2022)
University of California Merced, California, USA (https://www.ucmerced.edu/)

- Faculty Committee: Heather Bortfeld, Rose Scott, Ramesh Balasubramaniam, and Elif Isbell
- Project title**:** The Effect of Contextual Action-Based Timing on Human Brain Responses GPA: 3.98 out of 4

Certificate in Quantitative Methods, Quantitative Psychology (September 2021)
University of California Merced, California, USA (https://www.ucmerced.edu/)

Master of Science, Biomedical Engineering (September 2013- August 2016)
University of Tehran. Tehran, Iran (http://www.ut.ac.ir/en**)**

- Supervisors: Hossein Ahmadi Noubari and Seyed Kamaledin Setarehdan
- Project title**:** Investigation of fNIRS application for infant cerebral hemodynamic monitoring: A report of data analysis for feature extraction and infant classification into healthy and unhealthy
- GPA: 3.8 out of 4

Bachelor of Science in Biomedical Engineering (January 2008 – September 2012)
Sahand University of Technology, Tabriz, Iran (http://www.sut.ac.ir/en)

- GPA: 3.8 out of 4

Diploma, Physics and Mathematics
School of Exceptional Talents under supervision of Shahrekord University, Shahrekord, Iran

PUBLICATIONS & CONFERENCE PROCEEDINGS

Rahimpour, A., Pollonini, L., Comstock, D., Balasubramaniam, R., & Bortfeld, H. (2022). Multiple Levels of Contextual Influence on Action-Based Timing Behavior and Cortical Activation. (*Scientific Reports, 2022*)

Ghafari T., **Rahimpour A**., Esteky H. (2022). Where and When Matter in Visual Working Memory. (*Attention, Perception, & Psychophysics, 2022)*

Heravi, H., **Rahimpour, A**., Delgarmi, M., & Ebrahimi, A. (2021). Automatic landmark detection of human back surface from depth images via deep learning. (*Biomedical Signal Processing and Control, 2021)*

Heravi, H., Aghaeifard, R., **Jounghani, A. R.**, Ebrahimi, A., & Delgarmi, M. (2020).

Extracting features of the human face from Rgb-D images to plan facial surgeries. *Biomedical Engineering: Applications, Basis and Communications*, *32*(06), 2050042.

Rahimpour, A., Pollonini, L., Comstock, D., Balasubramaniam, R., & Bortfeld, H. (2020). Tracking differential activation of primary and supplementary motor cortex across timing tasks: An fNIRS validation study. *Journal of Neuroscience Methods*, 108790.

Ebrahimzadeh, E., Shams, M., **Jounghani, A. R**., Fayaz, F., Mirbagheri, M., Hakimi, N., ... & Soltanian-Zadeh, H. (2020). Localizing confined epileptic foci in patients with an unclear focus or presumed multifocality using a component-based EEG-fMRI method. *Cognitive Neurodynamics*, 1-16.

Rahimpour, A., Noubari, H. A., & Kazemian, M. (2018). A case-study of NIRS application for infant cerebral hemodynamic monitoring: A report of data analysis for feature extraction and infant classification into healthy and unhealthy. *Informatics in Medicine Unlocked*, *11*, 44-50.

Rahimpour, A., Dadashi, A., Soltanian-Zadeh, H., & Setarehdan, S. K. (2017, April). Classification of fNIRS based brain hemodynamic response to mental arithmetic tasks. In *2017 3rd International Conference on Pattern Recognition and Image Analysis (IPRIA)* (pp. 113-117). IEEE.

Jahani, S., Berivanlou, N. H., **Rahimpour, A**., & Setarehdan, S. K. (2015, November). Attention level quantification during a modified stroop color word experiment: an fNIRS based study. In *2015 22nd Iranian Conference on Biomedical Engineering (ICBME)* (pp. 99-103). IEEE.

ABSTRACTS & PRESENTATIONS

R. O'Connell, S., **Rahimpour, A**., Papadopoulous, J., Nowlen, F., Bortfeld, H., Goldsworthy, R. (Feb 2022). *Tracking motor and auditory cortex activation during synchronous tapping in cochlear implant users and normal-hearing listeners: An fNIRS validation study*. 45th Annual Conference of Association for Research in Otolaryngology (ARO), San Jose, CA.

Ghafari, T., **Rahimpour, A**., Esteky, H. (September 2021). *Memory Performance is heterogeneous around visual field*. Brenstein Network Computational Neuroscience Conference, 2021.

Rahimpour, A., Pollonini, L., Comstock, D., Balasubramaniam, R., & Bortfeld, H. (October 2021). *The effect of study design context on timing behavior and cortical brain activation: fNIRS alternating vs. block design study.* Society for Virtual fNIRS Conference 2021.

Rahimpour, A., Comstock, D., Pollonini, L., Balasubramaniam, R., & Bortfeld, H. (January 2021). *Tracking differential activation of primary and supplementary motor cortex across timing tasks: An fNIRS validation study*. 4th Annual Boston University Neurophotonics

Symposium, Boston, MA.

Rahimpour, A., Comstock, D., Pollonini, L., Balasubramaniam, R., & Bortfeld, H. (January 2021). *The effect of study design context on timing behavior and cortical brain activation: fNIRS alternating vs. block design study*. 4th Annual Boston University Neurophotonics Symposium, Boston, MA.

Ebrahimzadeh, E., Shams, M., **Rahimpour Jounghani, A**., Fayaz, F., Mirbagheri, M., Hakimi, N., ... & Soltanian-Zadeh, H. (2019). *Epilepsy Presurgical Evaluation of Patients with Complex Source Localization by a Novel Component-Based EEG-fMRI Approach*. Iranian Journal of Radiology, 16(Special Issue).

Rahimpour, A., Pollonini, L., Comstock, D., Balasubramaniam, R., & Bortfeld, H. (November 2019). *Tracking differential activation of primary and supplementary motor cortex across timing tasks: an fNIRS validation study***.** 60th Annual Meeting of Psychonomic Society, Montreal, Quebec, Canada.

Rahimpour, A., Pollonini, L., Comstock, D., Balasubramaniam, R., & Bortfeld, H. (June 2019). *Tracking differential activation of primary and supplementary motor cortex across timing tasks: an fNIRS validation study***.** 20th Annual UC Systemwide Bioengineering Symposium, Merced, CA.

Rahimpour, A., Comstock, D., Pollonini, L., Balasubramaniam, R., & Bortfeld, H. (May 2019). *Tracking differential activation of primary and supplementary motor cortex across timing tasks: An fNIRS validation study*. Berkeley/Stanford Developmental Psychology Symposium, Berkeley, CA.

Rahimpour, A., Pollonini, L., Comstock, D., Balasubramaniam, R., & Bortfeld, H. (March 2019). *Tracking differential activation of primary and supplementary motor cortex across timing tasks: an fNIRS validation study***.** 26th Annual Meeting of the Cognitive Neuroscience Society, San Francisco, CA.

Borjkhani, M., Khazenifard A., & **Rahimpour, A**. (May 2014). *Probabilistic Study of different synchronization measures: Application to electroencephalographic.* Poster presented at Brain and Clinical Neuroscience Congress (BCNC), Tehran, Iran.

TEACHING EXPERIENCE

• Teaching Assistant of Cognitive Psychology, Spring 2022, Instructor: Robert Yancey
• Teaching Fellow of Industrial/Organizational Psychology, Fall 2021, Instructor: Ross Avilla
• Teaching Fellow of Developmental Cognitive Neuroscience, Spring 2021, Instructor: Heather Bortfeld
Teaching Assistant of Physiological Psychology, Fall 2020, Instructor: Meaghan Altman

• Teaching Assistant of Industrial/Organizational Psychology, Fall 2020, Instructor: Ross Avilla
• Teaching Assistant of Cognitive Psychology, Spring 2020, Instructor: Robert Yancey
• Teaching Assistant of Cognitive Development, Fall 2019, Instructor: Robert Yancey
• Guest lecturing of Introduction of Neuropsychology, Summer 2019, Instructor: Anabel Castillo
• Guest lecturing of Introduction of Neuroimaging Methods, Summer 2019, Instructor: Anabel Castillo
• Teaching Assistant of Developmental Cognitive Neuroscience, Spring 2019, Instructor: Heather Bortfeld
• Teaching Assistant of Alcohol, Drugs and Behaviors, Fall 2017 & 2018, Instructor: Robert Yancey
• Teaching Assistant of Clinical Neuropsychology, Spring 2018. Instructor: Alex Khislavsky
• Teaching Assistant of Statistical Pattern Recognition, Fall 2015, Instructor: Babak Nadjar Araabi
• Teaching Assistant of Biomedical Instruments, Fall 2015, Instructor: Kamaledin Setarehdan
• Teaching Assistant of Designing Linear Control Systems, Spring 2012, Instructor: Ahmad Akbari
• Teaching Assistant of Advanced Electronics, Spring 2011, Instructor: E Najafi Aghdam
• Teaching Assistant of Engineering Mathematics, Fall 2010**,** Instructor**:** Sadeghi Yazdankhah

AD HOC REVIEWER

• Associate editor of the Frontiers in Humans Neuroscience *(November 2021-Present)*
• Reviewer of the Society of SfNIRS Conference 2021 *(August 2021)*
• Reviewer of Medical and Biological Engineering and Computing (MBEC) *(July 2021)*
• Contributing reviewer of the Cortex journal *(August 2021)*
• Contributing reviewer of the journal of Cognitive Neuroscience *(June 2021)*
• Contributing reviewer of the PNAS journal *(March 2021)*
• Contributing reviewer of the Frontiers Human Neuroscience journal *(Jan 2021)*
• Contributing reviewer of the Cerebral Cortex journal *(Dec 2020)*
• Reviewer of the Biomedical Engineering: Applications, Basis, and Communications journal *(July 2020)*
• Contributing reviewer of the journal of Infant, Behavior and Development *(Dec 2020)*
• Reviewer of the IEEE/ Transaction on Neural Systems & Rehabilitation Engineering *(Jan 2020)*
• Contributing reviewer of the Elsevier journals: Hearing Research- Medical Hypothesis- Computer Methods and Programs in Biomedicine. *(Dec 2017)*
• Contributing reviewer of research project grant proposal- Leverhulme Trust. *(August 2019)*

HONORS & AWARDS

• Competitive Hatano Cognitive Development Research fellowship award, UC Merced, CA, USA *(May 2021)*
• Accepted innovative proposal and attending advances workshop in UC Berkeley NSF-Innovation Corps program *(Oct 2020)*
• Competitive Developmental Student Research award, UC Merced, CA, USA *(June 2020)*
• Awarded Bobcat Research Support fellowship, UC Merced, CA, USA. *(Summers, 2018-2022)*
• Awarded University of California GSA Travel grant, UC Merced, CA, USA. *(Winter 2019)*
• Best master thesis award from institute for cognitive science studies (IRICSS). *(Winter 2017)*
• Second ranked in the M.Sc. program and selected as the exceptional talents of National Universities in Iran. *(Spring 2011)*
• Awarded research grant from Mofid children's hospital. *(Spring 2017)*
• Awarded research grant from Cognitive Sciences and Technologies Council (CSTS) of Iran. *(Summer 2016)*
• Ranked 6th out of 128 among biomedical students in the B.Sc. program and selected as the exceptional talents of National Universities in Iran. *(Spring 2011)*
• Ranked first in the annual festival of scientific magazines of universities in Iran for publishing a national magazine in biomedical engineering, Harkat festival- Editor in chief. *(Spring 2010)*

EXTRACURRICULAR ACTIVITIES

• Organizing committee member of SfNIRS conference 2021 (http://fnirs2021.org/) *(May 2021- present)*
• Member of Iranian Students of California (ISC) *(Aug 2020- May 2021)*
• fNIRS laboratory tour guide of high school students, Bortfeld lab, University of California, Merced, California *(Feb 2020)*
• Graduate student organizer of Developmental Psychology Colloquium Series *(Jan 2020-May 2020)*
• Member of Cognitive Neuroscience Society (CNS) *(Jan 2019- Jan 2020)*

Abstract

The Effect of Contextually Specific, Action-Based Timing Behavior on Human Brain Responses

by

Ali Rahimpour Jounghani

Doctor of Philosophy in Psychological Sciences

University of California, Merced, 2022

Professor Heather Bortfeld, Ph.D., Chair

Timing is an essential component of human actions, and is the foundation of any sort of sequential behavior, from picking up a glass to playing an instrument or dancing. Because of this, our understanding of how we represent time in the brain (i.e., the human timing system) critically relies on basic research on simple behaviors. Perception of temporal regularities is central to a wide range of basic actions, but also underpins abilities unique to humans such as the creation of complex musical scores. This dissertation is an in-depth examination of endogenously and exogenously guided timing behavior, and how context is a critical component of understanding rhythmic entrainment in humans.

We previously validated "gold standard" functional magnetic resonance imaging (fMRI) findings on action-based timing behavior using functional near infrared spectroscopy (fNIRS) (Rahimpour et al., 2020). In particular, we observed significant hemodynamic responses in cortical areas in direct relation to the complexity of the behavior being performed. To do so, we probed multiple levels of contextual influence on action-based timing behavior and patterns of cortical activation as measured using fNIRS. Our findings highlighted several distinct, context-dependent parameters of specific timing behaviors. Here we further interrogate human timing abilities by introducing variations of our original experimental design, observing that subtle contextual variations have a significant impact on the degree of rhythmic entrainment given the presence/absence of metronomic input. We used electroencephalogram (EEG) to further validate our fNIRS findings, demonstrating that single trial neurobiological activity can be used to predict whether behavior is exogenously or endogenously guided. We also found that patterns of neural activity correspond to differential use of the internal timing system, and that specific differences in neural activity correlate with accuracy of action-based timing behavior. These findings emerged from our use of a novel deep learning approach to extract person-specific, neural-based features as predictors of behavioral performance. Finally, we examined whether fNIRS and EEG produced similar localization information, finding that the influence of training factors on cortical localization must be accounted for to make such comparisons.

Keywords: action-based timing behavior, fNIRS, EEG, rhythmic entrainment, hemodynamic response, event related potential, neurobiological activity, coordination modes, phase of maintenance task, synchronization, syncopation, pacing, continuation, deep learning, difference in difference approach, piecewise grow curve model, coordination dynamics

Chapter 1: Introduction

In traditional Persian music (https://www.youtube.com/watch?v=D5W4GJod8qU), both performers execute and synchronize a rhythmic pattern together. Sometimes one stops while the other maintains the tempo but over time, both performers and listeners entrain to the rhythm. These temporal rhythmic interactions make it difficult to ignore the music and underpin what makes it enjoyable. More broadly, this highlights how we perceive and respond to complex temporal information, abilities that serve as the basis for a range of questions relevant to research in psychology, cognitive science, and neuroscience. Not surprisingly, complex temporal processing has been studied extensively using a range of methodological approaches (Grondin, 2010; Haigh et al., 2021).

In my dissertation, I aim to answer some fundamental questions about action-based timing. First, I review recent findings from this area of research, with a focus on the neural bases of timing action and behavioral entrainment in humans. Second, I identify gaps in the extant scientific literature and formulate hypotheses that are as yet unanswered in this field of study. Finally, I present a series of studies in which I investigated action-based timing using both behavioral and brain-based experimental approaches, in addition to introducing a novel machine-learning approach.

Timing Scales

In humans, the development of sensitivity to time is essential, as accurate timing guides many aspects of social behavior, including speaking, dancing, listening to speech, playing music, performing a wide variety of sports, and driving a car. Four different timing scales have been identified as relevant to characterizing human timing mechanisms: 1) microseconds (e.g., echolocation); 2) milliseconds (e.g., music, dance and speech); 3) seconds to minutes to hours (e.g., conscious perception of time); 4) circadian rhythms (e.g., sleep-wake cycle) (Merchant & De Lafuente, 2014). Here, I focus on the millisecond scale as it is applied to the study of human timing behavior.

Timing With Millisecond Resolution

Timing that is calibrated to the hundreds of milliseconds (200–1,000 ms) is the basis for a broad range of activities, from speech perception/communication to the execution and appreciation of music and dance. Processing in the auditory, visual, and tactile modalities relies on timing, as does the coordination of movements that occur in this time range (Clarke, 1999). Thus, the human ability to quantify time on the millisecond scale needs to be precise, yet flexible. Indeed, individuals must be able to control the onset and offset of their time estimation depending on the contingencies of the environment.

Such flexibility in perception of time is well described by Weber's law, which quantifies human perceptual ability by predicting a linear relationship between sensitivity and duration on interval timing tasks (Getty, 1976; Killeen & Weiss, 1987). Weber law predicts a linear psychophysical function, such that as the duration of an event increases, the amount of error in timing action also increases linearly (Grondin, 2014; Merchant et al., 2008); but see (Grondin, 2012, 2014). Thus, according to this law, the resulting

Weber fraction (i.e., the parameter that indicates the coefficient of variation) should be constant (Merchant & De Lafuente, 2014).

Timing Interval Properties

However, more recent studies have shown that there are violations in such scalar timing properties (Bizo et al., 2006). For example, it has been shown that Weber's law does not hold or holds only for a restricted range of durations depending on the particular task context (Bangert et al., 2011; Merchant et al., 2008). Merchant et al (2008) found that performance variability was larger in perceptual tasks compared to timing action tasks, and for visual compared to auditory stimuli. Variability also decreased as a function of the number of intervals. These researchers suggested that their findings may indicate the existence of different timing mechanism. Bangert et al (2011) also reported that there is a violation of Weber's law for time. For example, depending on the specific numbers, the Weber fraction indicates that the scalar property is nonlinear. Indeed, these researchers reported that the Weber fraction is higher at 1,700 ms than at 1,350 ms, where the Weber fraction is already higher than at 1,175 or 1,000 ms. Thus, for brief intervals (270–1,175 ms), their data showed no violation of Weber's law, but beyond that range, the Weber fraction increased.

Timing depends on a wide range of factors, including perception, learning and memory, and voluntary motor action and control (Grondin, 2010). Timing perception alone is complex, and timing-based action depends on the interaction of a dynamic network of brain structures, which associate temporally dependent sensory information dynamically with memory traces of time to generate behavior based on perceptual decisions (Roseboom et al., 2015). Integration of time across multiple sensory modalities is necessary for the recognition and interpretation of temporal aspects of the sensory information that are guiding action. Thus, the ability to adjust behavior dynamically in different contexts is a critical component of the execution of voluntary movements with strict temporal control.

Implications of Timing Behavior

Action-based timing plays an important role in timing behavior. Generally speaking, the human motor system is hierarchically organized, guided by sensory input (Pinel, 2009) and mediated by voluntary control (Wing, 2002). This hierarchical structure allows the motor system to organize a large number of different movement sequences involving various complexities, including the number of limbs used, number of trajectories, sequence length, and relative timing of movement (Wolpert & Ghahramani, 2000).

Because the ability to perform time-dependent behavior accurately is critical for various skills, a large body of research has focused on how temporal mechanisms control behavior, with focus shifting more recently to whether and how timing is represented in the central nervous system (Repp, 2005). In real-life behavior, hierarchically-timed action interfaces with perceptual and cognitive systems (Cisek, 2019). In other words, timing behavior dynamically interfaces perception, action, and cognition, with different states/parameters changing over time (Balasubramaniam et al., 2021). This dynamic system synergistically integrates different elements of timing, including different coordination modes (Schöner & Kelso, 1988). Here, coordination mode refers to the way a motor action, in this case tapping, is timed relative to an external stimulus. By linking changes in coordination mode to behavioral outcomes, we can try to understand how the brain dynamically organizes perception and action. The dynamic movements produced

by the motor system based on both endogenous and endogenous processes is referred to be researchers as coordination dynamics (Tognoli et al., 2020).

Examples of behaviors whose performance relies fundamentally on the coordination of perceptual processes, timing, and motion—on coordination dynamics—include professional dancers' performance on the stage, musicians' performances in concert, and pro-gamers' gaming performances, to name just a few. Even within a specific class of movement, such skills differ further still across individuals and are impacted by age, as well as neurological disorders or neural degradation. Impacts on different characteristics of timing-based action can be observed in people with, for example, neurologically-based motor deficits (e.g., people with Parkinson's Disease) or auditory deficits (e.g., cochlear implant users), meaning that there are practical reasons to better understand how coordination dynamics work. There are theoretical reasons for understanding coordination dynamics too. Critically, understanding the mechanisms underlying timing behavior will help address questions about the nature of our internal clock. More specifically, if humans organize sequential events internally when there are no environmental or other external cues to guide such behavior, one must ask whether such processing is idiosyncratic, differing from person-to-person, or rather whether a "universal" or standard internal clock guides timing for everyone in the same way.

One perspective that helps delineate the connection between internal timing and its consequences is studied through the use of maintenance tasks in an experimental setting. Maintenance tasks are those in which participants are asked to first produce a behavior linked to an externally presented stimulus, and their behavior is further assessed (i.e., for changes in accuracy) after removal of the external cue. One task that uses maintenance is the continuation paradigm (Rao et al., 1997), which has been an important source of information about the accuracy of internal timing mechanisms relative to timing as it is guided by external information.

Maintenance has been shown in findings from participants *performing a routine task at different fixed time intervals* (Matell & Meck, 2000). Investigations of maintenance have demonstrated that short-term memory is essential for measuring timing performance (Schon et al., 2004). For example, maintenance based on temporal intervals in the sub-second and second range has been shown to interact with working memory and long-term memory, both of which are crucial to the elaboration of information to maintain different timing intervals (Rammsayer & Ulrich, 2011). Thus, it seems that internal generation of precisely timed movements is dependent on interrelated neural systems involved in sensorimotor processing (Rao et al., 1997), attention, and memory (Ruspantini et al., 2011).

Researchers who have used the continuation paradigm argue that time-associated brain regions respond in a context-dependent manner by maintaining the activation induced by stimulus-based input during the "pacing" phase to guide behavior in the "continuation" phase (Jantzen et al., 2004). Thus, contextual parameters of action-based timing systems play a major role in the variable behavioral and neural results obtained using the continuation paradigm. Furthermore, possible examination is to find a novel way to predict context-based behavioral accuracy by neurophysiological markers.

Timing and External Sensory Input

I have focused my research in part on understanding how people temporally coordinate their actions relative to external input. Specifically, I examine sensorimotor synchronization (SMS), a form of behavior in which an action is temporally coordinated with an external event (Repp, 2005). Usually, SMS refers to a situation in which both the action and the external stimulus are periodic. Therefore, SMS can be defined as the ability to temporally coordinate one's own motor rhythm with an external rhythm. Such coordination is essential, for example, in music and in dancing (Murta et al., 2017). Musicians and dancers must synchronize their actions with the audible and visible actions produced by other ensemble members. Orchestral musicians must follow a conductor. Musicians often use a metronome to pace their actions, or they coordinate their actions with beats produced by other musicians, such as those in the rhythm section. Even when people simply listen to music, they generate temporal expectations (internal synchronization), often moving in synchrony with the musical beat.

Despite the complexity of these domains of relevance, SMS studies often focus on the simple task of finger tapping to an auditory sequence that consists of pure tones, and there are many variants of SMS tasks that engage different forms of movement (e.g., tapping on a hard surface versus finger flexion or limb movement without contact) (Balasubramaniam et al., 2004), modalities of stimulation (e.g., auditory or visual) (Hove et al., 2013), and coordination (e.g., in-phase (synchronization) or anti-phase (syncopation)) (Jantzen et al., 2004). Finger tapping in synchrony with an external rhythm remains a popular paradigm because of its simplicity. SMS tasks in neuroscience research most often involve a modified version of finger tapping, which allows investigation of the internal timing system.

Interestingly, the findings on rhythm and beat perception suggest that people have different capacities for synchronization to rhythms presented across different modalities (Grahn & Brett, 2007). Findings generally show an auditory advantage, with stronger neural coupling between sensory and motor areas of the brain when people coordinate their actions to an auditory stimulus. Consistent with this, auditory rhythms generally lead in terms of the accuracy of sensorimotor synchronization relative to visual rhythms (Comstock et al., 2018). The auditory cortex of many vertebrates contains cells that are tuned to the duration of auditory stimuli in the range of tens of milliseconds (10–100 ms); in contrast, the range of durations represented in the visual area begins at around 100 ms (Toussaint & others, 2002). These findings all support the argument that time is a fundamental component of auditory processing, in particular.

Timing Parameters Available for Manipulation

Two central coordination dynamics of interest that I have used in the studies presented here are maintenance (already discussed) and in-phase (synchronization, i.e., movement in time with a pacing metronome) versus anti-phase timing (syncopation, i.e., movement in between successive metronome) (Jantzen et al., 2004). While in-phase synchronization of motor action to auditory input can be performed relatively automatically with little planning or monitoring, anti-phase syncopation involves planning and executing each movement individually. Thus, syncopation is more attention-demanding and involves learning-related mechanisms far beyond those required for synchronization. A person must repeatedly predict the midpoint of an interval, with

minute timing errors accumulating as the task progresses (Mayville et al., 2002). Thus, syncopation is a less stable form of coordination than synchronization, and relative to synchronization, syncopation decreases in stability as rate increases (Jantzen et al., 2004; Wilson et al., 2014). A further manipulation of timing can be achieved by having participants engage in paced tapping, followed by continuation tapping, whereby they continue tapping without an accompanying external stimulus. This manipulation can be combined with the in-phase/anti-phase manipulation (Lewis et al., 2004).

Neural Representation of Timing Action

The motor system is organized in a hierarchical structure that involves the spinal cord, subcortex, and cerebral cortex (Pinel, 2009). Finger tapping tasks generally recruit primary sensory and motor cortex (S1 and M1), supplementary motor area (SMA), premotor cortex (PMC), inferior parietal cortex, basal ganglia, and cerebellum (Witt et al., 2008). Although the SMA is involved primarily in motor planning, its activity also reflects an active supervisory role of M1 during motor processing (Kasess et al., 2008). Different task-specific parameters may modulate the neural mechanisms engaged during motor performance. For example, motor areas are recruited to a greater extent in tone-syncopated than tone-synchronized tapping (Byblow & Stinear, 2006; Chen et al., 2008; Jantzen et al., 2004; Mayville et al., 2002).

The similarities and differences in the neural circuits engaged during tapping can be investigated further by adding a pacing-continuation component to the task. While simple synchronized finger tapping engages the motor-cerebellar network, continuation of synchronized tapping without an accompanying sound engages a broader range of cortical regions due to its load on working memory. Motor areas such as M1, S1, SMA, and anterior cerebellum are commonly activated during both pacing and continuation tapping (Witt et al., 2008). Thus, more complex SMS tasks result in greater activation in related motor areas (e.g., pre-SMA, PMC, & cerebellum), as well as in stronger coupling to the auditory area (in the presence of a tone).

Our group previously investigated neural activity patterns underlying movements paced according to an external sound, which they then maintained without that sound. Our findings demonstrated that temporal representation depends on how that representation is established (i.e., for continuation, how it was established during a previous pacing phase) (Rahimpour et al., 2020). Furthermore, while we found that synchronization was achieved relatively automatically, with little planning or monitoring, syncopation involved planning and executing each movement individually. Moreover, syncopation was also generally more attention-demanding and appeared to involve learning-related mechanisms, because it required participants to identify the break point of an empty interval over and over with no feedback on the accuracy of their performance (Mayville et al., 2002). This effect was exaggerated further by introducing a stimulus-free continuation phase. Thus, syncopation appears to be a less stable form of coordination than synchronization. Consistent with this, other findings have shown that, relative to synchronization, syncopation decreases in stability as the rate of the behavior (i.e., tapping) increases (Jantzen et al., 2004; Wilson et al., 2014) (More details in Chapter 2 and 3).

Aims

The neural activity elicited from timing behavior depends on several timing parameters, including duration of timing movement, the effect of training (musician vs. non-musician) (Chen et al., 2008), interval ratio (metrical vs. non-metrical rhythmic form) (Sakai et al., 1999), rhythmic complexity (Mathias et al., 2020), movement rate (Kelso et al., 1998), number of stimuli (Jantzen et al., 2009), kinematics (e.g., the velocity of acceleration) (Paek et al., 2014), body effector (Serrien, 2008), movement trajectory (Pabst & Balasubramaniam, 2018), left versus right (dominant versus non-dominant) hand movement (Bai et al., 2005), and unimanual versus bimanual movement (Serrien, 2008). Chapter 2 focuses on how multiple levels of parameters affect timing behavior and neural activity. This study focused specifically on the impact of study design (i.e., block design—validated in our previous study—compared to alternating design) on timing performance and neural engagement.

Thus far, the neural data I have described have been obtaining using an indirect, blood-based measurement tool, functional near-infrared spectroscopy (fNIRS), to examine timing-based action. I describe fNIRS in detail in Chapter 2. For now, it is important to keep in mind that cortical hemodynamics are slow relative to neural activity itself. We are able to establish long-range connections between timing behavior and hemodynamic activity, but we are unable to observe moment-to-moment changes in the brain during such action. FNIRS is a good indirect measure of timing-based influences on the brain, but it is fundamentally constrained in terms of its temporal details. Given that, Chapter 3 explores insights provided by neural activation of previously trained individuals as measured via EEG. These activations should reflect and predict context-oriented timing behavior and thus allow us to study more nuanced aspects of the temporal characteristics of coordination dynamics. In the study presented in Chapter 3, neural activations—and their corresponding event-related potentials (ERPs)—are tracked in participants while they engage in the same alternating timing paradigm described in Chapter 2. These brain-based measures together with carefully acquired behavioral data, will further inform our understanding of the temporal changes in sensory-motor related brain activity as it responds in support of time-based action. Specifically, in this study we ask how ERPs relate to [specifically predict] behavioral accuracy the tapping task we established in previous studies.

These two forms of brain-based information (collected using fNIRS and EEG) tell us different things about how the brain supports timing-based action, together they can inform us about the measures themselves. ERPs (as collected using EEG) are limited in terms of the precise localization they can indicate regarding the neural source of their effects. Source modeling is a tool to help interpret the source localization of EEG-acquired signals, but due to the inverse problem (Koles, 1998), this is an imperfect method. It is important to better understand the accuracy of such source localization techniques, something we can achieve using a neuroimaging method with a better spatial resolution (e.g., fNIRS). Thus, in Chapter 4, I explore the degree to which fNIRS can validate source localization findings for EEG data and explore the influence of training effect on precise brain locals. Specifically, this chapter gives insight into the ability of fNIRS system to validate results obtained using the ICA-DIPFIT source localization

technique, with a focus on data collected using the same timing-based actions described in Chapters 2 and 3.

References

Aasted, C. M., Yücel, M. A., Cooper, R. J., Dubb, J., Tsuzuki, D., Becerra, L., Petkov, M. P., Borsook, D., Dan, I., & Boas, D. A. (2015). Anatomical guidance for functional near-infrared spectroscopy: AtlasViewer tutorial. *Neurophotonics*, *2*(2), 20801.

Bai, O., Mari, Z., Vorbach, S., & Hallett, M. (2005). Asymmetric spatiotemporal patterns of event-related desynchronization preceding voluntary sequential finger movements: a high-resolution EEG study. *Clinical Neurophysiology*, *116*(5), 1213–1221.

Balasubramaniam, R., Haegens, S., Jazayeri, M., Merchant, H., Sternad, D., & Song, J.-H. (2021). Neural encoding and representation of time for sensorimotor control and learning. *Journal of Neuroscience*, *41*(5), 866–872.

Balasubramaniam, R., Wing, A. M., & Daffertshofer, A. (2004). Keeping with the beat: Movement trajectories contribute to movement timing. *Experimental Brain Research*, *159*(1), 129–134. https://doi.org/10.1007/s00221-004-2066-z

Bangert, A. S., Reuter-Lorenz, P. A., & Seidler, R. D. (2011). Dissecting the clock: Understanding the mechanisms of timing across tasks and temporal intervals. *File:///C:/Users/Ali/Dropbox/PC/Desktop/References/76.Txt*, *136*(1), 20–34.

Barker, J. W., Aarabi, A., & Huppert, T. J. (2013). Autoregressive model based algorithm for correcting motion and serially correlated errors in fNIRS. *Biomedical Optics Express*, *4*(8), 1366–1379.

Bell, A. J., & Sejnowski, T. J. (1989). *An information-maximisation approach to blind separation and blind deconvolution*. *1034*(February 1995), 1004–1034.

Bizo, L. A., Chu, J. Y. M., Sanabria, F., & Killeen, P. R. (2006). The failure of Weber's law in time perception and production. *Behavioural Processes*, *71*(2–3), 201–210. https://doi.org/10.1016/J.BEPROC.2005.11.006

Bortfeld, H., Fava, E., & Boas, D. A. (n.d.). *Identifying Cortical Lateralization of Speech Processing in Infants Using Near- Infrared Spectroscopy Identifying Cortical Lateralization of Speech Processing in Infants Using Near-Infrared Spectroscopy*. *October 2014*, 37–41. https://doi.org/10.1080/87565640802564481

Bortfeld, H., Fava, E., & Boas, D. A. (2009). Identifying cortical lateralization of speech processing in infants using near-infrared spectroscopy. *Developmental Neuropsychology*, *34*(1), 52–65.

Bortfeld, H., Wruck, E., & Boas, D. A. (2007). Assessing infants' cortical response to speech using near-infrared spectroscopy. *NeuroImage*, *34*(1), 407–415. https://doi.org/10.1016/j.neuroimage.2006.08.010

Branas, C. C., Cheney, R. A., MacDonald, J. M., Tam, V. W., Jackson, T. D., & ten Havey, T. R. (2011). A Difference-in-Differences Analysis of Health, Safety, and Greening Vacant Urban Space. *American Journal of Epidemiology*, *174*(11), 1296–1306. https://doi.org/10.1093/AJE/KWR273

Byblow, W. D., & Stinear, Æ. C. M. (2006). *Modulation of short-latency intracortical inhibition in human primary motor cortex during synchronised versus syncopated finger movements*. 287–293. https://doi.org/10.1007/s00221-005-0205-9

Chen, H.-C., Vaid, J., Boas, D. A., & Bortfeld, H. (2011). Examining the phonological neighborhood density effect using near infrared spectroscopy. *Human Brain Mapping*, *32*(9), 1363–1370.

Chen, J. L., Penhune, V. B., & Zatorre, R. J. (2008). Moving on time: brain network for auditory-motor synchronization is modulated by rhythm complexity and musical training. *Journal of Cognitive Neuroscience*, *20*(2), 226–239.

Chou, C. P., Yang, D., Pentz, M. A., & Hser, Y. I. (2004). Piecewise growth curve modeling approach for longitudinal prevention study. *Computational Statistics & Data Analysis*, *46*(2), 213–225. https://doi.org/10.1016/S0167-9473(03)00149-X

Cisek, P. (2019). Resynthesizing behavior through phylogenetic refinement. *Attention, Perception, \& Psychophysics*, *81*(7), 2265–2287.

Clarke, E. F. (1999). Rhythm and timing in music. In *The psychology of music* (pp. 473–500). Elsevier.

Collective, B. M., & Shaw, D. (2012). Makey Makey: improvising tangible and nature-based user interfaces. *Proceedings of the Sixth International Conference on Tangible, Embedded and Embodied Interaction*, 367–370.

Comstock, D. C., & Balasubramaniam, R. (2018). Neural responses to perturbations in visual and auditory metronomes during sensorimotor synchronization. *Neuropsychologia*, *117*, 55–66.

Comstock, D. C., Hove, M. J., & Balasubramaniam, R. (2018). Sensorimotor synchronization with auditory and visual modalities: Behavioral and neural differences. *Frontiers in Computational Neuroscience*, *12*, 53.

Dyer, S. A., & Dyer, J. S. (2001). Cubic-Spline Interpolation: Part 1. *IEEE Instrumentation and Measurement Magazine*, *4*(1), 44–46. https://doi.org/10.1109/5289.911175

Ebrahimzadeh, E., Shams, M., Rahimpour Jounghani, A., Fayaz, F., Mirbagheri, M., Hakimi, N., Hashemi Fesharaki, S. S., & Soltanian-Zadeh, H. (n.d.). Epilepsy Presurgical Evaluation of Patients with Complex Source Localization by a Novel Component-Based EEG-fMRI Approach. *Iranian Journal of Radiology*, *16*(Special Issue).

Getty, D. J. (1976). Counting processes in human timing. *Perception \& Psychophysics*, *20*(3), 191–197.

Grahn, J. A., & Brett, M. (2007). Rhythm and beat perception in motor areas of the brain. *Journal of Cognitive Neuroscience*, *19*(5), 893–906.

Grondin, S. (2010). Timing and time perception: a review of recent behavioral and neuroscience findings and theoretical directions. *Attention, Perception, \& Psychophysics*, *72*(3), 561–582.

Grondin, S. (2012). Violation of the scalar property for time perception between 1 and 2 seconds: evidence from interval discrimination, reproduction, and categorization. *Journal of Experimental Psychology: Human Perception and Performance*, *38*(4), 880.

Grondin, S. (2014). About the (non) scalar property for time perception. *Neurobiology of Interval Timing*, 17–32.

Haigh, A., Apthorp, D., & Bizo, L. A. (2021). The role of Weber's law in human time perception. *Attention, Perception, \& Psychophysics*, *83*(1), 435–447.

Hoppes, C. W., Sparto, P. J., Whitney, S. L., Furman, J. M., & Huppert, T. J. (2018). *Functional near-infrared spectroscopy during optic flow with and without fixation*. 1–14.

Hove, M. J., Fairhurst, M. T., Kotz, S. A., & Keller, P. E. (2013). Synchronizing with auditory and visual rhythms: an fMRI assessment of modality differences and modality appropriateness. *Neuroimage*, *67*, 313–321.

Huppert, T. J., Diamond, S. G., Franceschini, M. A., & Boas, D. A. (2009). HomER: a review of time-series analysis methods for near-infrared spectroscopy of the brain. *Applied Optics*, *48*(10), D280--D298.

Ivry, R. B., & Keele, S. W. (1989). Timing Functions of The Cerebellum. *Journal of Cognitive Neuroscience*, *1*(2), 136–152. https://doi.org/10.1162/jocn.1989.1.2.136

Jahani, S., Berivanlou, N. H., Rahimpour, A., & Setarehdan, S. K. (2015). *Attention level quantification during a modified stroop color word experiment : An fNIRS based study*. *November*, 25–27.

Jahani, S., Berivanlou, N. H., Rahimpour, A., & Setarehdan, S. K. (2016). Attention level quantification during a modified stroop color word experiment: An fNIRS based study. *2015 22nd Iranian Conference on Biomedical Engineering, ICBME 2015*. https://doi.org/10.1109/ICBME.2015.7404124

Jantzen, K. J., Steinberg, F. L., & Kelso, J. A. S. (2004). Brain networks underlying human timing behavior are influenced by prior context. *Proceedings of the National Academy of Sciences*, *101*(17), 6815–6820.

Jantzen, K. J., Steinberg, F. L., & Kelso, J. A. S. (2009). Coordination dynamics of large-scale neural circuitry underlying rhythmic sensorimotor behavior. *Journal of Cognitive Neuroscience*, *21*(12), 2420–2433.

Kasess, C. H., Windischberger, C., Cunnington, R., Lanzenberger, R., Pezawas, L., & Moser, E. (2008). *The suppressive influence of SMA on M1 in motor imagery revealed by fMRI and dynamic causal modeling*. 1–10. https://doi.org/10.1016/j.neuroimage.2007.11.040

Kelso, J. A. S., Fuchs, A., Lancaster, R., Holroyd, T., Cheyne, D., & Weinberg, H. (1998). Dynamic cortical activity in the human brain reveals motor equivalence. *Nature*, *392*(6678), 814–818.

Killeen, P. R., & Weiss, N. A. (1987). Optimal timing and the Weber function. *Psychological Review*, *94*(4), 455.

Kocsis, L., Herman, P., & Eke, A. (2006). The modified Beer--Lambert law revisited. *Physics in Medicine \& Biology*, *51*(5), N91.

Koles, Z. J. (1998). *Trends in EEG source localization*. *106*, 127–137.

Lawhern, V. J., Solon, A. J., Waytowich, N. R., Gordon, S. M., Hung, C. P., & Lance, B. J. (2018). EEGNet: a compact convolutional neural network for EEG-based brain–computer interfaces. *Iopscience.Iop.Org*. https://iopscience.iop.org/article/10.1088/1741-2552/aace8c/meta

Lewis, P. A., Wing, A. M., Pope, P. A., Praamstra, P., & Miall, R. C. (2004). Brain activity correlates differentially with increasing temporal complexity of rhythms during initialisation, synchronisation, and continuation phases of paced finger tapping. *Neuropsychologia*, *42*(10), 1301–1312.

Lin, C. C., Barker, J. W., Sparto, P. J., Furman, J. M., & Huppert, T. J. (2017). Functional near-infrared spectroscopy (fNIRS) brain imaging of multi-sensory integration during computerized dynamic posturography in middle-aged and older adults. *Experimental Brain Research*, *0*(0), 0. https://doi.org/10.1007/s00221-017-4893-8

Matell, M. S., & Meck, W. H. (2000). Neuropsychological mechanisms of interval timing behavior. *Bioessays*, *22*(1), 94–103.

Mathias, B., Zamm, A., Gianferrara, P. G., Ross, B., & Palmer, C. (2020). Rhythm Complexity Modulates Behavioral and Neural Dynamics During Auditory--Motor Synchronization. *Journal of Cognitive Neuroscience*, *32*(10), 1864–1880.

Mayville, J. M., Jantzen, K. J., Fuchs, A., Steinberg, F. L., & Kelso, J. A. S. (2002). Cortical and subcortical networks underlying syncopated and synchronized coordination revealed using fMRI. *Human Brain Mapping*, *17*(4), 214–229.

Merchant, H., & De Lafuente, V. (2014). Introduction to the neurobiology of interval timing. *Neurobiology of Interval Timing*, 1–13.

Merchant, H., Zarco, W., & Prado, L. (2008). Do we have a common mechanism for measuring time in the hundreds of millisecond range? Evidence from multiple-interval timing tasks. *File:///C:/Users/Ali/Dropbox/PC/Desktop/References/76.Txt*, *99*(2), 939–949.

Murta, T., Chaudhary, U. J., Tierney, T. M., Dias, A., Leite, M., Carmichael, D. W., Figueiredo, P., & Lemieux, L. (2017). Phase--amplitude coupling and the BOLD signal: a simultaneous intracranial EEG (icEEG)-fMRI study in humans performing a finger-tapping task. *Neuroimage*, *146*, 438–451.

Ning, L., & Luo, W. (2017). Specifying Turning Point in Piecewise Growth Curve Models: Challenges and Solutions. *Frontiers in Applied Mathematics and Statistics*, *3*, 19. https://doi.org/10.3389/FAMS.2017.00019/BIBTEX

Pabst, A., & Balasubramaniam, R. (2018). Trajectory formation during sensorimotor synchronization and syncopation to auditory and visual metronomes. *Experimental Brain Research*, *236*(11), 2847–2856.

Paek, A. Y., Agashe, H., & Contreras-Vidal, J. L. (2014). Decoding repetitive finger movements with brain activity acquired via non-invasive electroencephalography. *Frontiers in Neuroengineering*, *7*, 3.

Pinel, J. P. J. (2009). *Biopsychology*. Pearson education.

Pollonini, L., Olds, C., Abaya, H., Bortfeld, H., Beauchamp, M. S., & Oghalai, J. S. (2014). Auditory cortex activation to natural speech and simulated cochlear implant speech measured with functional near-infrared spectroscopy. *Hearing Research*, *309*, 84–93. https://doi.org/10.1016/j.heares.2013.11.007

Rahimpour, A., Dadashi, A., Soltanian-Zadeh, H., & Setarehdan, S. K. (2017, April). Classification of fNIRS based brain hemodynamic response to mental arithmetic tasks. In *2017 3rd International conference on pattern recognition and image analysis (IPRIA)* (pp. 113-117). IEEE.

Rahimpour, A., Dadashi, A., Soltanian-Zadeh, H., & Setarehdan, S. K. (2017). Classification of fNIRS based brain hemodynamic response to mental arithmetic tasks. *3rd International Conference on Pattern Analysis and Image Analysis, IPRIA 2017*. https://doi.org/10.1109/PRIA.2017.7983029

Rahimpour, A., Noubari, H. A., & Kazemian, M. (2018). A case-study of NIRS application for infant cerebral hemodynamic monitoring: A report of data analysis for feature extraction and infant classification into healthy and unhealthy. *Informatics in Medicine Unlocked*, *11*, 44–50. https://doi.org/10.1016/J.IMU.2018.04.001

Rahimpour, A., Pollonini, L., Comstock, D., Balasubramaniam, R., & Bortfeld, H. (2020). Tracking differential activation of primary and supplementary motor cortex across timing tasks: An fNIRS validation study. *Journal of Neuroscience Methods*, *341*, 108790.

Rammsayer, T., & Ulrich, R. (2011). Elaborative rehearsal of nontemporal information interferes with temporal processing of durations in the range of seconds but not milliseconds. *Acta Psychologica*, *137*(1), 127–133.

Rao, S. M., Harrington, D. L., Haaland, K. Y., Bobholz, J. A., Cox, R. W., & Binder, J. R. (1997). Distributed neural systems underlying the timing of movements. *Journal of Neuroscience*, *17*(14), 5528–5535.

Repp, B. H. (2005). Sensorimotor synchronization: A review of the tapping literature. In *Psychonomic Bulletin and Review* (Vol. 12, Issue 6, pp. 969–992). https://doi.org/10.3758/BF03206433

Roseboom, W., Linares, D., & Nishida, S. (2015). Sensory adaptation for timing perception. *Proceedings of the Royal Society B: Biological Sciences*, *282*(1805), 20142833.

Ruspantini, I., Mäki, H., Korhonen, R., D'Ausilio, A., & Ilmoniemi, R. J. (2011). The functional role of the ventral premotor cortex in a visually paced finger tapping task: a TMS study. *Behavioural Brain Research*, *220*(2), 325–330.

Sakai, K., Hikosaka, O., Miyauchi, S., Takino, R., Tamada, T., Iwata, N. K., & Nielsen, M. (1999). Neural representation of a rhythm depends on its interval ratio. *Journal of Neuroscience*, *19*(22), 10074–10081.

Santosa, H., Zhai, X., Fishburn, F., & Huppert, T. (2018). The NIRS brain AnalyzIR toolbox. *Algorithms*, *11*(5), 73.

Schon, K., Hasselmo, M. E., LoPresti, M. L., Tricarico, M. D., & Stern, C. E. (2004). Persistence of parahippocampal representation in the absence of stimulus input enhances long-term encoding: a functional magnetic resonance imaging study of subsequent memory after a delayed match-to-sample task. *Journal of Neuroscience*, *24*(49), 11088–11097.

Schöner, G., & Kelso, J. A. S. (1988). A synergetic theory of environmentally-specified and learned patterns of movement coordination. *Biological Cybernetics*, *58*(2), 71–80.

Sergent, J. (1993). Mapping the musician brain. *Human Brain Mapping*, *1*(1), 20–38. https://doi.org/10.1002/hbm.460010104

Serrien, D. J. (2008). The neural dynamics of timed motor tasks: Evidence from a synchronization--continuation paradigm. *European Journal of Neuroscience*, *27*(6), 1553–1560.

Spencer, N. J., Bywater, R. A. R., Holman, M. E., & Taylor, G. S. (1998). *Inhibitory neurotransmission in the circular muscle layer of mouse colon*. *June 1997*, 10–14.

Tognoli, E., Zhang, M., Fuchs, A., Beetle, C., & Kelso, J. A. S. (2020). Coordination Dynamics: A foundation for understanding social behavior. *Frontiers in Human Neuroscience*, *14*.

Toussaint, G. T., & others. (2002). A mathematical analysis of African, Brazilian, and Cuban clave rhythms. *Proceedings of BRIDGES: Mathematical Connections in Art, Music and Science*, 157–168.

Vahid, A., Bluschke, A., Roessner, V., Stober, S., & Beste, C. (2019). Deep Learning Based on Event-Related EEG Differentiates Children with ADHD from Healthy Controls. *Journal of Clinical Medicine 2019, Vol. 8, Page 1055*, *8*(7), 1055. https://doi.org/10.3390/JCM8071055

Vahid, A., Mückschel, M., Stober, S., Stock, A. K., & Beste, C. (2020). Applying deep learning to single-trial EEG data provides evidence for complementary theories on action

control. *Communications Biology 2020 3:1*, *3*(1), 1–11. https://doi.org/10.1038/s42003-020-0846-z

Wilson, T. W., Kurz, M. J., & Arpin, D. J. (2014). Functional specialization within the supplementary motor area: a fNIRS study of bimanual coordination. *Neuroimage*, *85*, 445–450.

Wing, A. M. (2002). Voluntary timing and brain function: an information processing approach. *Brain and cognition*, *48*(1), 7-30.

Wing, A. M., & Kristofferson, A. B. (1973). Response delays and the timing of discrete motor responses. *Perception & Psychophysics*, *14*(1), 5–12. https://doi.org/10.3758/BF03198607

Wing, C., Simon, K., & Bello-Gomez, R. A. (2018). Designing difference in difference studies: best practices for public health policy research. *Annu Rev Public Health*, *39*(1), 453-469.

Witt, S. T., Laird, A. R., & Meyerand, E. (2008). Functional neuroimaging correlates of finger-tapping task variations: an ALE meta-analysis. *Neuroimage*, *42*(1), 343–356.

Wolpert, D. M., & Ghahramani, Z. (2000). *Computational principles of movement neuroscience*. *3*(november).

Ye, J. C., Tak, S., Jang, K. E., Jung, J., & Jang, J. (2009). NIRS-SPM: statistical parametric mapping for near-infrared spectroscopy. *Neuroimage*, *44*(2), 428–447.

Chapter 2
Multiple Levels of Contextual Influence on Action-Based Timing Behavior and Cortical Activation

Abstract

Procedures used to elicit both behavioral and neurophysiological data to address a particular cognitive question can impact the nature of the data collected. Previously, we used functional near-infrared spectroscopy (fNIRS) to assess performance of a modified finger tapping task (Rahimpour et al., 2020), in which participants performed synchronized or syncopated tapping relative to a metronomic tone. Both versions of the tapping task included a pacing phase (tapping with the tone) followed by a continuation phase (tapping without the tone). Both behavioral and brain-based findings revealed two distinct timing mechanisms underlying the two forms of tapping. Here we investigate the impact of an additional—and extremely subtle—manipulation of the study's experimental design. We measured responses in 23 healthy adults as they performed the two versions of the finger-tapping tasks either *blocked* by tapping type or *alternating* from one to the other type the course of the experiment. As in our previous study, behavioral tapping indices and cortical hemodynamics were monitored, allowing us to compare results across the two study designs. Consistent with previous findings (Jantzen et al., 2004a, 2007a; Rahimpour et al., 2020), results reflected distinct, context-dependent parameters of the tapping. Moreover, our results demonstrated a significant impact of study design on rhythmic entrainment in the presence/absence of auditory stimuli. Tapping accuracy and hemodynamic responsivity collectively indicate that the blocked design context is ideal for studying action-based timing behavior.

Keywords: rhythmicity, rhythm entrainment, synchronization, syncopation, block study design, alternating study design, fNIRS, coordination mode, maintenance paradigm, finger-tapping task, causal inference, temporal trend, HRF, AR-IRLS, coordination dynamics

Introduction

Timing and coordination in human behavior can be described as a function of motor and acoustic interactions within a larger complex dynamical system (Proksch et al., 2022). The behavior of such a complex dynamical system can be affected by changes in the timing of both externally observed stimuli and endogenous motor and auditory processes. Thus, it is critical to characterize an appropriate contextual approach to study human timing ability. Sensorimotor synchronization is a scientific approach to investigate timing entrainment behavior in humans, which fundamentally underlies more complex rhythmic behaviors such as dancing. Finger-tapping is a common sensorimotor synchronization task used to explore timing control of rhythmic entrainment (i.e., stable temporal relationship between external periodic inputs and endogenous rhythmic process) and, as a result, coordinate with environmental rhythm (McPherson et al., 2018; Repp & Su, 2013). Finger-tapping studies assess how participants use their mental timing system in a manner that is independent of other motor behavior or feedback mechanisms (Ivry & Keele, 1989; Sergent, 1993; Wing & Kristofferson, 1973). Two leading derivatives of the sensorimotor synchronization approach are synchronization-continuation and syncopation-continuation tasks (tapping on the beat, or off the beat respectively) (Jantzen et al., 2004; Rahimpour et al., 2020). In those approaches, participants are initially entrained with an external stimulus. When the stimulus train is extinguished, they are required to maintain and sustain the entrainment (on or off the beat) based on the internal timekeeping mechanism.

Two stable modes of human behavioral coordination with external signals are synchrony and syncopation (or anti-synchrony). Synchronized tapping to an external pacing signal generally requires little preparation and self-monitoring (Chauvigné et al., 2014). By contrast, syncopated tapping requires substantial monitoring of the perception-action cycle across time (Mayville et al., 2002a). Participants may also be asked to continue tapping after the cessation of the externally presented stimulus, allowing researchers to contrast pacing along to an external stimulus and continuing without it. Such a continuation phase depends on an internal mental representation of the duration of the intervals and thus can provide insights into specific aspects of timing behavior and endogenous timing processes.

The ability to accurately and precisely perform timing behavior is critical to various real-world skills (Nachev et al., 2008). Different task-specific timing parameters may be manipulated to further target specific neural and/or cognitive mechanisms. The behavioral performance and associated neural activity elicited from timing behavior depend on several timing parameters, including duration of timing movement, the effect of training in rhythmic timing activities (e.g. musicians vs. non-musicians) (Chen et al., 2008), stimulus interval ratio (metrical vs. non-metrical rhythmic form) (Sakai et al., 1999), rhythmic complexity (Mathias et al., 2020), movement rate (Kelso et al., 1998), number of stimuli (Jantzen et al., 2009), kinematics (e.g., the velocity of acceleration) (Paek et al., 2014), body effector (Serrien, 2008), movement trajectory (Pabst & Balasubramaniam, 2018), left versus right (dominant versus non-dominant) hand movement (Bai et al., 2005), and unimanual versus bimanual movement (Serrien, 2008a). It is important to understand how subtle decisions in the initial study design of timing

tasks may impact both behavioral and neural processes, and the conclusions that can be drawn from these studies.

Study Designs in Timing Research

The intricacies of timing behavior and variety of contexts in which humans make use of different timing mechanisms make it important to carefully design experimental tasks to ensure we are observing stable characteristics of timing behavior. Motor control and movement research employing tapping has often alternated coordination modes across the course of an experiment. to minimize behavioral confounds across trials (Merel et al., 2019). However, much fMRI research relies on blocked design to improve signal to noise ratio in neural data across conditions (Amaro & Barkera, 2006), given the sluggish nature of cortical hemodynamics (relative to, for example, electrical brain potentials). In what follows, we describe the impact of two contrasting study designs – with coordination mode either blocked or alternating – on the behavioral and neural correlates of timing.

In our previous study (see Rahimpour et al., 2020), participants were asked to perform a synchronized and syncopated finger-tapping in a standard continuation task. The synchronized and syncopated tapping trials were presented in a blocked manner, so participants did not have to switch back and forth between the two types of tapping. Participants were asked to pace their tapping relative to the auditory metronome tone and then continue tapping without the tone. This represents a canonical blocked design, with synchronized and syncopated trials performed consecutively. Such a design allows researchers use to examine the accuracy of timing ability, while lending itself to hemodynamic-based measures such as fMRI. These synchronization/syncopation-continuation tasks have been found to recruit sensorimotor cortex (S1/ M1), supplementary motor area (SMA), premotor cortex (PMC), inferior parietal cortex, basal ganglia, and cerebellum to different degrees depending on the specific coordination mode and task phase (Lewis et al., 2004; Witt et al., 2008). In our previous findings, we observed significant hemodynamic changes directly related to the complexity of the tapping task. Specifically, we observed recruitment of a broader cortical network during the syncopated continuation condition compared to other conditions (synchronized pacing, synchronized continuation, or syncopated pacing). We also observed overall differences in hemodynamic activity in the synchronized versus syncopated coordination mode, which points to distinct processing networks for these different forms of coordination dynamics. Our block study design activated a network compatible with the motor-related timing network (M1 and SMA) in the syncopated and synchronization tasks, but additional activity was observed during syncopated tapping in central, frontal, and parietal areas. This a finding is compatible with an increase in memory and attentional processes, as well as increases in cognitive control, required for syncopated tapping (Rahimpour et al., 2020).

In contrast, in a design in which coordination mode alternates from trial to trial participants are asked to alternate their tapping pattern between synchronized and syncopated tapping across trials. When adding the continuation paradigm to this design. Each trial includes a period of tapping paced to an auditory tone and then continued in the absence of the tone (Comstock et al., 2018; Comstock & Balasubramaniam, 2018; Pabst & Balasubramaniam, 2018). As previously mentioned, the coordination modes of

synchrony and syncopation can create two stable attractors in human movement. However, the less stable coordination mode—syncopation—has a tendency to transition to the more stable timing of synchronous tapping, particularly given increasing task demands, such as by increasing the complexity of the task by including a continuation condition with no externally guiding stimulus (Jantzen et al., 2009). Additionally, it takes time to develop an internal representation of pulse and to entrain tapping behavior to complex rhythmic stimuli (Chapin, et al., 2010). Thus, alternating between synchronized and syncopated tapping may increase task demand as well as shorten the amount of time available to develop a stable pulse percept, particularly in the syncopated coordination mode. Therefore, we predict relatively less accurate and lower rhythmic entrainment performance from participants in an alternating design than a block study design across both synchronization- and syncopation-continuation tasks. Also, we predict that complexity and difficulty of study design (given the alternating versus block design) will lead to broader patterns of neural activation overall.

Current Study

In this study, we examined whether the study's design, with tapping either blocked by coordination mode or alternating across modes, influenced behavioral and cortical indicators of rhythmic entrainment. We used a sensorimotor synchronization finger-tapping task from our previous study, which included two coordination (tapping) modes (synchronized vs. syncopated), and two forms of maintenance (pacing with a metronome vs. continuing without the metronome). Critically, one set of participants performed the experiment with task trials blocked by coordination mode, and a second set was asked to alternate from one coordination mode to the other across the course of the experiment. Thus, four conditions were included for each of the two study designs: 1) synchronized pacing, 2) synchronized continuation, 3) syncopated pacing, and 3) syncopated continuation.

Our previous study used tapping tracking for behavioral measurement (MakeyMakey™ kit) and functional near-infrared spectroscopy (fNIRS) for hemodynamics. Compared to functional magnetic resonance imaging (fMRI), fNIRS provides fine-grained temporal information and a more vibrant picture of cortical hemodynamic activity in terms of concentration changes of both [Oxy-Hb] and deoxygenated [deoxy-Hb] hemoglobin (Cutini et al., 2014). Moreover, it has a higher temporal resolution than fMRI and PET and better spatial resolution than EEG. It also has less sensitivity to movement than all other methods.

We hypothesize that switching back and forth between coordination modes over the course of the study will increase demand on timing control mechanisms, and thus impact the behavioral performance and cortical hemodynamics we observe during the finger-tapping task. We propose that the neural representation of timing behavior may be flexibly determined by the sensorimotor systems engaged during pacing and continuation phases for synchronized and syncopated coordination modes, and that this neural representation may differ based on the study design—blocked or alternating—that is used. To test our hypothesis, we compared findings across the two study designs. Specifically, we measured relative changes in cortical hemodynamics while participants performed the maintenance task given its systematically varied difficulty levels. This allowed us to probe the neural representation and continuity of timing

behavior across two different coordination modes (synchronization and syncopation) in two different maintenance contexts (pacing and continuation) across two different design contexts (block and alternating). We predicted that the finger-tapping task would produce markedly different behavioral and cortical outcomes depending on the specific context in which the forms of tapping were embedded.

Materials and Methods

Participants

Twenty-three healthy adult volunteers (16 females, 7 males; mean age 26.1, range 19-41) from the University of California, Merced were recruited in the study. Thirteen participants were randomly assigned to perform the tapping task in an alternating design and the remainder were assigned to perform the task in a block design. All participants successfully completed the tapping task and participated in fNIRS data collection. All participants were strongly right-handed, according to self-report. No participants reported any neurological or skeletomuscular disorder or injury that would prevent them from performing a timing-based tapping task. Informed consent was obtained from each participant before any data collection. This study was approved by the University of California, Merced Institutional Review Board for research ethics and human participants.

Task Procedure

Participants performed a rhythmic coordination task in a mixed-method study design containing two different study designs: block design and alternating design (See Figure 2 in Chapter 2). This task involved tapping on a custom-built metal plate connected to a MakeyMakey™ kit (Comstock et al., 2018; Comstock & Balasubramaniam, 2018) in time with an auditory metronome presented at 1 Hz in order to register the timing of each tap relative to an auditory metronome tone (Rahimpour et al., 2020). The time point of a participant's plate finger-tapping was corrected by 25 ms (to correct for temporal device delay due to the time it took the internal circuitry of the MakeyMakey™ to process the input, a built-in delay for input registration that reduces accidental double inputs) to define the onset of each behavioral response.

Two different timing relations were examined: synchronized tapping (pressing on each beat) and syncopated tapping (pressing between successive beats). The orders of coordination modes were counterbalanced across the trials (i.e., half of the participants were randomly selected to start with synchronization and the rest with syncopation), and half of the participants completed the tapping task in either blocked (Figure 1A-Chapter 2) or alternating design (Figure 1B-Chapter 2). Each coordination mode consisted of two phases of pacing and continuation at a rate of 1 Hz. For each coordination mode, participants were instructed to perform the task condition’s timing relation as best as possible when the metronome was on, and to continue after the metronome stopped. Seated participants performed repetitive right finger movements in the presence of an auditory metronome that produced a 1kHz tone for 20ms every 1000ms (1Hz). There were ten trials for each of the four timing conditions (i.e., synchronized pacing, synchronized continuation, syncopated pacing, syncopated continuation), with each trial involving 27 cycles of responses.

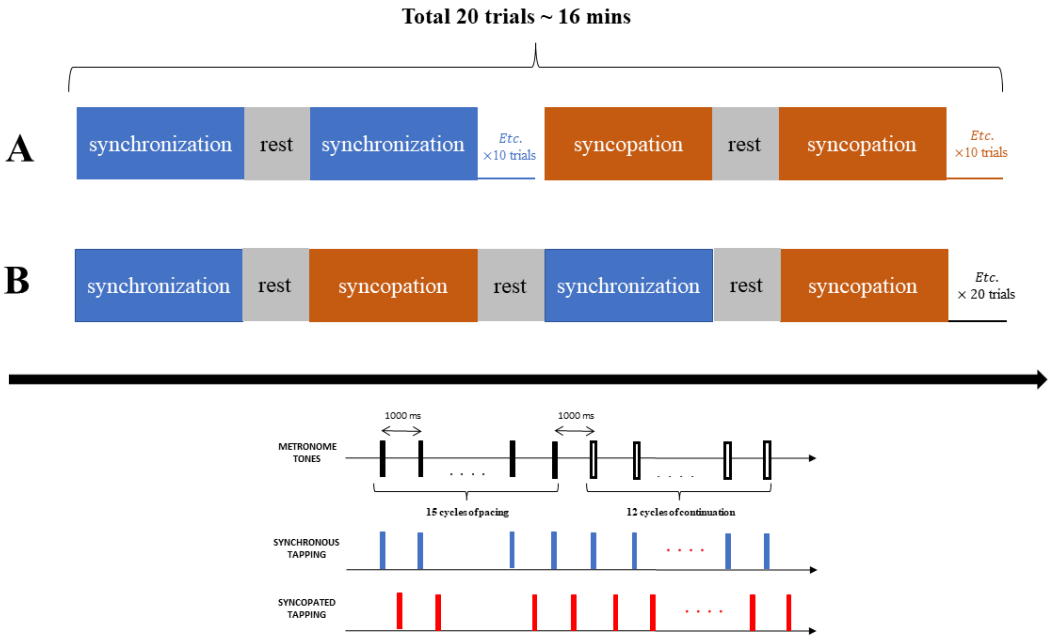

Figure 1. Schematic diagrams stimulus design A) blocked and B) alternating study designs. Participants perform repetitive finger tapping in the presence and then absence of an auditory metronome tone. The task consisted of 20 tapping trials. Each trial began with a pacing phase (15 cycles of tapping with the tone) followed by a continuation phase (12 tapping cycles continued in the same manner established during pacing but without the tone). Tapping patterns were performed in two different coordination modes: synchronized tapping (blue color) or syncopated tapping (red). Ten trials of tapping in each coordination mode were performed corresponding to block or alternating study design. During each trial, participants fixated a crosshair (+).

Statistical Analysis

Behavioral Analysis

For behavioral analysis, two relative measures of performance were calculated: asynchrony as a measure of accuracy, and inter-response interval as a measure of tapping fluency. We defined asynchrony as the time difference between a participant's response and the stimulus for each tapping cycle ($tap_i - beat_i, i \in n; cycle\ number$) (Bavassi et al., 2017; Delignières et al., 2009). We defined "virtual" asynchrony in syncopation as the time difference between a participant's response and the middle time point of each cycle ($tap_{mid\ \{i,i+1\}} - tap_i, i \in n; cycle\ number$). The term "mean asynchrony" (i.e., coordination error) is used to refer to accuracy for both synchronization and syncopation. Lower mean asynchrony (i.e., an asynchrony value close to 0) indicates higher levels of tapping accuracy. Further, negative mean asynchrony indicates that a participant is predicting the onset of each successive stimulus, while positive mean asynchrony indicates that a participant is reacting to a stimulus onset (Repp & Su, 2013). Note that

virtual mean asynchrony is also defined and computed by considering the taps and the extrapolated silent beats in continuation phases (Repp, 2005). Lastly, we measured the fluency of tapping, the inter-response interval (IRI), which we defined as the time between consecutive taps ($IRI_i = tap_{i+1} - tap_i \, , i \, \epsilon \, n; cycle \, number$). Negative asynchrony indicated that a tap occurred before the stimulus onset; a positive asynchrony indicated that the tap occurred after the stimulus onset. Thus, positive asynchronies represent reactions to stimuli, rather than their anticipation (Repp & Su, 2013). A negative IRI indicated that the interval produced behaviorally by the participant was shorter than the target time interval. Although the reasons for this phenomenon are not fully understood, anticipation errors in general are assumed to arise because the brain synchronizes the sensory consequences of the action with the event (e.g., auditory tone) without accounting for the afferent-conductance delay (Rose et al., 2021).

For our analyses, we first removed outliers from mean asynchrony and IRI indices using the interquartile range (IQR) based method. IQR is defined as the difference between the 25th percentile (Q1) and the 75th percentile (Q3) of our two behavioral markers. We considered an observation to be an outlier if it had a value 1.5 times greater than the IQR or 1.5 times less than the IQR (Rousseeuw & Croux, 1993). The average amount of missing data (due to single tap outliers or missing taps) within each timing condition was 3.2 (outliers= 2.98; missing taps=1.22). We then balanced data using a bootstrapping resampling method by selecting the constant sample size (=5) within each timing condition block (Berkovits et al., 2000).

Regression:

We analyzed our data using a multiple linear regression (MLR) model estimated by ordinary least squares (OLS) in order to assess the strength of the association between a set of independent variables (predictors) and single dependent (predicted) variable. Our model defined IRI and mean asynchrony as two separate dependent variables, and phase (pacing vs continuation), coordination mode (synchronization vs syncopation), and study design (blocked vs alternating) as three independent variables. The main equations can be presented as:

$$Y_{Asynchrony} = X.\beta + \varepsilon \qquad (1)$$

and

$$Y_{IRI} = X.\beta + \varepsilon \qquad (2)$$

Where Y is a $n \times 1$ $(n = 23)$ matrix containing n total observations of each mean asynchrony and IRI variables, the matrix X has dimensions $n \times (k + 1)$ for $three$ independent variables. The vector β_k $(dimention: (k + 1) \times 1; \; k\epsilon \; 0, \dots, 3)$ and ε $(dimention: n \times 1)$ represent regression coefficient and error, respectively. After observing no violation of MLR assumptions, we estimated our model to predict our mean asynchrony and IRI variables based on our three independent variables and generate the main effect and interaction effect of each independent variable (predictor) on the dependent (predicted) variable.

After estimating our regression coefficients, we used Tukey's honestly significant difference (HSD) post-hoc test as a multiple pairwise comparison technique (Abdi &

Williams, 2010) to find the ANOVA contrast effects between all possible group pairing sub categorical observations.

Cubic Spline Growth Curve Model:

A flexible statistical approach to model the nonlinear form of temporal trend growth is the piecewise growth curve model (PGCM) (Chou et al., 2004). We estimate PGCM by cubic spline interpolation approach (Dyer & Dyer, 2001) to perform piecewise interpolation and find the turning point of the curve (Ning & Luo, 2017). This allows us to formulate the function of growth forms for pacing and the subsequent continuation phases such that the second derivative of the model represents the turning point of the fitted model. This point is essential since we are interested in comparing growth rates across the pacing and continuation phases. The specification of a turning point is important (Ning & Luo, 2017), since it may happen before or after the intervention (the transition from pacing to continuation).

Causal Inference:

Finally, we implemented the difference in differences (DID) method (Branas et al., 2011; Wing et al., 2018) to compare the changes in our behavioral indices over time between averaged indices of the alternating design (as the manipulated group) and the block design (as the control group). We were then able to investigate the causal effect of study design on rhythmic entrainment. The DID technique is ideal for use with the continuation paradigm, given that randomization of pacing and continuation phases at the level of the individual is impossible. No violation of assumptions has been observed in our DID approach. First, the functions and covariates in the model are correctly defined. Second, the expectation value of the error term is zero and the corresponding distributions of covariates are independent. Third, both study designs follow the same trends over time in the absence of intervention. The DID regression model was implemented as shown in the following equations:

$$Y = \beta_0 + \beta_1.[Block] + \beta_2.[Alternating] + \beta_3.[Block \times Alternating] + \varepsilon \qquad (3)$$

‘

Block’ and ‘*Alternating*’ represent control and manipulated groups, respectively, in which dummy variables of time are defined as pacing:0 and continuation:1. The variable ‘$Block \times Alternating$’ is defined as the interaction between behavioral performance changes of block and alternating designs. Also, β_i $(j\epsilon\{0,1,2,3\})$ are defined as regression coefficients of the model. Because timing coordination is randomized over time, we were able to control for its effect and exclude it from the model as a confounding variable.

A post hoc power analysis was conducted using the software package, GPower (Faul & Erdfelder, 1992). The sample size of 23 was used for the statistical power analyses, and a three-predictor variable equation was used as a baseline. The recommended effect sizes used for this assessment were as follows: small ($Cohen's\ f\ =$ 0.14), medium ($Cohen's\ f\ =$ 0.39), and large ($Cohen's\ f\ =$ 0.59) (see Cohen et al., 2014). The α −level used for this analysis was $p < .05$. The post hoc analyses revealed the statistical power for this study was 0.2 and 0.8 for detecting a small and medium effects, respectively, whereas the power exceeded .95 for detecting a moderate to large

effect size. Thus, there was sufficient power (i.e., power= 0.8) at the moderate to large effect size level, although less than adequate statistical power at the small effect size level.

fNIRS Instrument and Analysis

During the finger-tapping task, cortical hemodynamics were monitored and recorded using a multichannel continuous-wave fNIRS system (NIRScout, NIRx Medical Technologies, LLC) with a probe comprising 16 light-source emitter positions containing 760 and 850 nm LED light and 20 APD light detectors. Data were collected at 3.785 Hz, and the average inter-optode distance was 3 cm (Rahimpour et al., 2020). Figure 2 illustrates our fNIRS probes and channel placement mapped relative to typical 10-10 scalp landmarks.

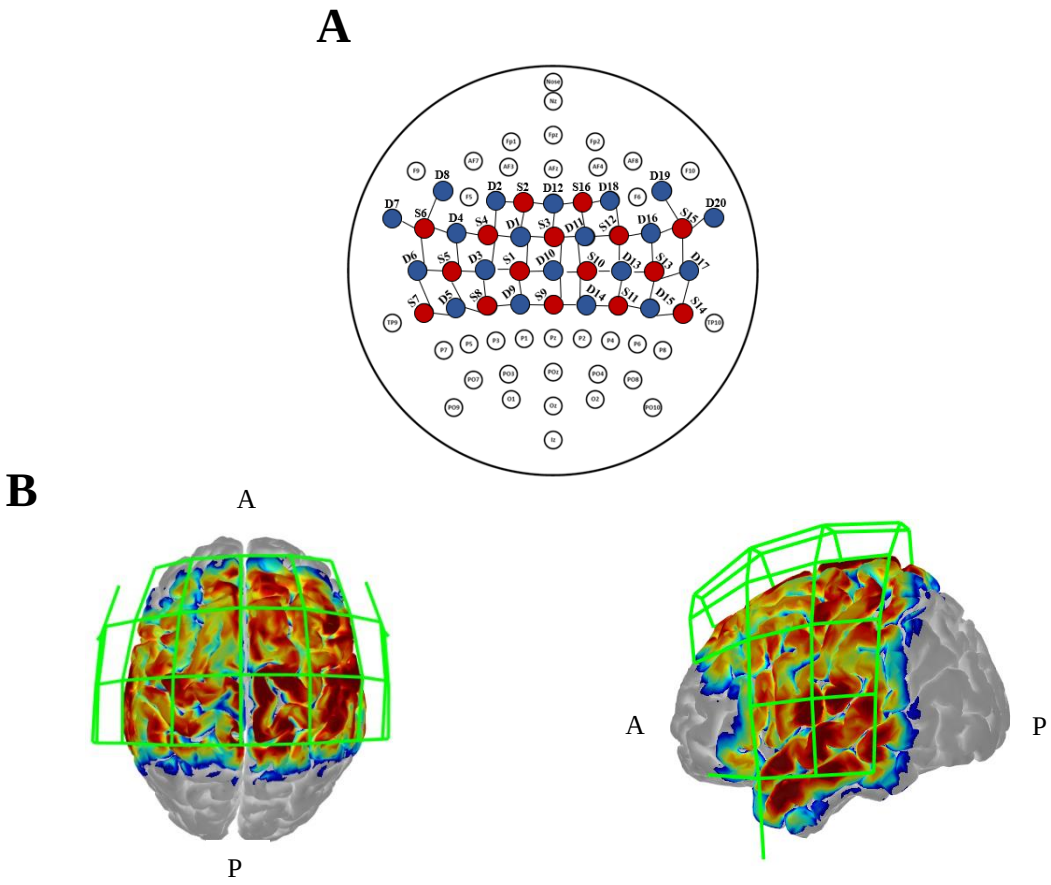

Figure 2. fNIRS probes and channel placement adapted from (Rahimpour et al., 2020). Depiction of the geometrical layout of sources (S, red) and detectors (D, blue) concerning the international 10-10 EEG system (A) and the corresponding sensitivity maps (B) of the probe in a 3D head model. A and P indicate anterior and posterior, respectively.

Raw fNIRS intensity signals were first converted to optical density changes and then oxygenated [Oxy-Hb] and deoxygenated [deoxy-Hb] hemoglobin concentration estimates, via the modified Beer-Lambert law (partial pathlength factor: 6.0) (Kocsis et

al., 2006). Both preprocessing and activation analyses were measured using the NIRS Brain AnalyzIR toolbox, a MATLAB-based open-source analysis package (Huppert et al., 2009; Santosa et al., 2018) which is computed using an autoregressive iterative reweighted least square (AR-IRLS) algorithm (Huppert, 2016).

Extracerebral components such as scalp hemodynamics, heartbeat, and respiration, and motion artifacts were corrected using AR-IRLS thoroughly described in Barker et al. (2013) and implemented in the NIRS Brain AnalyzIR software described in Santosa et al. (2018). Therefore, it makes the algorithm robust to physiological and motion artifacts (Hoppes et al., 2018; Lin et al., 2017). We used a canonical model to estimate the general linear model's regression coefficients and finally generate the hemodynamic response functions (HRFs).

We first checked the data quality at the participant level and then computed group-level results. At the group level, we performed a linear mixed-effects model that included the β value (together with t-value) per channel and timing condition as the dependent variable and independent variable, respectively, to model group-level correlations (Abdelnour et al., 2009). For each channel, estimates of the t-value for oxy-Hb and deoxy-Hb were computed across all trials for all participants. Our analyses only include the significantly active channels (i.e., statistically non-zero β) with FDR corrected p-value (q-value). However, we focus our analyses on [oxy-Hb] hemoglobin concentration due to its higher signal-to-noise ratio (SNR) and lower inter-participant variability relative to [deoxy-Hb] (see Rahimpour et al., 2020).

Results

Our focus is on the impact of the two study designs on the behavioral and hemodynamic measures of the finger-tapping task, above and beyond the contextual influences of coordination mode and phase of the maintenance paradigm. We first report and compare the behavioral results from the IRI and mean asynchrony indices, followed by a comparison of the channel maps for each timing condition across the block and alternating study designs.

Behavior

Mean Asynchrony

Our estimated multiple regression model was calculated to predict mean asynchrony based on coordination mode, maintenance phase, and study design. A significant effect of all independent variables on the mean synchrony index was found ($F_{1,24} = 430.08, P < 0.001$), with an R^2 of 0.78 in our full estimated regression model. Moreover, there was a main effect of phase on mean asynchrony ($F_{1,24} = 269.09, P < 0.001, \eta 2 = 0.4$), with a 48.82 ms average shift toward more positive mean asynchrony during continuation compared to pacing. We also observed an average increase of 8.44 ms in mean asynchrony for syncopation compared to synchronization that was significant ($F_{1,24} = 5.83, P = 0.02, \eta 2 = 0.14$), and an average increase of 23.15 ms in mean asynchrony for the alternating compared to block design, which was also significant ($F_{1,24} = 96.22, P < 0.001, \eta 2 = 0.33$). Thus, all three independent variables—coordination mode, maintenance phase, and study design—significantly impacted mean

asynchrony. Moreover, a significant phase × study design interaction ($F_{1,24} = 5.97, P < 0.02, \eta 2 = 0.24$) and coordination × study design interaction ($F_{1,24} = 7.29, P < 0.01, \eta 2 = 0.28$) were observed.

We also observed a contrast effect between pacing and continuation in synchronization ($F_{1,24} = 10.8, P = 0.001, \eta 2 = 0.34$) and syncopation ($F_{1,24} = 22.4, P < 0.001, \eta 2 = 0.4$) when controlling for study design. A contrast effect was also observed for synchronization and syncopation in the continuation phase ($F_{1,24} = 7.5, P < 0.001, \eta 2 = 0.3$) when controlling for study design.

Block study design:

In order to find the accuracy of synchronized and syncopated paced tapping, the average mean asynchronies were measured as -33.75 ± 130.5 (ms) (mean$\pm$SD) and -38.03 ± 145.34 (ms), respectively (see Figure 3). This clearly shows negative mean asynchrony (NMA) (i.e., the anticipation of tapping response with respect to the auditory stimulus) (Repp & Su, 2013) in the pacing phase for synchronization and syncopation. Moreover, the average continuation phase with no metronome present was estimated at 14.71 ± 210.8 (ms) for synchronized tapping and 62.91 ± 244.25 (ms) for syncopated tapping conditions. This indicates more variability for continuation than pacing in both coordination modes.

By using Tukey's HSD posthoc test, we observed significant differences between pacing and continuation in synchronization mode ($F_{1,24} = 8.18, P < 0.001, \eta 2 = 0.24$); between phases in syncopation $F_{1,24} = 18.62, P < 0.001, \eta 2 = 0.34$; and synchronization and syncopation in continuation phase ($F_{1,24} = 8.26, P < 0.001, \eta 2 = 0.23$).

Alternating study design:

For participants in the alternating study design, for synchronized and syncopated pacing and continuation, the mean asynchronies were 24.03 ± 106.22 (ms)(mean $\pm$ SD), 5.33 ± 127.93 (ms), 62.99 ± 212.73 (ms), and 76.59 ± 218.92 (ms), respectively, as illustrated in Figure 3. The results reveal that pacing resulted in more accurate and stable tapping compared to the continuation phase. Significant differences between pacing and continuation were observed for synchronization ($F_{1,24} = 6.13, P < 0.001, \eta 2 = 0.13$) and syncopation ($F_{1,24} = 12.46, P < 0.001, \eta 2 = 0.33$) coordination modes; however, no significant differences between coordination modes in each phase were observed.

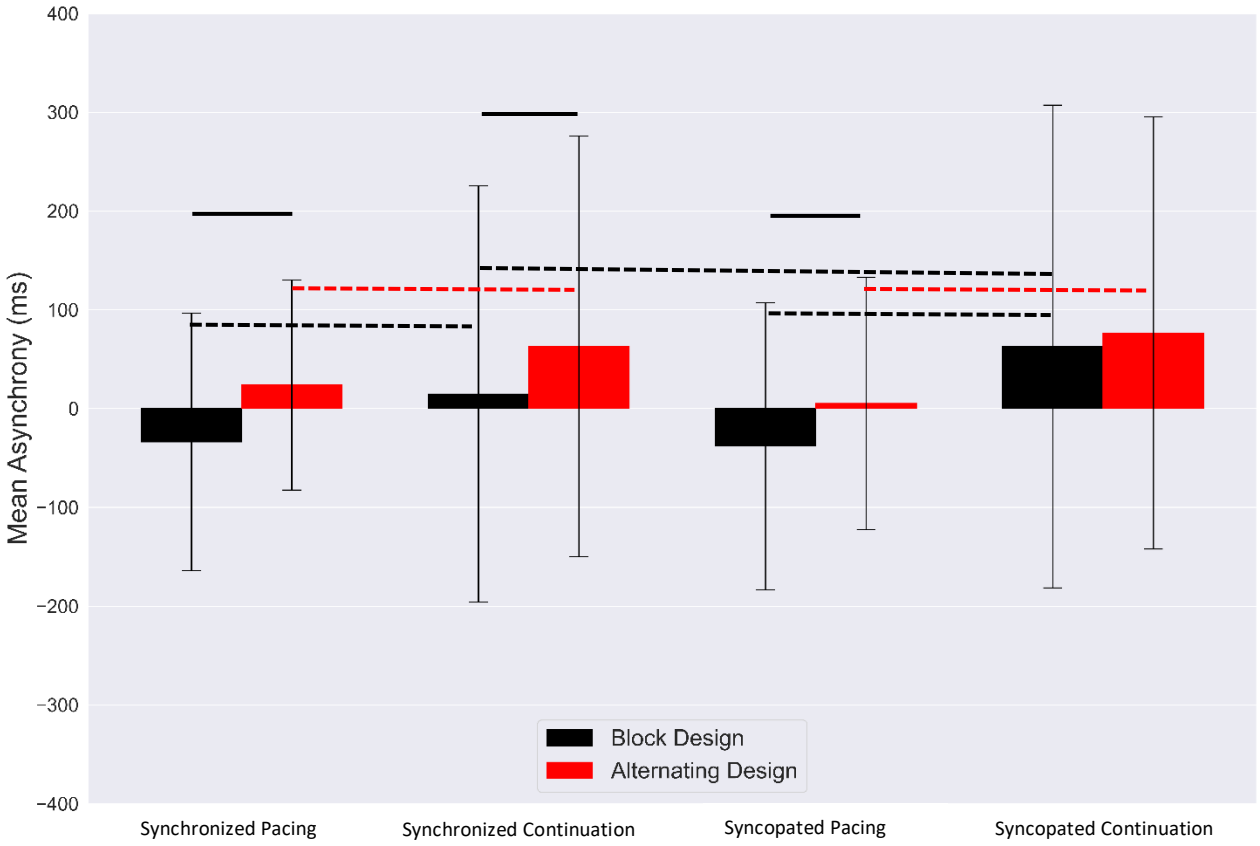

Figure 3. Mean asynchronies of each timing condition (i.e., synchronized pacing, synchronized continuation, syncopated pacing, and syncopated continuation) for the block design (black) and alternating design (red). Error bars show standard deviation (SD). Dashed brackets indicate statistically significant comparisons between timing conditions and solid brackets represent significant contrast effect between two study designs (block vs. alternating designs)

Block vs. Alternating study design:

Specifically, we found a significant contrast effect between pacing and continuation phases ($F_{1,24} = 23.65, P = 0.001, \eta 2 = 0.2$), and also between the block and alternating study designs when averaging across the two coordination modes ($F_{1,24} = 14.96, P = 0.001, \eta 2 = 0.18$). Significant contrast effects were observed between the block and alternating design in synchronized pacing ($F_{1,24} = 9.04, P < 0.001, \eta 2 = 0.31$), synchronized continuation ($F_{1,24} = 8.24, P < 0.001, \eta 2 = 0.28$), and syncopated pacing ($F_{1,24} = 8.27, P < 0.001, \eta 2 = 0.29$).

As can be seen in Figure 4, the average mean asynchrony index in syncopated and synchronized continuation is higher than in pacing for both coordination modes. This is consistent with our previous findings (Rahimpour et al., 2020) that more complex timing behavior results in less accurate behavioral performance.

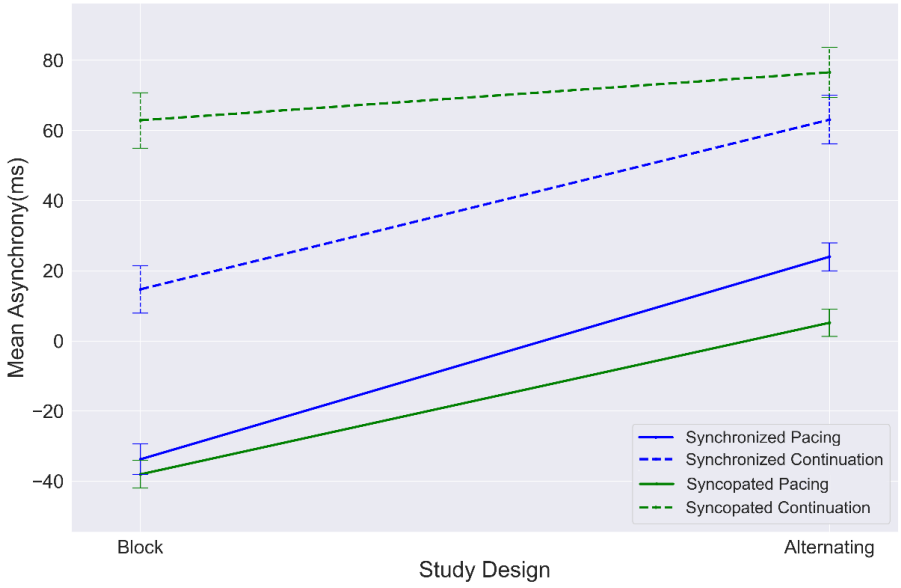

Figure 4. Values of mean asynchrony from block design to alternating design for each coordination mode and phase of maintenance task: synchronization (blue); syncopation (green); pacing (solid line); continuation (dashed line). Error bar indicates standard error (SE).

Temporal trend and causal inference on mean asynchrony:

We used cubic spline interpolation to estimate the fitted model of averaged pacing and continuation tapping trial cycles, as shown in Figures 5 and 6. Figure 5A shows the temporal trends for the averaged tapping cycles corresponding to the two coordination modes across the two study designs. The trend for synchronization over time shows a lower level of mean asynchrony than for syncopation; however, an incremental increase in asynchrony in the alternating compared to the blocked design was observed in all timing conditions, particularly at the continuation onset time point. Figure 5B shows the second derivative of the trends specifying the turning point estimated by our interpolated model. As can be seen, the estimated turning point for the block design falls (accurately) at the continuation onset time point (15 seconds). However, for the alternating study design, the turning point for both synchronized and syncopated tapping occurs at 10 seconds (5 seconds before the phase transition time point) and again at 24 seconds (9 seconds after phase transition) due to incomplete timing entrainment in the alternating design context.

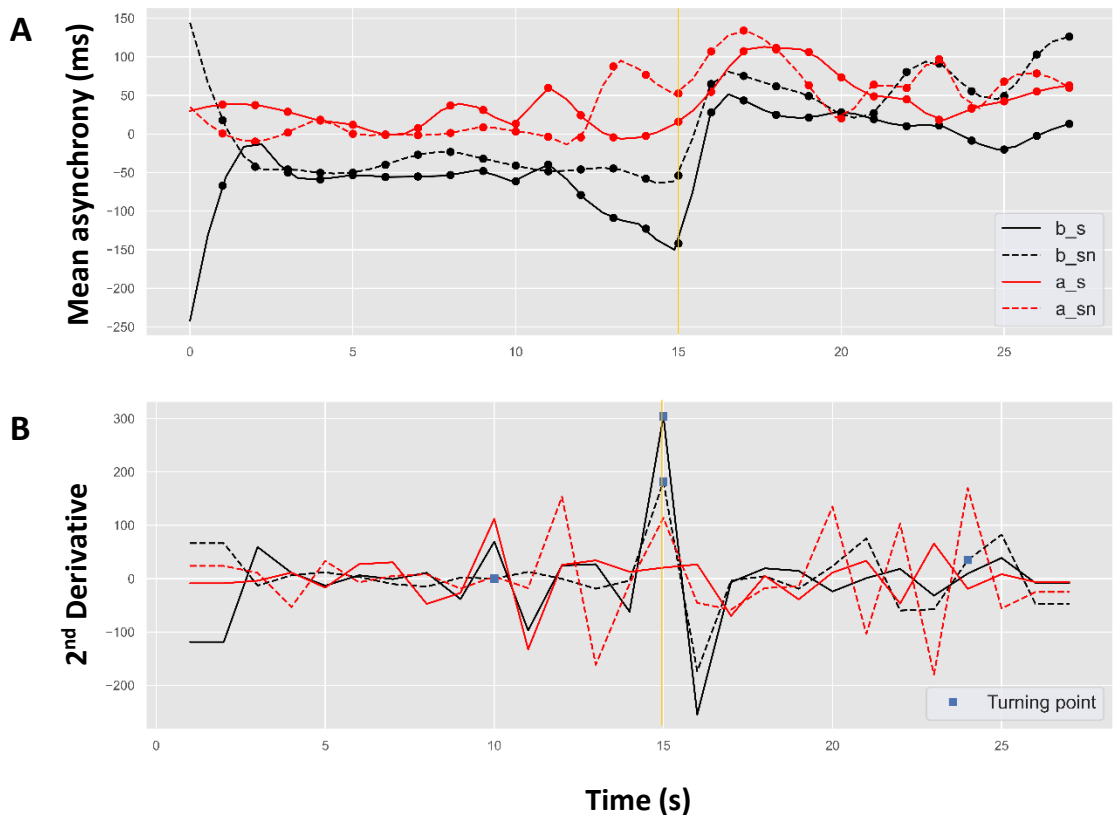

Figure 5. (A) Estimated asynchrony trend during maintenance (pacing followed by continuation) and (B) second derivatives of the corresponding trends locating the turning points (blue square marks) in: blocked synchronization (b_s as solid black line); blocked syncopation (b_sn as dashed black line); alternating synchronization (a_s as solid red line); and alternating syncopation (a_sn as dashed red line). Gold vertical solid line represents continuation phase onset.

Figure 6A depicts the temporal trends for the averaged tapping cycles across all timing conditions corresponding to the two study designs. The temporal trend for the alternating design has a higher asynchrony level than the block design; however, the incremental growth of asynchrony is observed in both, particularly in the transition to the continuation phase. Figure 6B shows the second derivative of the estimated asynchrony trends (Figure 6A) in which the maximum value represents the turning point of our model (see section Cubic Spline Growth Curve Model). As shown, the estimated turning point for the block design occurs at the continuation onset time point (second: 15). However, the turning point for the alternating design appears at time point 12 (3 seconds before the phase transition).

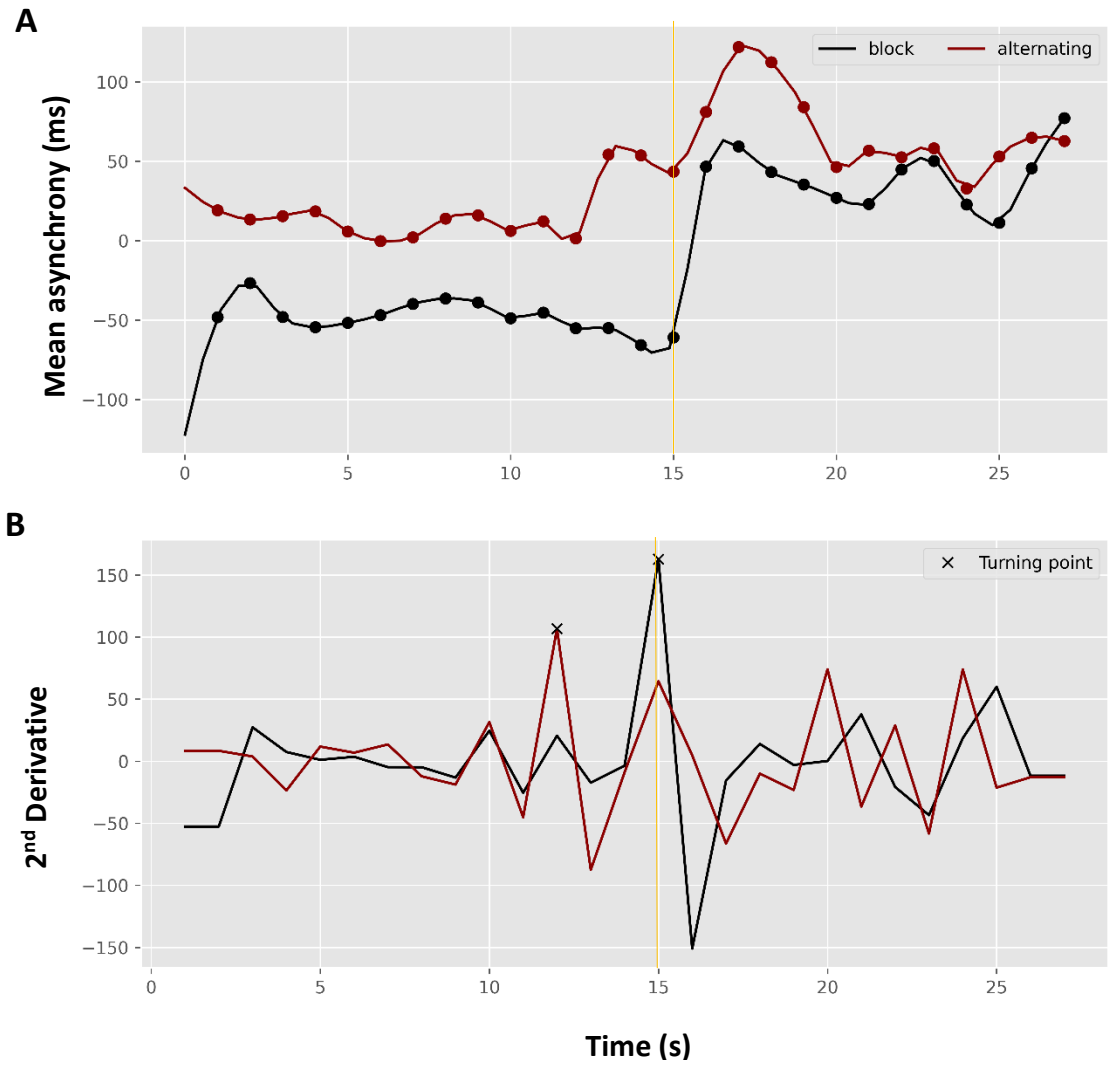

Figure 6. (A) Estimated asynchrony trend for the maintenance paradigm (pacing followed by continuation) averaged for coordination mode, and (B) second derivatives of the corresponding trends locating the turning points (x-marks) in the block design (black line) and alternating design (red line). The gold vertical solid line represents continuation phase onset.

As shown in Figure 7, the DID approach estimated by OLS was implemented to find the causal effect of study design on what we will refer to as rhythmic entrainment (Kurtosis= 3.03, Skewness=-0.1). From a total of 7842 observations (trials), we observed

a significant causal effect of study design on mean asynchrony output ($F_{2,7839} = 187.02, P < 0.001$), with an R^2 of 0.04. As shown in equation (3), four defined regression coefficients were used to estimate the effect of each of the following on the outcome: β_0: baseline mean asynchrony during pacing for block design; β_1: mean asynchrony temporal changes of block design; β_2: mean asynchrony temporal changes of alternating design; β_3: interaction of mean asynchrony between the two study designs. The coefficients were estimated as reported in Table 1. As shown, all coefficients were significant. These results demonstrate the causal impact of the study design on a behavioral measure obtained during performance of the maintenance task using different modes of coordination.

Table 1. Basic DID models of mean asynchrony for study design causality

	$\boldsymbol{\beta}$	SE	T statistics	R
Constant	-36.12	1.22	-5.343*	0.3
Block	75.21	3.392	16.213**	0.66
Alternating	54.33	4.107	9.543**	0.33
Block × Alternating	-10.19	4.113	9.796**	0.63
Obs	7842			
BIC	442.33			
Likelihood-ratio test of alpha=0	Chibar2(01) =883.3 Prob≥chibar2=0.000			

Abbreviation: SE, standard error. β, regression coefficient**.** Prob, probability. obs, observation. BIC, Bayesian information criterion

* $P < 0.01$, ** $P < 0.001$

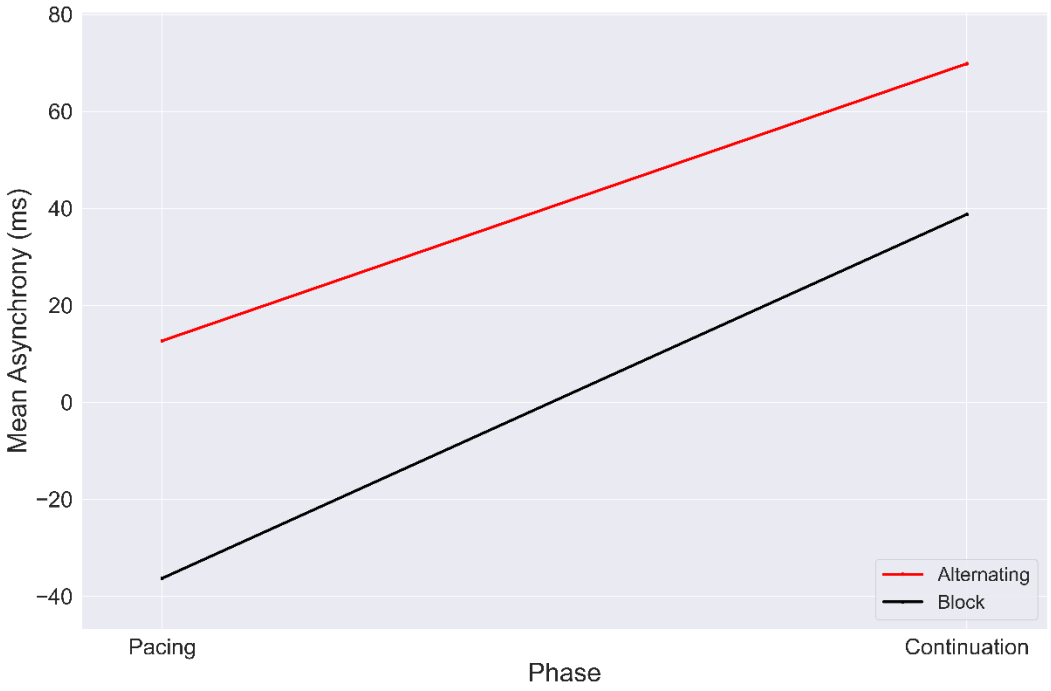

Figure 7. Graphic illustration of the DID estimator. Values of mean asynchrony averaged by timing coordination modes from pacing to continuation for each study design: block (black) and alternating (red).

IRI

MLR was also used to predict IRI based on timing type, maintenance phase, and study design; the outcome was significant ($F_{1,24} = 366.28, P < 0.001$), for the full model with an R^2 of 0.52. We observed a main effect of phase on IRI ($F_{1,24} = 166.05, P < 0.001, \eta 2 = 0.42$) with superior performance for pacing relative to continuation. We also found an average increase of IRI (ΔIRI =13.77 ms) during syncopation relative to synchronization ($F_{1,24} = 98.05, P < 0.001, \eta 2 = 0.44$), and an average increase (ΔIRI=15.44 ms) for the alternating compared to block design ($F_{1,24} = 14.16, P < 0.001, \eta 2 = 0.22$), thus favoring block design for accuracy. Likewise, all three independent variables—phase, coordination mode, and study design—significantly impacted IRI. Moreover, the phase and study design significantly interacted with each other ($F_{1,24} = 16.3, P < 0.001, \eta 2 = 0.14$).

When controlling for coordination mode, we observed a significant difference between the block design and alternating design ($F_{1,24} = 6.02, P = 0.001, \eta 2 = 0.22$). Specifically, a significant contrast effect between block design and alternating design was observed for synchronized pacing ($F_{1,24} = 4.69, P < 0.02, \eta 2 = 0.16$). We also observed a contrast effect between pacing and continuation for synchronization ($F_{1,24} =$

$6.83, P = 0.001, \eta 2 = 0.24$) and syncopation ($F_{1,24} = 18.5, P = 0.001, \eta 2 = 0.3$) coordination modes when controlling for study design. A contrast effect was observed between synchronization and syncopation for the continuation phase ($F_{1,24} = 14.9, P = 0.001, \eta 2 = 0.33$) when controlling for study design.

Block study design:

Synchronized tapping was performed with a mean IRI of 998.32 ± 52.24 (ms) and 994.8 ± 65.34 (ms) for the pacing and continuation phases, showing performance was very close to one second, thus on-time with the metronome. The average response rate was slower during syncopated tapping, with a mean IRIs of 998.76 ± 59.93 (ms) for pacing and 1022.18 ± 70.7 (ms) for continuation phases.

Post-hoc analyses of our regression model revealed a significant contrast effect for syncopated pacing and syncopated continuation ($F_{1,24} = 12.1, P < 0.001, \eta 2 = 0.31$). We also observed a contrast effect for synchronized continuation and syncopated continuation ($F_{1,24} = 13.13, P < 0.001, \eta 2 = 0.3$).

Alternating study design:

Synchronized tapping was performed with a mean IRI of 986.65 ± 54.03 (ms) and 1013.41 ± 61.69 (ms) for the pacing and continuation phases. Moreover, during syncopated tapping, the average response rate was slower, with a mean IRIs of 1001.76 ± 56.42 (ms) for pacing and 1030.75 ± 70.51 (ms) for continuation phases.

A post-hoc analysis of the linear regression model for the alternating design revealed a contrast effects at every level for the alternating study design: synchronized pacing and synchronized continuation ($F_{1,24} = 11.32, P < 0.001, \eta 2 = 0.34$), syncopated pacing and syncopated continuation ($F_{1,24} = 16.18, P < 0.001, \eta 2 = 0.37$), synchronized pacing and syncopated pacing ($F_{1,24} = 5.41, P < 0.001, \eta 2 = 0.19$), synchronized continuation and syncopated continuation conditions ($F_{1,24} = 8.19, P < 0.001, \eta 2 = 0.27$) (see Figure 8)

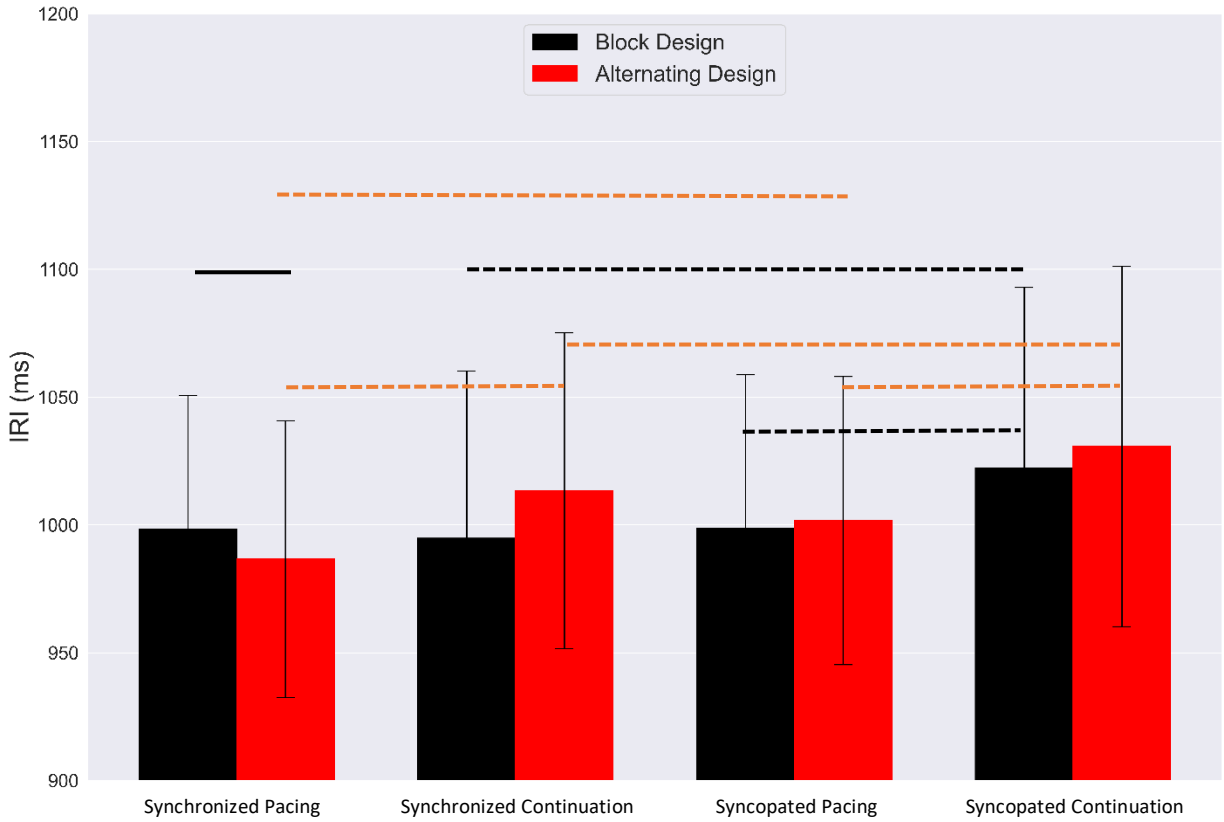

Figure 8. Averaged IRIs with SDs for each condition (i.e., synchronized pacing, synchronized continuation, syncopated pacing, and syncopated continuation) for block (black) and alternating designs (red). solid brackets indicate statistically significant contrasts between the two study designs and dashed brackets represent significant comparisons between timing conditions.

Block vs. Alternating study design:

We observed a significant contrast effect for synchronization and syncopation coordination modes ($F_{1,24} = 11.15, P = 0.001, \eta 2 = 0.28$), as well as for the block and alternating study designs ($F_{1,24} = 6.02, P = 0.001, \eta 2 = 0.22$). A main effect of coordination mode ($F_{3,36} = 85.01, P < 0.001, \eta 2 = 0.4$) and study design ($F_{1,24} = 14.88, P < 0.001, \eta 2 = 0.33$) on the IRI marker was also observed. We also observed an interaction between coordination mode and study design on IRI. ($F_{3,36} = 15.32, P < 0.001, \eta 2 = 0.26$).

Figure 9 shows that the IRI mean value in syncopated continuation is significantly higher than all other timing conditions regardless of study design. While supporting our prior findings (Rahimpour et al., 2020) that more complex timing behavior leads to less accuracy of behavioral performance, the results also show that participants in general performed better in the block design than in the alternating design across timing conditions.

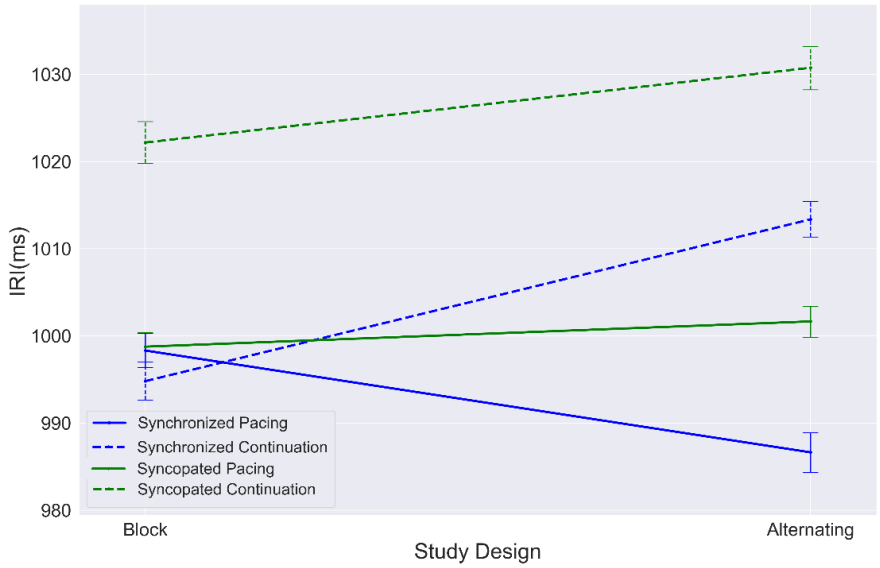

Figure 9. Mean values of IRIs from block and alternating designs for each condition: synchronization (blue); syncopation (green); pacing (solid line); continuation (dashed line). Error bar indicates standard error (SE).

Temporal trend and causal inference on IRI:

Using cubic spline interpolation, we estimated the fitted model of averaged pacing and continuation tapping trial cycles, as shown in Figures 10 and 11. Figure 10A shows four different IRI temporal trends of the averaged tapping cycles corresponding to the two types of coordination modes of the study designs. Syncopated tapping in both designs shows an abrupt increase in at 16 seconds (at first unpaced tap). However, gradual decrease has been observed in all trends during continuation of both study designs. In this regard, as shown in Figure 10B, the estimated turning points of all trends occur at the continuation onset time point (15 seconds); however, the turning point for syncopated tapping occurs at 6 seconds (9 seconds before phase transition time point) in the alternating study design.

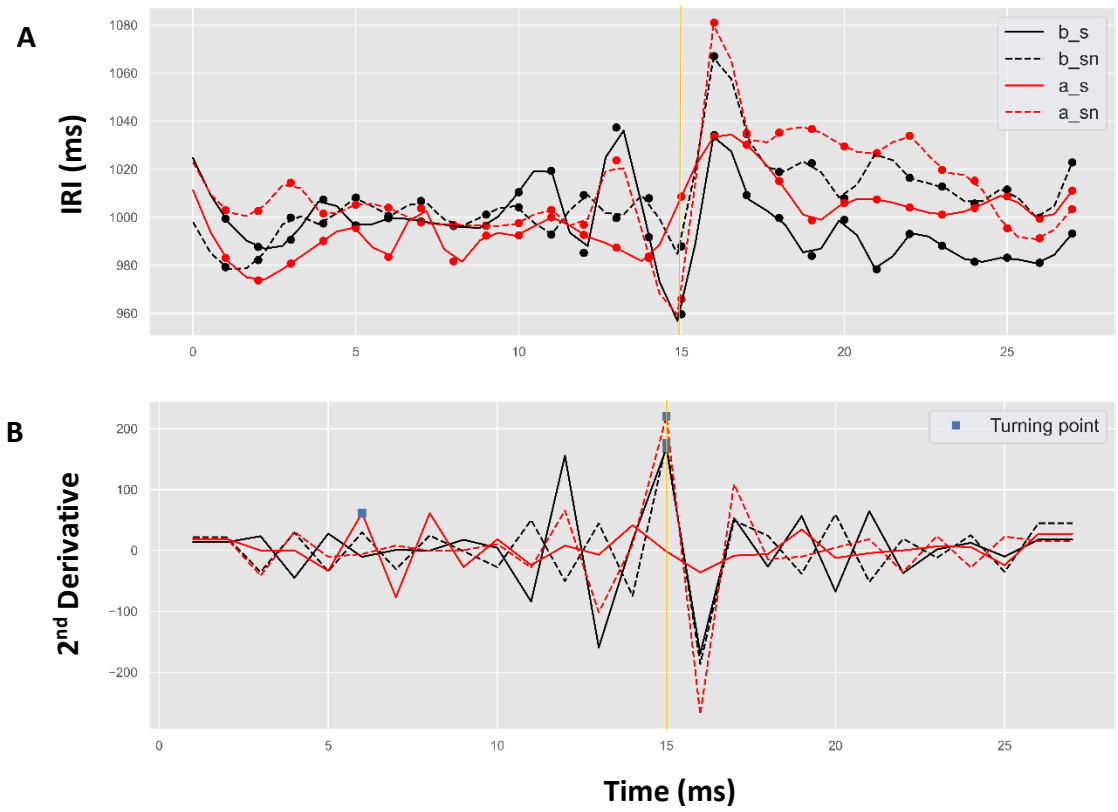

Figure 10. (A) Estimated IRI trend of maintenance paradigm (pacing followed by continuation), and (B) second derivatives of the corresponding trends locating the turning points (blue square marks) in synchronization + block design (b_s as solid black line); syncopation + block design (b_sn as dashed black line); synchronization + alternating design (a_s as solid red line); and syncopation + alternating design (a_sn as dashed red line). Gold vertical solid line represents continuation phase onset.

Figure 11A depicts temporal traces of the mean IRI cycles corresponding to the two study designs. The temporal trace corresponding to alternating design is higher than the block design in continuation phase; however, the abrupt growth of IRI was observed in both designs in the transition to continuation phase. Figure 11B shows the second derivative of the trend in which the estimated turning points for both study designs fall on the continuation onset time point (15 seconds).

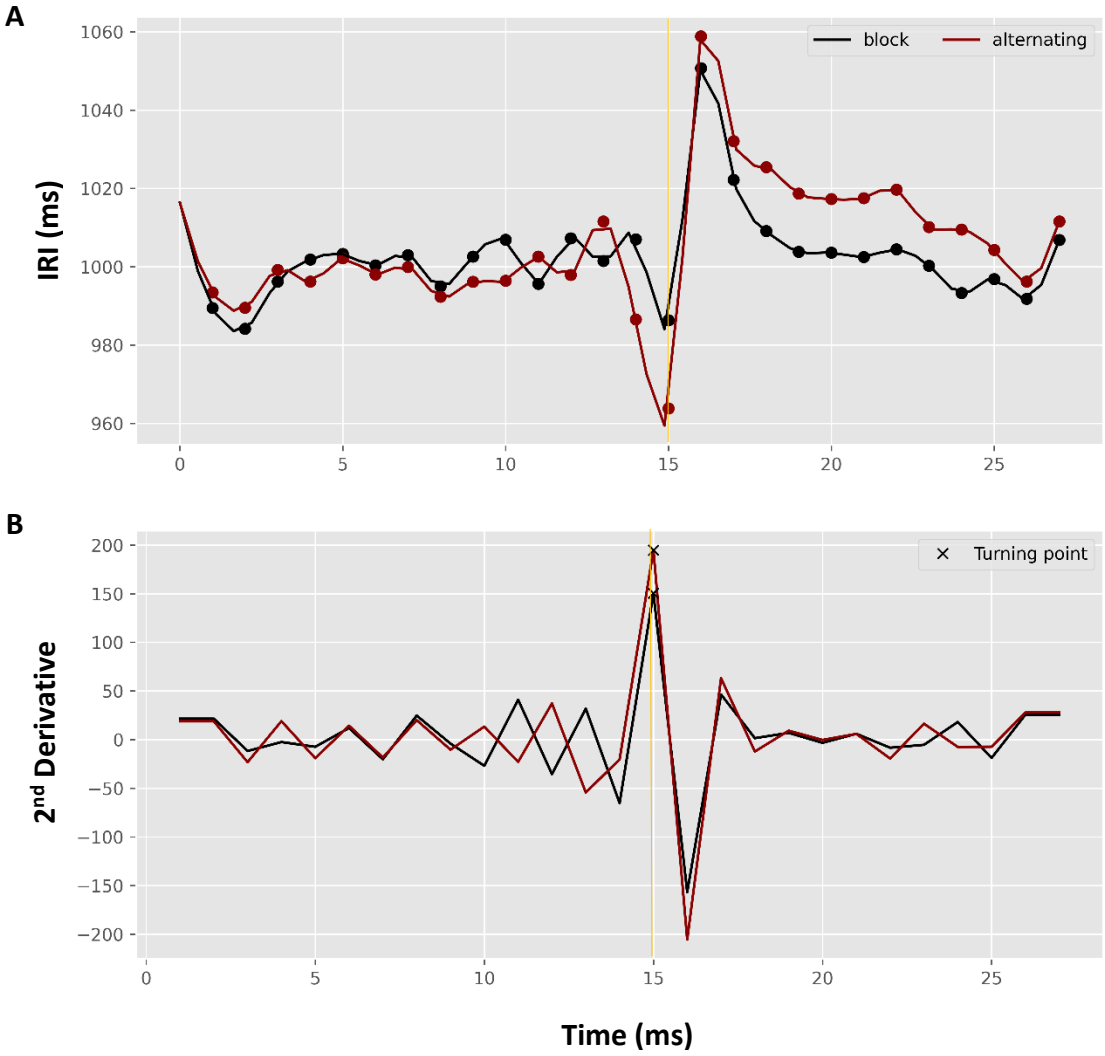

Figure 11. (A) Estimated IRI trend for maintenance paradigm (pacing followed by continuation) across coordination mode by design type, and (B) second derivatives of the corresponding trends locating the turning points for the block design (black line) and alternating design (red line). Gold vertical solid line represents continuation phase onset.

We implemented the DID approach estimated by OLS to find the causal effect of study design on accuracy (Figure 12). From a total 7023 observations, we observed a significant causal effect of the manipulation on mean asynchrony output ($F_{2,7020} = 73.78, P < 0.001$), with an R^2 of 0.02 (Kurtosis= 3.170, Skewness=0.085). Four

regression coefficients (β_0: baseline mean IRI of block design in pacing period; β_1: IRI temporal changes of block study design group; β_2: IRI temporal changes of alternating study design; β_3: interaction of IRI changes between two study designs) were estimated to determine whether there were the main effects of independent variables (see Causal Inference section for more information). Accordingly, as reported in Table 2, all regression coefficients were significant, revealing the causal effect of study design on the tapping accuracy in the maintenance paradigm.

Table 2. Basic DID models of IRI for study design causality

	$\boldsymbol{\beta}$	SE	T statistics	R
Constant	998.24	0.82	795.011*	0.13
Block	10.29	1.252	10.273**	0.46
Alternating	25.63	1.449	13.255**	0.53
Block × Alternating	15.41	1.502	3.685**	0.33
Obs			7023	
BIC			393.5	
Likelihood-ratio test of alpha=0			Chibar2(01) =143.3 Prob≥chibar2=0.001	

Abbreviation: SE, standard error. β, regression coefficient**.** Prob, probability. obs, observation. BIC, Bayesian information criterion

* $P < 0.01$, ** $P < 0.001$

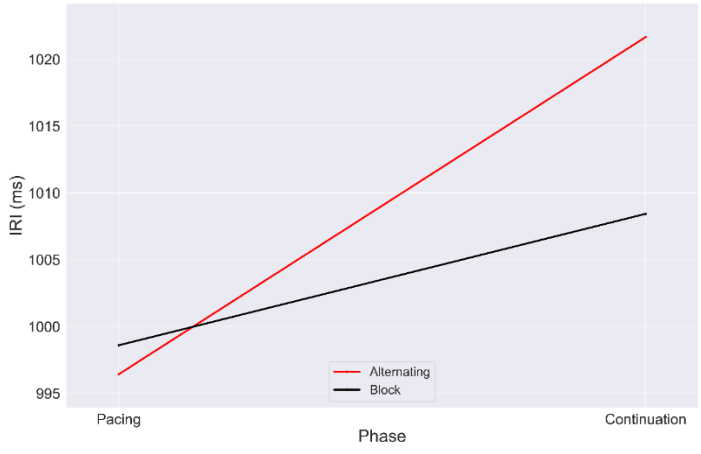

Figure 12. Graphic illustration of the DID estimator. The values of IRIs averaged across coordination mode with pacing to continuation phase for each study design: block (black line); alternating (red line).

Cortical Hemodynamics

Here we investigate the result of the hemodynamic activity for each timing condition (i.e., synchronized pacing, synchronized continuation, syncopated pacing, and syncopated continuation) in two different methodological designs of the fNIRS experiment (block versus alternating design). We depict and compare group-level channel maps' results via AR-IRLS regression model.

Synchronized Pacing

Channels with significant activation for synchronized pacing conditions obtained by block design and alternating design are shown in Figure 13. In the blocked design, we observed highly significant [Oxy-Hb] activations in left temporal, frontal channels ($t_{FT7-F7} = 7.3, q = 0.01$; $t_{FT7-FT9} = 6.5, q = 0.03$; $t_{FT7-FC} = 5.3, q < 0.05$), right parietal temporal ($t_{CP2-C2} = 5, q < 0.05$) and left parietal area ($t_{CPz-CP1} = 7.5, q < 0.01$) extending anteriorly into central ($t_{Cz-C1} = 6.1, q = 0.03$; $t_{Cz-FCz} = 5.9, q = 0.03$), and frontal ($t_{FCz-Fz} = 5.1, q = 0.04$; $t_{FCz-FC1} = 6.4, q = 0.01$; $t_{FC1-F1} = 4.4, q = 0.05$) regions in block design study (Figure 13A); however no significant activation was observed in alternating design (Figure 13B).

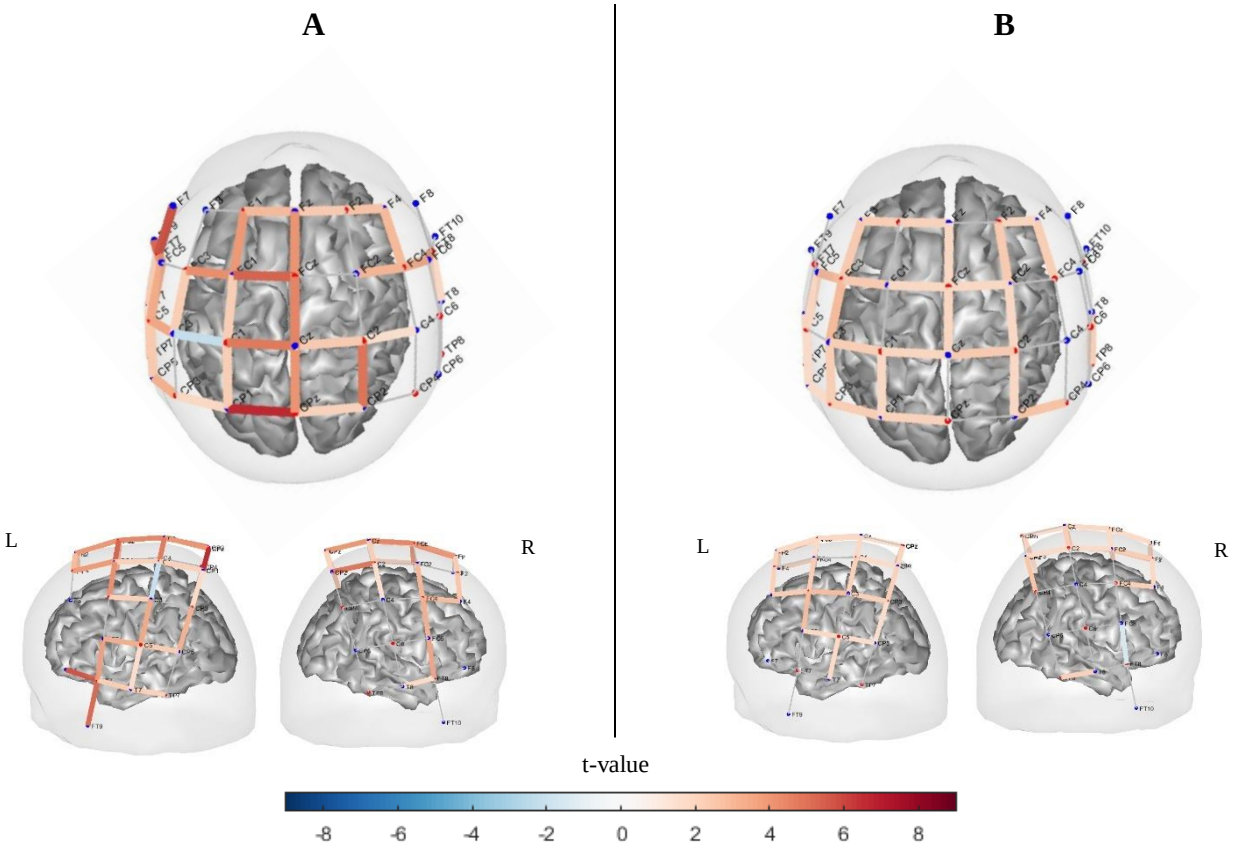

Figure 13. Channel maps of the main effect (q<0.5) of synchronized pacing condition on [Oxy-Hb] hemodynamic activation obtained by (A) Block design and (B) Alternating design. Color bars represent the t-value range.

Synchronized Continuation

In Figure 14, we see different patterns, with mostly nonsignificant activation of channels in both the block and alternating designs, although here is a significantly activated channel within the left parietal region ($t_{CPz-CP1} = 4.7, q = 0.05$) and right central parietal area ($t_{CP2-C2} = 4.6, p = 0.05$) in the block design. We also observed marginally significant activation in the left central (motor) area ($t_{FCz-FC1} = 4, q = 0.055$; $t_{FC1-FC3} = 4.1, q = 0.053$). The highly activated area has been observed in frontotemporal areas ($t_{FT7-FT9} = 7.4, q < 0.01$; $t_{FT7-F7} = 6.1, q = 0.02$) as well as right frontotemporal area ($t_{FC7-FC} = 5.4, q < 0.05$). However, similar to synchronized pacing, no significant activation was observed during the synchronized continuation condition of the alternating design.

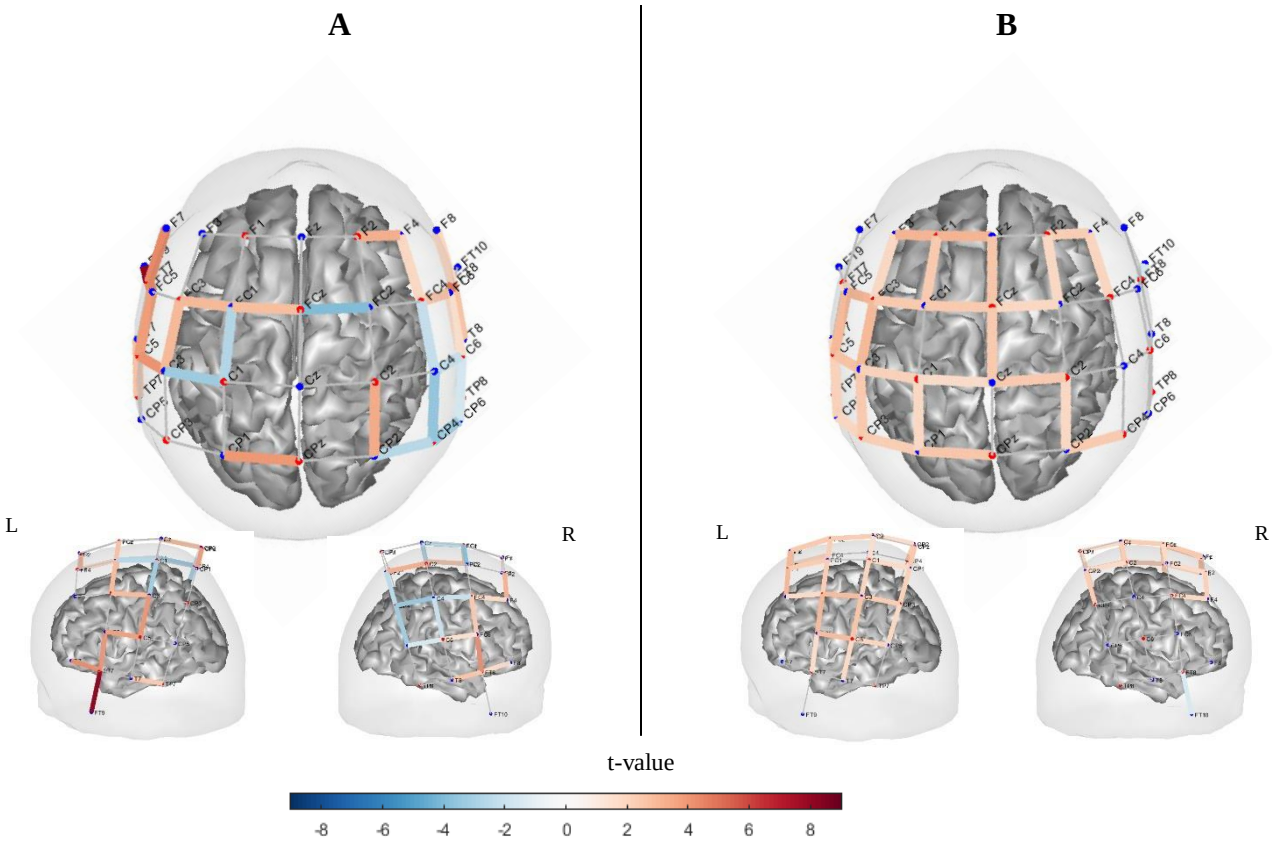

Figure 14. Channel maps of the main effect (q<0.5) in synchronized continuation condition obtained by (A) block design and (B) alternating design. Color bars represent the t-value range.

Syncopated Pacing

In the block design, the most highly activated electrode was found in the right central frontal area ($t_{FCz-Fz} = 7.2, q < 0.01$; $t_{FCz-FC2} = 8.5, q < 0.01$). In addition,

other significantly activated channels in the block design were observed in the central and frontal areas ($t_{Cz-C1} = 6.8, q = 0.02$; $t_{C1-FC1} = 6.2, q = 0.03$; $t_{FCz-FC1} = 5.8, q < 0.05$) (Figure 15A). However, as shown in Figure 15B, the most activated channels for the alternating design are observed in left central areas ($t_{C1-C3} = 4.65, q = 0.05$; $t_{C1-FC1} = 4.66, q = 0.05$) and bilateral temporal areas ($t_{T7-TP7} = 4.92, q < 0.05$; $t_{T8-TP8} = 4.88, q < 0.05$, and $t_{C5-T7} = 4.7, q < 0.05$).

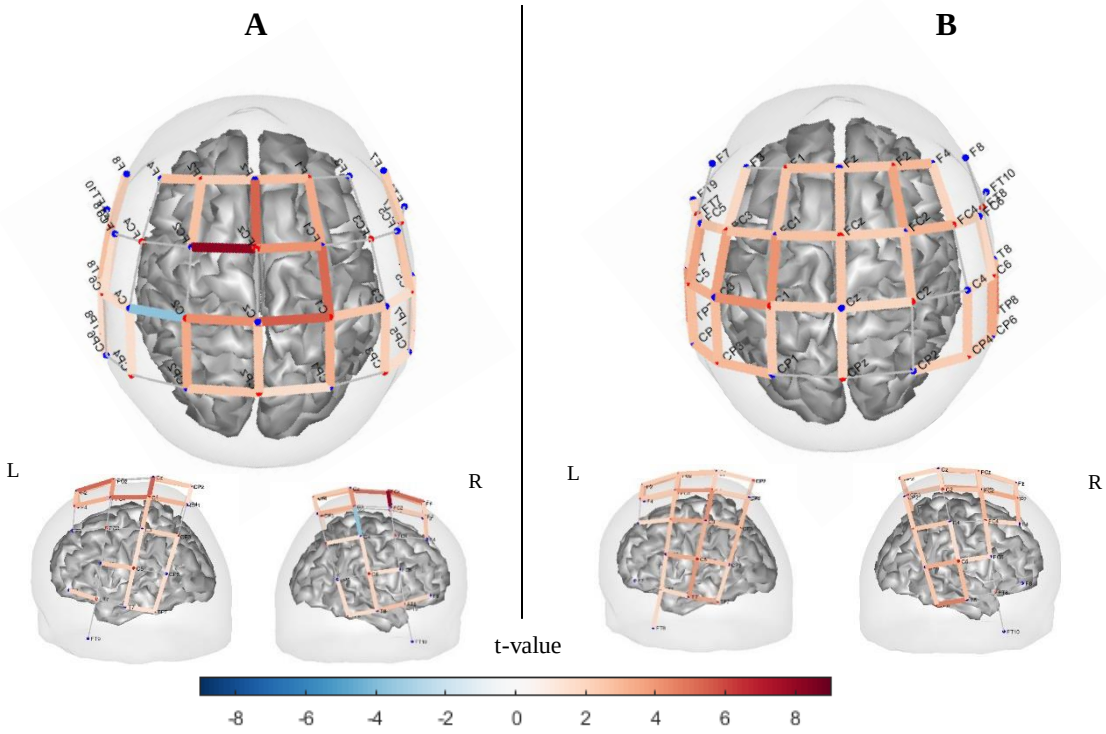

Figure 15. [Oxy-Hb] channel maps of the main effect (q<0.5) in syncopated pacing condition obtained by (A) block design and (B) alternating design. Color bars represent the t-value range.

Synchronized Continuation

Similar to syncopated pacing, syncopated continuation produced several significant channels of activation, particularly in the frontal, central, and parietal areas in both block and alternating designs. Figure 16 illustrates the [Oxy-Hb] channel maps with significant main effects in the syncopated continuation condition for the block design and a few marginally significant channels for the alternating design. As with syncopated pacing, the block design produced stronger [oxy-Hb] activation than the alternating design.

A few marginally significant areas of activation were observed in the alternating design ($t_{C3-FC3} = 4.71, q = 0.05$; $t_{C3-FC3} = 4.76, q = 0.05$), with a broad distribution of channels showing nonsignificant levels of activation in central, temporal, parietal, and frontal areas (none of these reached significance). In contrast, we observed highly

significant activation in the frontal area ($t_{FCz-Fz} = 8.1: q < 0.01$; $t_{FCz-FC2} = 8.4: q < 0.01$) for the block design. Moreover, other significantly activated channels in the block study design can be observed in the left central frontal area ($t_{FC1-FCz} = 6.2: q = 0.04$), right parietal area ($t_{CP2-C2} = 6.8: q = 0.03$), and left parietal, temporal areas ($t_{CP3-C3} = 5.8: q < 0.05$; $t_{C1-C3} = 5.7: q < 0.05$).

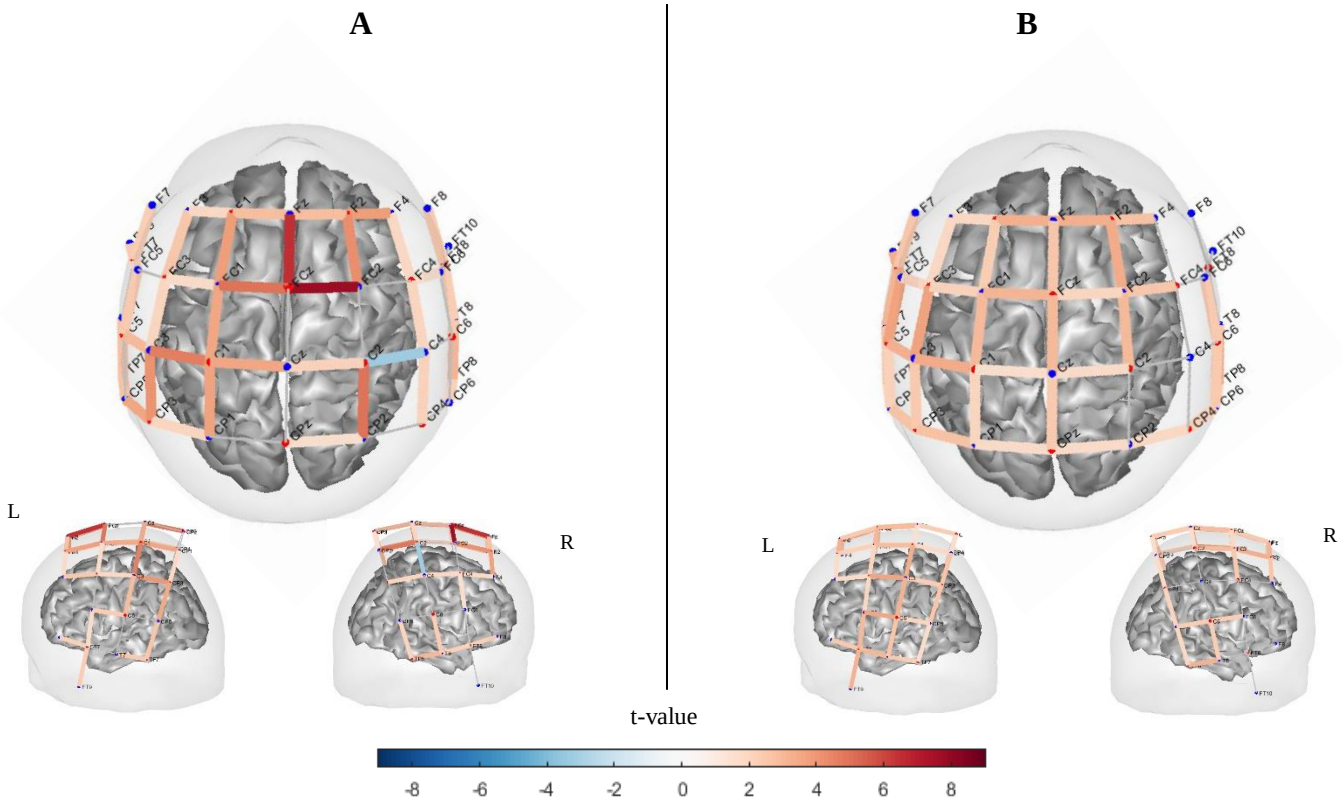

Figure 16. [Oxy-Hb] channel maps of the main effect (q<0.5) in the syncopated continuation condition obtained by (A) block design and (B) alternating design. Color bars represent the t-value range.

Discussion

The current study aimed to determine whether a subtle manipulation of experimental design influences overall accuracy in a tapping task and affects corresponding cortical hemodynamics. We observed a causal effect of study design on behavioral performance. Moreover, there was a meaningful influence of study design on the estimated temporal interpolation was indicated by GCM. The turning points in the block design were the indicators of accurate computational interpolation for the experimental transition between pacing and continuation. However, they did not perform in this way for the alternating design. In general, more complex behavior leads to less stable and less accurate individual performance. To this end, we measured the behavioral accuracy and hemodynamic activation associated with different timing behaviors. Manipulation of timing behaviors was achieved by manipulating coordination mode

(syncopated vs synchronized tapping) and phase of the maintenance task (pacing and continuation) (Jantzen et al., 2004) across two study designs (block vs. alternating study designs). Results showed that both block and alternating study designs engaged primary temporal and motor areas of the brain, and specific forms of motor timing behavior differentially engaged frontal and parietal areas. Therefore, study design strongly influenced overall cortical engagement.

We observed significant differences in the behavioral results for both study designs between coordination modes (synchronized vs. syncopated tapping) and phase (pacing vs. continuation). In our original fNIRS validation study, which used a block design (Rahimpour et al., 2020), recruitment of a broader cortical network during syncopated continuation compensated for the increased timing demands on the motor system, allowing for stable interval production performance. In our study, the differences in neural activity that we observed during blocked synchronized and syncopated tapping may reveal reliance on distinct processing networks in support of more automatic versus cognitively controlled timing behavior. For example, increased activity within subsystems associated with motor planning and preparation (SMA and dorsal-premotor) (Mayville et al., 2002) and working memory and attention (prefrontal cortex, superior parietal lobe, and MTG) (Smith & Jonides, 1998) have been postulated to reflect increases in cognitive demand for performance of the off-beat (syncopated) coordination mode. Such differences were even more pronounced during continuation (when no metronome was present), when the absence of the external auditory stimulus no longer served as a timing guide and cognitive load was greater.

Across both study designs, finger tapping activated cortical areas compatible with the automatic, motor-related timing network (sensorimotor regions). The additional activity observed during syncopated tapping in central, frontal, and parietal areas is consistent with greater engagement of memory and attention processes, and an overall increase in levels of cognitive control. This interpretation is consistent with behavioral findings showing that motor production of anti-phase relationships imposes higher cognitive and attentional demand than in-phase patterns (Meyer-Lindenberg et al., 2002; Monno et al., 2002). This was observed across both study designs.

A significant difference between the two study designs was observed in the average neural activation as reflected by [Oxy-Hb] levels. In particular, the two designs produced different activation patterns for the synchronized versus syncopated rhythms, and for the pacing and continuation phases. These findings suggest that not only are different cortical networks engaged during externally guided performance of different coordination modes across study designs, but that once established, those different networks continue to operate even when the external guide is no longer present. Although there are likely other mediating factors, one distinct possibility is that these hemodynamic response patterns reflect the differential representation of temporal information given two distinct coordination dynamics. Indeed, process models of interval timing propose specific mechanisms for representing and storing temporal intervals (Treisman, 1963), and the consequence of the existence of two different timing mechanisms is that substantially different networks are recruited to perform the same temporal task (Wing, 2002). Results presented here strongly suggest that the neural activity supporting continuation of an initially externally guided rhythm not only generalizes across different

coordination modes but that it is also strongly influenced by the study context in with initial that mode is initially established. Thus, the context of a study's design plays an integral role in which neural networks are engaged during the continuation paradigm.

These findings lead to the interesting consequence that the complexity and difficulty of a study's design (here, block vs. alternating) impacts the extent of neural activation, with lower levels of activation observed when entrainment is not allowed to take place, as in the alternating design context. In contrast, greater levels of neural activation were observed in sensorimotor areas across all timing conditions in the block design. These differences may reflect differences in overall entrainment, with ongoing changes in coordination in the alternating study design relative to the block design interrupting any consistent entrainment of motor timing behavior. There is some evidence that hemodynamic responses are modulated by movement parameters (Harrington et al., 1998; Thickbroom et al., 1998), further supporting our interpretation that a study's design impacts context-dependent neural engagement.

Future research will be needed to understand the details of this impact. For example, an increase in the overall length of trials in the alternating design context may lead to sufficient entrainment so as to produce comparable levels of hemodynamic activity to those observed in the blocked context. Moreover, contrasting hemodynamic-based measures with other, more direct measures of neurophysiological activity, such as electroencephalography, will be important to further substantiating these findings.

Conclusion

The present study interrogates behavioral and brain responses when different rhythmic patterns of motor coordination are introduced into a pacing-continuation task, and further compares responses across a rhythmically blocked versus a rhythmically alternating study design. Behavioral results point to the substantial influence of study design on complex timing behavior. The complexity and difficulty of the particular study design likewise impacts the degree and breadth of neural activation elicited. Significantly higher levels of activity across all four tapping conditions in block design may reflect development of an internal representation of the timing patterns (i.e., entrainment), something that is not possible in the alternating design. Thus, our findings highlight the impact of a study's design on the degree of rhythmic entrainment that can be achieved given different forms of coordination dynamics. Thus, neural correlates of timing behavior reflect context-dependent parameters.

Our results provide insight into the influence of the broader experimental context on timing behavior and the underlying neural activity that supports it, an interpretation consistent with several previous findings (Jantzen et al., 2007; Jantzen et al., 2004; Rahimpour et al., 2020). Thus, representation of timing information is formed in a context-dependent manner, with the introduction of different cognitive states or expectations, as well as difficulty levels, impacting behavioral performance and the corresponding neural engagement supporting it. Here we have observed that it takes time to develop an internal timing representation and thus entrain motorically to complex rhythmic stimuli.

References

Abdelnour, F., Schmidt, B., & Huppert, T. J. (2009). Topographic localization of brain activation in diffuse optical imaging using spherical wavelets. *Physics in Medicine \& Biology*, *54*(20), 6383.

Abdi, H., & Williams, L. J. (2010). Tukey's honestly significant difference (HSD) test. *Encyclopedia of Research Design*, *3*(1), 1–5.

Bai, O., Mari, Z., Vorbach, S., & Hallett, M. (2005). Asymmetric spatiotemporal patterns of event-related desynchronization preceding voluntary sequential finger movements: a high-resolution EEG study. *Clinical Neurophysiology*, *116*(5), 1213–1221.

Barker, J. W., Aarabi, A., & Huppert, T. J. (2013). Autoregressive model based algorithm for correcting motion and serially correlated errors in fNIRS. *Biomedical Optics Express*, *4*(8), 1366–1379.

Bavassi, L., Kamienkowski, J. E., Sigman, M., & Laje, R. (2017). Sensorimotor synchronization: neurophysiological markers of the asynchrony in a finger-tapping task. *Psychological Research*, *81*(1), 143–156.

Berkovits, I., Hancock, G. R., & Nevitt, J. (2000). Bootstrap resampling approaches for repeated measure designs: Relative robustness to sphericity and normality violations. *Educational and Psychological Measurement*, *60*(6), 877–892.

Branas, C. C., Cheney, R. A., MacDonald, J. M., Tam, V. W., Jackson, T. D., & Ten Have, T. R. (2011). A difference-in-differences analysis of health, safety, and greening vacant urban space. *American Journal of Epidemiology*, *174*(11), 1296–1306.

Chauvigné, L. A. S., Gitau, K. M., & Brown, S. (2014). The neural basis of audiomotor entrainment: an ALE meta-analysis. *Frontiers in Human Neuroscience*, *8*, 776.

Chen, J. L., Penhune, V. B., & Zatorre, R. J. (2008). Moving on time: brain network for auditory-motor synchronization is modulated by rhythm complexity and musical training. *Journal of Cognitive Neuroscience*, *20*(2), 226–239.

Chou, C. P., Yang, D., Pentz, M. A., & Hser, Y. I. (2004). Piecewise growth curve modeling approach for longitudinal prevention study. *Computational Statistics & Data Analysis*, *46*(2), 213-225.

Cohen, P., West, S. G., & Aiken, L. S. (2014). *Applied multiple regression/correlation analysis for the behavioral sciences*. Psychology press.

Comstock, D. C., & Balasubramaniam, R. (2018). Neural responses to perturbations in visual and auditory metronomes during sensorimotor synchronization. *Neuropsychologia*, *117*, 55–66.

Comstock, D. C., Hove, M. J., & Balasubramaniam, R. (2018). Sensorimotor synchronization with auditory and visual modalities: Behavioral and neural differences. *Frontiers in Computational Neuroscience*, *12*, 53.

Cutini, S., Scarpa, F., Scatturin, P., Acqua, R. D., & Zorzi, M. (2014). *Number – Space Interactions in the Human Parietal Cortex : Enlightening the SNARC Effect with Functional Near-Infrared Spectroscopy*. *February*, 444–451. https://doi.org/10.1093/cercor/bhs321

Deligniéres, D., Torre, K., & Lemoine, L. (2009). Long-range correlation in synchronization and syncopation tapping: A linear phase correction model. *PLoS ONE*, *4*(11). https://doi.org/10.1371/journal.pone.0007822

Dyer, S. A., & Dyer, J. S. (2001). Cubic-spline interpolation. 1. *IEEE Instrumentation \& Measurement Magazine*, *4*(1), 44–46.

Faul, F., & Erdfelder, E. (1992). GPOWER: A priori, post-hoc, and compromise power analyses for MS-DOS [Computer program]. *Bonn, FRG: Bonn University, Department of Psychology*.

Harrington, D. L., Haaland, K. Y., & Knight, R. T. (1998). Cortical networks underlying mechanisms of time perception. *Journal of Neuroscience*, *18*(3), 1085–1095.

Hoppes, C. W., Sparto, P. J., Whitney, S. L., Furman, J. M., & Huppert, T. J. (2018). *Functional near-infrared spectroscopy during optic flow with and without fixation*. 1–14.

Huppert, T. J. (2016). Commentary on the statistical properties of noise and its implication on general linear models in functional near-infrared spectroscopy. *Neurophotonics*, *3*(1), 10401.

Huppert, T. J., Diamond, S. G., Franceschini, M. A., & Boas, D. A. (2009). HomER: a review of time-series analysis methods for near-infrared spectroscopy of the brain. *Applied Optics*, *48*(10), D280--D298.

Ivry, R. B., & Keele, S. W. (1989). Timing Functions of The Cerebellum. *Journal of Cognitive Neuroscience*, *1*(2), 136–152. https://doi.org/10.1162/jocn.1989.1.2.136

Jantzen, K. J., Oullier, O., Marshall, M. L., Steinberg, F. L., & Kelso, J. A. S. (2007). A parametric fMRI investigation of context effects in sensorimotor timing and coordination. *Neuropsychologia*, *45*(4), 673–684.

Jantzen, K. J., Steinberg, F. L., & Kelso, J. A. S. (2004). Brain networks underlying human timing behavior are influenced by prior context. *Proceedings of the National Academy of Sciences*, *101*(17), 6815–6820.

Jantzen, K. J., Steinberg, F. L., & Kelso, J. A. S. (2009). Coordination dynamics of large-scale neural circuitry underlying rhythmic sensorimotor behavior. *Journal of Cognitive Neuroscience*, *21*(12), 2420–2433.

Kelso, J. A. S., Fuchs, A., Lancaster, R., Holroyd, T., Cheyne, D., & Weinberg, H. (1998). Dynamic cortical activity in the human brain reveals motor equivalence. *Nature*, *392*(6678), 814–818.

Kocsis, L., Herman, P., & Eke, A. (2006). The modified Beer--Lambert law revisited. *Physics in Medicine \& Biology*, *51*(5), N91.

Lewis, P. A., Wing, A. M., Pope, P. A., Praamstra, P., & Miall, R. C. (2004). Brain activity correlates differentially with increasing temporal complexity of rhythms during initialisation, synchronisation, and continuation phases of paced finger tapping. *Neuropsychologia*, *42*(10), 1301–1312.

Lin, C. C., Barker, J. W., Sparto, P. J., Furman, J. M., & Huppert, T. J. (2017). Functional near-infrared spectroscopy (fNIRS) brain imaging of multi-sensory integration during computerized dynamic posturography in middle-aged and older adults. *Experimental Brain Research*, *0*(0), 0. https://doi.org/10.1007/s00221-017-4893-8

Mathias, B., Zamm, A., Gianferrara, P. G., Ross, B., & Palmer, C. (2020). Rhythm Complexity Modulates Behavioral and Neural Dynamics During Auditory--Motor Synchronization. *Journal of Cognitive Neuroscience*, *32*(10), 1864–1880.

Mayville, J. M., Jantzen, K. J., Fuchs, A., Steinberg, F. L., & Kelso, J. A. S. (2002). Cortical and subcortical networks underlying syncopated and synchronized coordination revealed using fMRI. *Human Brain Mapping*, *17*(4), 214–229.

McPherson, T., Berger, D., Alagapan, S., & Fröhlich, F. (2018). Intrinsic rhythmicity predicts synchronization-continuation entrainment performance. *Scientific Reports*, *8*(1), 1–14.

Merel, J., Botvinick, M., & Wayne, G. (2019). Hierarchical motor control in mammals and machines. *Nature communications*, *10*(1), 1-12.

Meyer-Lindenberg, A., Ziemann, U., Hajak, G., Cohen, L., & Berman, K. F. (2002). Transitions between dynamical states of differing stability in the human brain. *Proceedings of the National Academy of Sciences*, *99*(17), 10948–10953.

Monno, A., Temprado, J.-J., Zanone, P.-G., & Laurent, M. (2002). The interplay of attention and bimanual coordination dynamics. *Acta Psychologica*, *110*(2–3), 187–211.

Nachev, P., Kennard, C., & Husain, M. (2008). Functional role of the supplementary and pre-supplementary motor areas. *Nature Reviews Neuroscience*, *9*(11), 856–869.

Ning, L., & Luo, W. (2017). Specifying turning point in piecewise growth curve models: challenges and solutions. *Frontiers in Applied Mathematics and Statistics*, *3*, 19.

Pabst, A., & Balasubramaniam, R. (2018). Trajectory formation during sensorimotor synchronization and syncopation to auditory and visual metronomes. *Experimental Brain Research*, *236*(11), 2847–2856.

Paek, A. Y., Agashe, H., & Contreras-Vidal, J. L. (2014). Decoding repetitive finger movements with brain activity acquired via non-invasive electroencephalography. *Frontiers in Neuroengineering*, *7*, 3.

Proksch, S., Reeves, M., Spivey, M., & Balasubramaniam, R. (2022). Coordination dynamics of multi-agent interaction in a musical ensemble. *Scientific Reports*, *12*(1), 1–14.

Rahimpour, A., Pollonini, L., Comstock, D., Balasubramaniam, R., & Bortfeld, H. (2020). Tracking differential activation of primary and supplementary motor cortex across timing tasks: An fNIRS validation study. *Journal of Neuroscience Methods*, *341*, 108790.

Repp, B. H. (2005). Sensorimotor synchronization: A review of the tapping literature. In *Psychonomic Bulletin and Review* (Vol. 12, Issue 6, pp. 969–992). https://doi.org/10.3758/BF03206433

Repp, B. H., & Su, Y. H. (2013). Sensorimotor synchronization: A review of recent research (2006-2012). *Psychonomic Bulletin and Review*, *20*(3), 403–452. https://doi.org/10.3758/s13423-012-0371-2

Rose, D., Ott, L., Guérin, S. M., Annett, L. E., Lovatt, P., & Delevoye-Turrell, Y. N. (2021). A general procedure to measure the pacing of body movements timed to music and metronome in younger and older adults. *Scientific reports*, *11*(1), 1-16.

Rousseeuw, P. J., & Croux, C. (1993). Alternatives to the median absolute deviation. *Journal of the American Statistical Association*, *88*(424), 1273–1283.

Sakai, K., Hikosaka, O., Miyauchi, S., Takino, R., Tamada, T., Iwata, N. K., & Nielsen, M. (1999). Neural representation of a rhythm depends on its interval ratio. *Journal of Neuroscience*, *19*(22), 10074–10081.

Santosa, H., Zhai, X., Fishburn, F., & Huppert, T. (2018). *The NIRS Brain AnalyzIR Toolbox*. https://doi.org/10.3390/a11050073

Sergent, J. (1993). Mapping the musician brain. *Human Brain Mapping*, *1*(1), 20–38. https://doi.org/10.1002/hbm.460010104

Serrien, D. J. (2008). *The neural dynamics of timed motor tasks : evidence from a synchronization – continuation paradigm*. *27*(December 2007), 1553–1560. https://doi.org/10.1111/j.1460-9568.2008.06110.x

Smith, E. E., & Jonides, J. (1998). Neuroimaging analyses of human working memory. *Proceedings of the National Academy of Sciences*, *95*(20), 12061–12068.

Thickbroom, G. W., Phillips, B. A., Morris, I., Byrnes, M. L., & Mastaglia, F. L. (1998). Isometric force-related activity in sensorimotor cortex measured with functional MRI. *Experimental Brain Research*, *121*(1), 59–64.

Treisman, M. (1963). Temporal discrimination and the indifference interval: Implications for a model of the" internal clock". *Psychological Monographs: General and Applied*, *77*(13), 1.

Wing, A. M. (2002). *Voluntary Timing and Brain Function : An Information Processing Approach*. *30*, 7–30. https://doi.org/10.1006/brcg.2001.1301

Wing, A. M., & Kristofferson, A. B. (1973). Response delays and the timing of discrete motor responses. *Perception & Psychophysics*, *14*(1), 5–12. https://doi.org/10.3758/BF03198607

Wing, C., Simon, K., & Bello-Gomez, R. A. (2018). Designing difference in difference studies: best practices for public health policy research. *Annual Review of Public Health*, *39*.

Witt, S. T., Laird, A. R., & Meyerand, M. E. (2008). Functional neuroimaging correlates of finger-tapping task variations: an ALE meta-analysis. *Neuroimage*, *42*(1), 343-356.

Chapter 3
Exploring Neurophysiological Markers to Predict Action-Based Timing Performance

Abstract

Research on action-based timing has shed light on the temporal dynamics of behavioral transitions in rhythmic sensorimotor coordination. Here, we investigate the neural mechanisms underlying timing dynamics using a modified experimental paradigm that combines synchronized and syncopated tapping (i.e., distinct coordination dynamics) with auditory pacing and continuation phases. To track motor network engagement during timing-based action, we measured neural responses in twelve healthy volunteers while they performed a synchronized/syncopated finger-tapping task on which they had previous experience. This produced a 2 x 2 alternating design: trials of synchronous and syncopated tapping with pacing to a tone followed by continued tapping without the tone. The accuracy and fluency of participants' tapping was tracked while their neural responses were monitored using electroencephalography (EEG). For data analysis, we used a novel deep learning approach to extract participant-specific, neural features that were predictive of the four distinct behavioral conditions. We then established that these brain-based features correlated with our two measures of performance accuracy.

Our findings demonstrate that specific coordination dynamics in action-based timing behavior can be identified in the corresponding EEG signal at the single trial level, and further can be used to predict the presence and absence of auditory input guiding rhythmic entrainment. Applying deep learning to single trial EEG data predicted the timing phase 20% above chance. Neurophysiological features related to attentional, and motor processes in the central, temporal, and frontal electrode sites contributed most to prediction accuracy. Furthermore, the N1peak latency component of the EEG signal, which is related to attentional processes, was observed at the central parietal electrode site. Importantly, our novel approach to EEG data analysis identified predictive neurophysiological processes in single-trial neural dynamics, demonstrating that deep learning approaches can be used to establish links between action-based behavioral performance and neurophysiological processes.

Keywords: stimulus-locked ERP, response-locked ERP, finger tapping task, synchronization, syncopation, pacing, continuation, correlation, deep learning

Introduction

The human motor system supports motor function and organizes different movement sequences (Rizzolatti & Luppino, 2001). The motor system supports actions with a wide range of complexities, including the number of limbs used, number of trajectories involved, sequence length, and relative timing of movement (Wolpert & Ghahramani, 2000). The ability to accurately and precisely perform time-dependent actions is critical for a variety of skills, such as playing sports or playing a musical instrument. Research has demonstrated that temporal mechanisms in the brain support such behaviors, and there is substantial interest in *how* action-based timing is represented in the central nervous system. In this regard, finger tapping is a reliable and commonly used task for measuring motor performance and evaluating muscle control and motor ability in the upper extremities (Jantzen et al., 2007; Witt et al., 2008). Methodologically, finger tapping allows investigation of the mental timing systems associated with motor actions and feedback mechanisms of varying complexity (Ivry & Keele, 1989; Sergent, 1993; Wing & Kristofferson, 1973). For example, finger tapping has been used to probe the neural representation and maintenance of timing behavior, where *maintenance* refers to the accurate behavioral maintenance of temporal information following the removal of timing cues. Likewise, finger tapping allows for measurement of relative changes in neural responses that reflect changes in coordination dynamics as participants perform different patterns of tapping with systematically varied levels of difficulty (Jantzen et al., 2004; Spencer et al., 1998).

Here we used a modified finger-tapping task that builds on our previous examination of movement timing (Rahimpour et al., 2020) to investigate the process by which individuals entrain to an external periodic stimulus (i.e., a metronome) and then internally maintain that entrainment (i.e., endogenous rhythmic process). We investigated this across two different timing contexts: synchronized (i.e., on-beat) and syncopated (i.e., off-beat) tapping. Increased activity within neural subsystems associated with timing behavior has been postulated to reflect increases in cognitive demand during coordination of complex action patterns. Examples include internal timing (basal ganglia and cerebellum) (Harrington et al., 1998; Ivry & Keele, 1989; Serrien, 2008), motor planning and preparation (supplementary motor area (SMA), and dorsal-premotor cortex) (Mayville et al., 2002), and working memory and attention (prefrontal cortex, and parietal land occipital areas) (Davranche et al., 2011; Nobre, 2001; Smith & Jonides, 1998). Other studies indicate that the brain areas recruited during finger tapping include primary somatosensory-motor cortex (S1/M1), SMA, premotor cortex (PMC), the inferior parietal lobule, basal ganglia, and cerebellum (Nachev et al., 2008; Witt et al., 2008), with different task-specific parameters modulating the particular neural mechanisms that are engaged.

Much progress has been made in identifying neural correlates specific to different forms of sensory-motor synchronization. For example, the similarities and differences in the neural circuits engaged by tapping to a metronomic tone (i.e., the pacing phase) and continuing to tap without the tone (i.e., the continuation phase) have been investigated using the pacing-continuation paradigm (Serrien, 2008). Simple synchronized finger tapping engages the cerebellar-parietal network, while continuation tapping relies engages prefrontal regions due to its load on working memory (Lewis et al., 2004). More

complex sensory-motor synchronization tasks result in greater activation in motor-related areas (pre-SMA, PMC, and cerebellum), as well as stronger coupling to the auditory cortex, such that there is less variability in tap timing when participants are guided by a regular auditory tone akin to a metronome (Comstock et al., 2018; Comstock & Balasubramaniam, 2018). Indeed, the ability to perceive and respond to temporal periodicities (i.e., timing perception) requires tight coupling of the auditory and motor systems (Chen et al., 2008; Ebrahimzadeh et al., 2020; Grahn & Brett, 2007; Hove et al., 2013). Motor regions, such as the sensory-motor cortex (M1/S1) and the SMA, along with the anterior cerebellum, are activated during both pacing and continuation tapping (Witt et al., 2008), while frontal networks play an essential role in mediating coordination in tasks with increased complexity (Jantzen et al., 2007; Mayville et al., 2002).

To examine the interaction between pattern and timing complexity, Jantzen et al. (2004) used functional magnetic resonance imaging (fMRI) to track cortical hemodynamics as participants performing either synchronized or syncopated finger tapping in response to an auditory cue, and then continued their tapping in the absence of that cue. Results revealed that these timing-based behaviors engaged different neural regions depending on the initial pacing context and regardless of its complexity. Our recent findings using functional near-infrared spectroscopy (Rahimpour et al., 2020) likewise indicate that the cortical activity elicited from timing behavior is task-dependent, and that the motor timing network further adapts to the presence or absence of external metronome.

Neural Activation

Tracking neural responsivity to different timing patterns requires a temporally sensitive measure that can provide temporal resolution in the millisecond range. Electroencephalography (EEG) is just such a measure; event-related potentials (ERPs), in particular, measure phase-locked neural activity relative to a stimulus (i.e., auditory tone onset) or response (i.e., finger tap) (Lopez-Calderon & Luck, 2014). When combined with the continuation paradigm, EEG can be used to track patterns of neural engagement during both the pacing and continuation phases of the continuation task while tapping accuracy is also monitored. For example, Peper, Beek, and van Wieringen (1995) found that stimulus-locked ERPs (i.e., ERPs time-locked to the auditory metronome) during the pacing phase of the continuation paradigm were associated with the motoric act of tapping and were phased-locked with tap onsets. In another study, the amplitude of the event-related changes decreased with increases in tapping cycle frequency (Boonstra et al., 2006). Furthermore, Serrien (2008) found greater EEG coherence—a measure of the degree of similarity in activity across electrodes—at central scalp sites during the continuation relative to the pacing phase of the continuation paradigm, as well as higher variability in tapping accuracy. Because activity in these areas (Clark et al., 2001) is associated with working memory functions, Serrien (2008) interpreted the findings as reflecting increased demand on working memory to maintain the temporal representation of the now-absent auditory stimuli during the continuation phase. Engagement of the inferior frontal lobule (supporting auditory-motor coupling) during synchronized pacing, and of the inferior parietal lobule during continuation, was observed by researchers using EEG frequency-based steady-state evoked potentials (SSEP) (De Pretto et al., 2018). Pfurtscheller et al. (2003) found beta-band oscillation in the mid-central area reflecting

inhibition of neural subnetworks during synchronized continuation, and Ross et al. (2022) observed a significant role of mu rhythms in motor inhibition during beat perception.

Only a few studies have investigated neural activity associated with both the coordination dynamics (synchronization and syncopation) using EEG. For example, Mayville et al. (1999) observed topographical changes in neural activity correlated with an automatic switch of dynamic coordination (from synchronized to syncopated tapping). However, Wallenstein et al. (1995) found that this coordination switch most impacted activity at left central electrode sites, and that changes in neural activity increased significantly just prior to this transition. Thus, it seems that the transition from one to the other coordination mode introduces a point of instability in the brain-behavior entrainment pattern due to the change in coordination dynamics.

Finally, examination of how neural activity couples with different behavioral movements is contributing to our understanding of action-based timing perception. For example, Bavassi et al. (2017) observed that asynchrony between the tone and the tap during synchronized tapping (i.e., synchronization error) related to the first peak latency of the principal component analysis (PCA), particularly PC1 and PC2. Smit et al. (2013) likewise found a strong correlation between alpha-band oscillations and the dynamics of tapping behavior, and Nozaradan et al. (2016) reported a link between cortical and behavioral measures of rhythmic movement, finding beat-related SSEP activity associated with both synchronized and syncopated tapping. Researchers have observed high correlations between the kinematics accuracy of repetitive finger tapping and delta band activity, localized in contralateral central area (Paek et al., 2014), consistent with the negative lateralized readiness potential (LRP) that has been observed in contralateral motor cortex to the responding hand (review paper; Kappenman & Luck., 2011). Overall, there is greater neural responsivity during synchronized than syncopated rhythmic tapping (Chemin et al., 2014), higher amplitude of timing oscillations (associated with an increase in rhythmic movement to the metronome) during tapping compared to a listening-only task (Nozaradan et al., 2016), and greater spectral power during synchronized than rhythm hearing in both auditory and motor areas (Mathias et al., 2020).

Current Study

The analytical methods used in the studies reviewed thus far were averaged across trials and did not explore individuals' neurophysiological activity at the single trial level. In particular, the LRP is difficult to extract and is very sensitive to noise, making single-trial analysis difficult (Kappeman & Luck., 2011). Inter-trial phase coherence (ITPC) is also limited to averaging across trials (Van Diepen & Mazaheri, 2018). Because SSEP transfers EEG signal into the frequency domain, the temporal information is lost; this is a critical point as temporal resolution is one of the main advantages of doing EEG studies (Pretto et al., 2018). In a recent study, Nave et al. (2022) conducted trial by trial exploratory logistic regression analyses of a task on rhythm perception but were not able to generalize their approach to other forms of timing behavior. Finally, cluster-based permutation tests depend on a predetermined threshold for cluster size selection and is highly sensitive to estimation parameters, meaning it does not control for false positive rate (Sassenhagen & Draschkow, 2019). Here we apply a novel analytical technique to address these limitations.

The goal of the present study was to use a temporally sensitive measure of neural activation, EEG, to track neural activity during a tapping task whose complexity varied in both pattern and timing. To this end, we collected EEG data from well-trained participants while they completed a continuation task, as employed in our prior study (Rahimpour et al., 2020). The task involved both in-phase (i.e., synchronized) and anti-phase (i.e., syncopated) tapping. Each form of tapping took place across two phases: first relative to an auditory metronome and then continued without the metronome. However, where we blocked trials by tapping pattern in our original study, here we introduced an alternating design (Pabst & Balasubramaniam, 2018) whereby the pattern of tapping alternated trial-by-trial between synchronization and syncopation, with each trial still including both pacing to a tone and continuation without the tone. This change from blocked to alternating trials increased the task difficulty by isolating the specific tapping pattern to a particular trial.

Although few studies have reported a linear relationship between the amplitude of neurophysiological activity and accuracy of task performance, Nozaradan et al. (2016) found that average asynchrony of taps relative to the guiding tone (i.e., synchronization error) strongly correlates with neural entrainment to a beat. For example, Mathias et al (2020) observed that the N1 peak latency negatively correlates with the average divergence between the target and realized tap (i.e., mean tap asynchrony), meaning that as mean asynchrony in a complex timing task decreased, stimulus-locked N1 amplitude became more positive (Mathias et al., 2020). However, the interrelation between behavior and the associated neurophysiological dynamics is not linear (Amirali et al., 2020), even though most analytic approaches in the literature rely on the assumption of linearity when applying correlational approaches to relate behavioral and neurophysiological data. Moreover, because ERP data are inherently noisy, it is difficult to establish functional connections at the single-participant or single-trial level via statistical techniques alone (Amirali et al., 2020). These issues severely limit our capacity to relate specific patterns of neural activity to human behavior. However, these deficiencies may be addressed by employing machine learning techniques.

Thus far, only a small number of studies have used deep learning in cognitive neuroscience research; to our knowledge, none have focused on timing behavior. The current study tests a novel approach to predict behavior state based on neurophysiological activity. We aimed to establish a predictive relationship between neurophysiological features extracted via deep learning from the EEG signal collected while participants performed distinct action-based timing behaviors. Our primary hypothesis was that neural responsivity as measured by EEG would correspond to the dynamic coordination process that manifests across two forms of timing guidance, exogenous (i.e., during pacing) and endogenous (i.e., during continuation), and given two different tapping behaviors (i.e., synchronization and syncopation). To this end data were collected across four tapping conditions: synchronized pacing, synchronized continuation, syncopated pacing, and syncopated continuation.

Materials and Methods

Participants

We recruited fifteen healthy volunteers with self-reported normal hearing to participate in the study. All had participated in a prior study in which they performed the same tapping task used here, meaning each had experience with the task. Data from three participants were excluded from the analyses due to a high number of motion artifacts in their EEG data based on visual inspection. Thus, twelve healthy right-handed adult volunteers (mean age 26, range 20-41 years) successfully participated in the study. None of the participants reported any neurological or skeletomuscular disorder or injury that would prevent them from performing a timing-based tapping task. The Institutional Review Board approved the protocol for research ethics and the protection of human subjects at the University of California, Merced. All participants gave informed written consent after the experimental procedures were explained to them.

Stimuli and Task

Each participant performed the finger-tapping task using the index finger of their dominant (right) hand in response to a 20 ms long, 1kHz metronomic tone repeated every 1000 ms (1 Hz). A one-second-long tone indicated the end of a trial and the start of a 20-second resting state. The task involved two patterns of tapping: 1) taps with each tone (synchronization) and 2) taps between two consecutive tones (syncopation). In order to avoid any neural adaptation to the particular tapping pattern during the performance of the task, we modified the original blocked design introduced by Jantzen and colleagues (2004) to one in which the tapping pattern alternated between synchronized and syncopated tapping from trial to trial (a syncopation trial always follows a synchronization trial and vice versa) for a total of ten trials per timing condition (20 trials overall) (see Figure 17). Regardless of the tapping pattern, within a given trial, tapping was first paced relative to a metronomic tone (15 cycles) and then continued without the tone (12 cycles). Distinct from the designs used in Jantzen et al. (2004) and Rahimpour et al. (2020), participants had experience performing the task in a prior study.

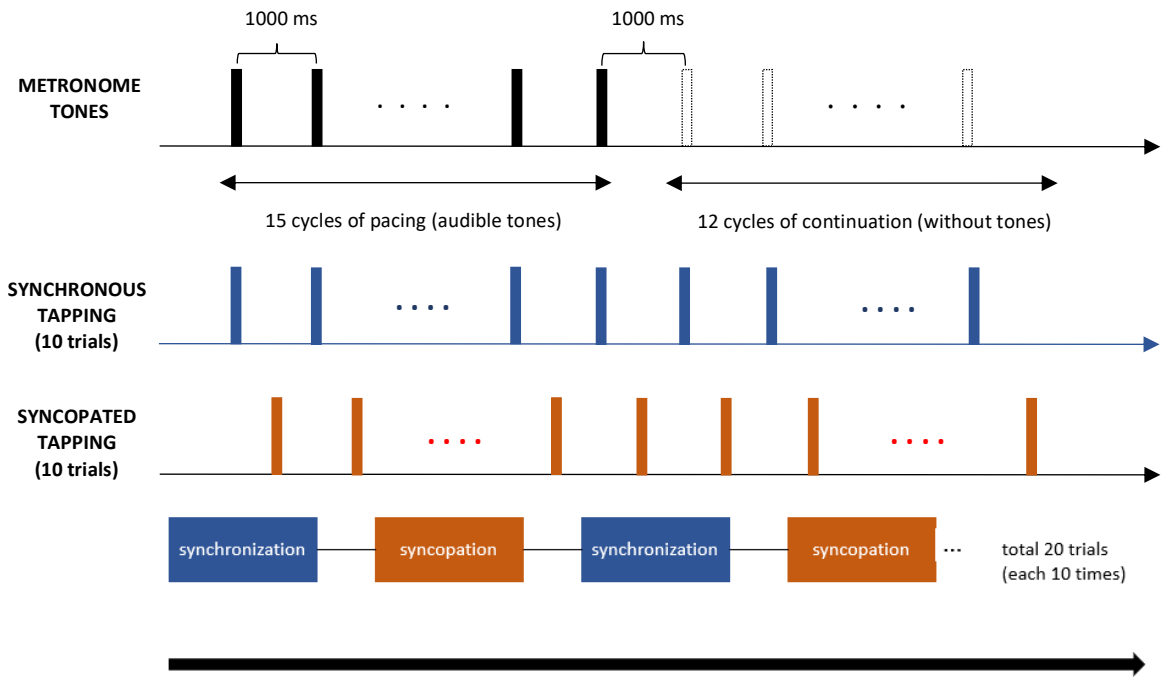

Figure 17. Schematic of the experimental paradigm adapted from Rahimpour et al (2020) to perform repetitive right finger tapping in the presence of the auditory metronome in the alternating study design. Blue and orange colors indicate synchronized and syncopated tapping, respectively.

To track tapping behavior, we used a temporally precise device—a smooth metal plate—that did not interfere with the accuracy of participants' tapping during their performance of the task. Two leads were connected to the plate, one connected to a custom-built electronic input device produced from a MakeyMakey™ kit (Comstock & Balasubramaniam, 2018) and the other held by the participant so that with each tap by the participant on the metal plate, the circuit was completed and delivered to the input device, which then sent a signal to the computer via USB, thus registering the tap (Collective & Shaw, 2012).

For analytical purposes, we used each finger tap on the plate as the mark of the onset of each behavioral response. The device introduced a temporal delay of approximately 25 ms. The delay is due to the time for the internal circuitry in the MakeyMakey™ to process the input, which has a built-in delay for input registration to reduce accidental double inputs (similar to a computer keyboard). The 25 ms delay was determined by a method recommended by the MakeyMakey™ engineers in which a high-speed camera (240 fps) was utilized to simultaneously record the timings of the tap and the corresponding computer registration via a tone output from the computer, a method that computed the delay to be approximately 25ms (+/- 2 ms from the camera frame rate). Thus, we adjusted the time recorded for each response post-hoc. Paradigm software was used to present the instructions and to synchronize the onset of each trial with a trigger sent to the EEG data.

EEG Data Recording

EEG data were continuously recorded with an ANT-Neuro 32 electrode cap with electrodes placed according to the 10–20 International electrode system (Figure 18), assigning Cz as the reference electrode. The data were recorded at a sampling rate of 1024 Hz with electrode impedance below five $k\Omega$ (Kappenman & Luck, 2010). Following acquisition, the EEG data were processed with EEGLAB (Delorme & Makeig, 2004) and ERPLAB (Lopez-Calderon & Luck, 2014).

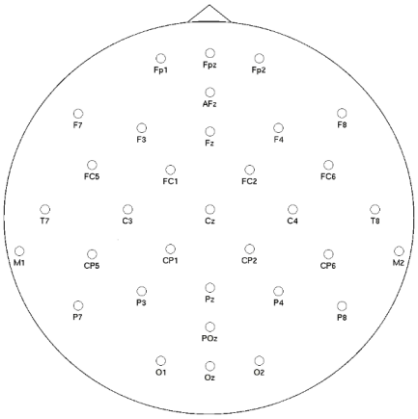

Figure 18. Channel locations according to the 10-20 international electrode system.

Data Analyses

Behavioral Measurement

We established two behavioral measures of performance. The first was accuracy asynchrony, defined as the time difference between the target onset and the participant's actual tap (asynchrony = tap onset − stimulus onset). In this case, the target time was 0 ms (onset of tone) for synchronization and 500 ms for syncopation. The second was inter-response interval (IRI), defined as the time between two consecutive taps.

We used multiple linear regression (MLR) and piecewise growth curve modeling (PGCM) to measure behavioral effects of each timing conditions (independent variables) on the dependent variables (i.e., mean accuracy asynchronies and IRIs recorded for each participant). No participants were categorized as outliers (3 SDs or more from the mean value). We also report Pearson correlation (R^2) (Benesty et al., 2009) to estimate linear similarities between ERPs and behavioral measures.

EEG Data Analysis

Preprocessing:

EEG data were preprocessed by first downsampling to 512 Hz, then applying a Butterworth high-pass filter with a cut-off set at 0.1 Hz, an order of 6, and a filter roll-off of 24 dB/octave. Data were then visually examined for artifacts, and corrupted sections were removed. Bad channels were detected and removed using an automated EEGLAB algorithm that compares channels with their surrounding channels (probability measure with z-score threshold set to 4). Four participants had one channel each removed from their data; the other eight participants had no channels removed from their data. ICA was performed using the Runica algorithm (with infomax rotation) within EEGLAB (Bell & Sejnowski, 1989) for further artifact rejection. Components were visually inspected, and components related to eye-blink and eye-movement artifacts were removed, resulting in an average of 1.2 components (range: 1 to 2 components) removed per participant. After running ICA, the bad channels (four channels total) were interpolated using spherical interpolation, and the data were re-referenced to the average reference. Data were

epoched using ERPLAB in two different ways. To create stimulus-locked ERPs, epochs were time-locked to the auditory stimulus onset. Thus, epochs were time-locked to the auditory stimulus onset, and for response-locked ERPs, epochs were time-locked to the participants' behavioral responses (i.e., taps) after adding 25 ms shift to account for the MakeyMakey device delay. Both stimulus-locked and response-locked ERPs were epoched from -100 to +500 ms relative to the time-locked event (total number of stimulus-locked epochs= 12960; response-locked=10031). After removing linear trends for an entire epoch, baseline correction was performed to the mean voltage between -100ms and the stimulus- or response-onset for each epoch.

Further data cleaning was performed at the epoch level with individual epochs removed (mean: 62; range: 9-147) if voltage exceeded $\pm 100 \mu V$ in any channels for total stimulus-locked and response-locked epochs. Next, we applied a Butterworth low-pass filter with a cut-off at 30 Hz, an order of 4, and a filter roll-off of 24 dB/octave. Finally, we generated each participant's stimulus-locked and response-locked ERPs for each of the four tapping conditions (i.e., synchronization-pacing, synchronization-continuation, syncopation-pacing, and syncopation-continuation). The total epochs included in the stimulus-locked ERP average per participants were 943 ± 46 $(mean \pm SD)$ for synchronized pacing, 912 ± 51 for syncopated pacing, 866 ± 51 for synchronized continuation, and 899 ± 86 for syncopated continuation. Also, the total epochs for response-locked were 741 ± 53, 754 ± 33, 844 ± 76, and 878 ± 29 respectively.

Deep Learning

We employed EEGNet (downloadable from https://github.com/vlawhern/arleegmodels) by using Python software (library: Tensorflow) to establish whether we could predict behavioral timing conditions based on single-trial EEG data. The architecture and procedure are almost identical to a previous study (Vahid et al., 2020) that investigated cognitive control using EEG. To apply EEGNet, we created two-dimensional arrays from single-trial EEG data in which channels (C) and time (T) are represented in columns and rows, respectively. EEGNet architecture is structured in two main stages (see Figure 19 and Table 3):

1. In the first stage of processing, temporal feature maps were generated by employing convolutional filters (width of 64 samples), after which D (a parameter that controls the number of spatial filters and covers all EEG channels) was learned by applying depth-wise convolution for each temporal feature map. Within each temporal map, the model then learned spatial features. After applying temporal and spatial filters, batch normalization followed an exponential linear unit (ELU) activation function. This included average pooling over 4-time steps with stride of 4.
2. In the second stage, a separate convolution was used consisting of depth-wise temporal filters of width 16 followed by a point-wise convolution. The following functions were each applied sequentially: batch normalization, ELU activation function, average pooling over 8-time steps, and dropout. Finally, a classification step finalized the processing using a dense layer with a softmax-activation function.

In the current study, we investigated how well single-trial neurophysiological data at the single-subject level could be used to classify trials into the pacing phase and the

continuation phase and across the two distinct coordination modes (i.e., synchronized and syncopated tapping). To this end, EEGNet was applied as a classifier to decode timing states. For evaluating classification performance, we used the "k-fold cross validation" approach (Refaeilzadeh et al., 2009), which allowed us to divide data into k-subsets and apply the holdout method, which was repeated k-times where each of the k subsets were used as test-sets and the other k-1 subsets were used for training the model. We set k to 10 and trained the model for a total of 7466 epochs and then tested it on 747 epochs in the validation set. The number of temporal and spatial filters (F1,D) were employed as (4,2), and the batch size was set to 32. To train EEGNet, the ADAM optimization was used (Kingma & Ba et al., 2014). Because our datasets were unbalanced due to variable numbers of trials across participants and timing conditions, we applied a class weight that was the inverse of the proportion in the training data, with the majority class set to one. To evaluate the model's performance, here we report the entire confusion matrix and accuracy. To investigate which kinds of features (i.e., single timepoints in single channels) had the highest impact on the classification decision, we used a "saliency map" approach (Simonyan e al., 2013). This made it possible for us to identify which EEG timepoints and electrode sites contributed most to classification accuracy. Saliency map generation required us to take the gradient of the classification score (i.e., before applying the softmax-activation function to the input data). This map showed to what degree the model's output changed when there were small changes in the input data at the single-subject level. For visualization, saliency maps for each trial belonging to a class were averaged and are shown in the results section. In order to standardize the visualization map, we also performed a normalization step in which the averaged saliency map scores were set between 0 and 1. Using this scale, values close to 1 indicated that a particular feature/time point strongly contributed to classification accuracy. To ensure that the model's classification performance in the 2-class (pacing-continuation) problem was significantly above chance for a particular participant, we calculated a threshold indicating classification accuracies significantly above chance level by assuming that the classification error obeys a binomial cumulative distribution (Amirali et al., 2019).

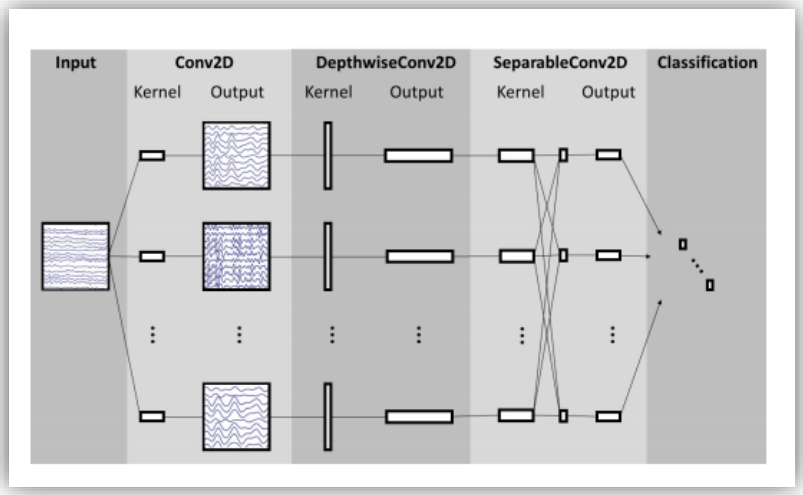

Figure 19. Structure of the EEGNet architecture adopted from Lawhern et al (2018). Lines denote the convolutional kernel connection between inputs and feature maps. Full details about the network architecture can be found in Table 3.

Table 3. Details of EEGNet architecture for single trial EEG classification adapted from Amirali et al (2020)

Block	**Layer Type**	**Filter**	**Size**	**Parameters**	**Output Dimension**	**Activation**	**Mode**
1	Input				(C, T)		
	Reshape				$(1, C, T)$		
	Conv2D	F_1	(1,64)		(F_1, C, T)	Linear	Same
	BatchNorm			$2 * F_1$	$(F_1, 1, T)$		
	DepthwiseConv 2D	$D * F_1$	$(C, 1)$	$C * D * F_1$	$(D * F_1, 1, T)$	Linear	Valid
	BatchNorm			$2 * D * F_1$	$(D * F_1, 1, T)$		
	Activation				$(D * F_1, 1, T)$	ELU	
	AveragePool2D		(1,4)		$(D * F_1, 1, \frac{T}{4})$		
	Dropout				$(D * F_1, 1, \frac{T}{4})$		
2	SeparableConv 2D	F_2	(1,16)	$16 * D * F_1 + F_2 * (D + F_1)$	$(F_2, 1, \frac{T}{4})$	Linear	Same
	BatchNorm			$2 * F_2$	$(F_2, 1, \frac{T}{4})$		
	Activation				$(F_2, 1, \frac{T}{4})$	ELU	
	AveragePool2D		(1,8)		$(F_2, 1, \frac{T}{32})$		
	Dropout				$(F_2, 1, \frac{T}{32})$		
	Flatten				$(F_2, 1, \frac{T}{32})$		
	Dense	$2 * F_2 * \frac{T}{32}$			N	Softmax	

Abbreviation: C, number of channels. T, number of timepoints. F, number of temporal filters. D, number of spatial filters. N, number of classes

Statistical Analyses of Behavior-Brain Relations

The relationship between extracted single-trial features generated via the deep learning method and participants' behavioral accuracy measures were estimated using MLR analysis (Using Python software; Libraries Scipy and StatsModels). Based on our findings of deep learning classification and brain state prediction, we used Pearson's correlation (FDR comparison corrected) to investigate the relationship between extracted features of single-trial stimulus-locked and response-locked ERPs and corresponding behavioral indices (i.e., mean asynchrony and IRI).

Results

Behavioral results

We first calculated the mean asynchronies and IRIs for the four timing conditions: (i) synchronized pacing, (ii) synchronized continuation, (iii) syncopated pacing, and (iv) syncopated continuation. We then used MLR to estimate a regression model and find the contrast effect between timing conditions post-hoc. Moreover, PGCM approach is calculated to estimate and interpolate the temporal trend of timing conditions on each dependent variable (i.e., mean asynchrony and IRI, separately).

Mean Accuracy Asynchrony

Our estimated MLR model was calculated to predict mean accuracy asynchrony based on two factors: phase (pacing, continuation) and coordination mode (synchronization, syncopation). A significant main effect of entire model on the mean synchrony index was found ($F_{1,11} = 118.1, P < 0.02$), with an R^2 of 0.48 in our estimated regression model. There was a main effect of phase on mean accuracy asynchrony ($F_{1,11} = 212.23, P < 0.01, \eta 2 = 0.47$), with a 41.12 ms average increase in accuracy asynchrony during continuation compared to pacing. However, the average change in mean accuracy asynchrony for syncopation compared to synchronization was not significant. Thus, the phase variable significantly impacted mean accuracy asynchrony.

For synchronized and syncopated pacing and continuation, the mean accuracy asynchronies were -43.7 ± 13.3 (ms)(mean $\pm$ SD), -50.3 ± 116.8 (ms), 12.2 ± 208.3 (ms), and -8.3 ± 206.5 (ms), respectively, as illustrated in Figure 20A. The results revealed that tapping during the continuation phase was more accurate but less stable relative to tapping during the pacing phase. We also observed negative mean accuracy asynchrony (NMAA) in the syncopated continuation condition, as well as for both synchronized and syncopated pacing conditions. NMAA describes an averaged accuracy asynchrony that is negative, meaning a participant demonstrates anticipatory timing behavior (rather than reactive tapping). This was only observed in the more complex tapping conditions. In untrained participants, performance in the pacing phase is often less accurate than what we observed in this study. Thus, our results appear to reflect faster rhythmic entrainment in these participants, each of whom had prior experience with the task. Nonetheless, significant differences in mean accuracy asynchrony were observed between pacing and continuation phases for both synchronized ($F_{1,11} =$

$11.54, P < 0.001, \eta 2 = 0.43$) and syncopated ($F_{1,11} = 8.36, P < 0.001, \eta 2 = 0.35$) tapping. Specifically, we found a significant contrast effect between pacing and continuation phases averaged across coordination modes ($F_{1,24} = 14.56, P < 0.01, \eta 2 = 0.25$).

As great be seen in Figure 20B, the average accuracy asynchrony during the continuation phase was greater than during pacing for both coordination modes. This is consistent with our previous findings (Rahimpour et al., under review) that behavioral performance based on endogenous cues is less accurate than that based on exogenous cues.

We used PGCM to estimate the fitted model for trial cycles for both pacing and continuation tapping, as shown in Figure 20C. The top plot in this figure shows the temporal trends for the averaged tapping cycles corresponding to the two coordination modes. The two modes follow each other closely across the first 10 seconds, at which point the trend towards synchronization across time reveals more variation than syncopation (during timepoints 10-17 s); subsequent to that, the time series for synchronization stabilizes (during timepoints 17-27 s), albeit to a pattern closer to that seen during syncopation. This means that although behavioral accuracy of syncopation is less accurate overall, it is stably so. The bottom plot shows the second derivative of the trends specifying the turning point estimated by our interpolated model. As can be seen, the estimated turning point for both synchronized and syncopated tapping occurs at 10 seconds (5 seconds before the phase transition timepoint) and at 25 seconds (10 seconds after phase transition). This effect is consistent with our previous finding reported in Chapter 2.

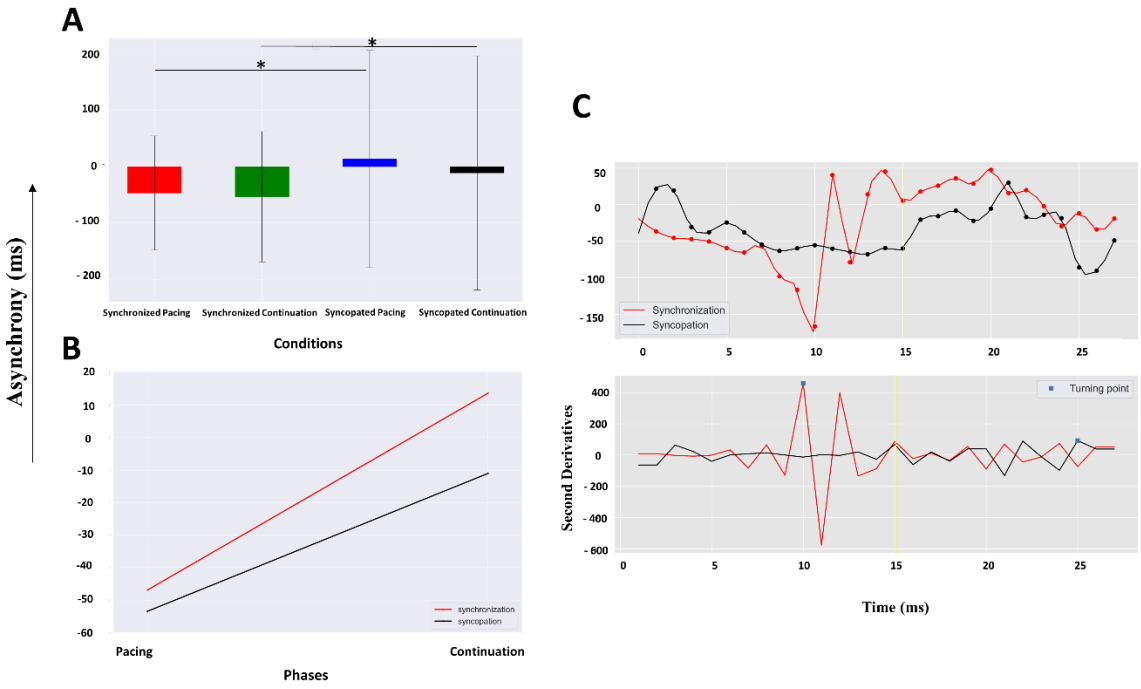

Figure 20. (A) Mean accuracy asynchronies for each timing condition. Error bars show standard deviation (SD). Solid brackets indicate statistically significant comparisons between timing conditions. (B) Values of mean accuracy asynchrony from each timing condition: synchronization (red); syncopation (black); Error bar indicates standard error (SE). (C- Top) Estimated accuracy asynchrony trend during maintenance (pacing followed by continuation). (C-Bottom) Second derivatives of the corresponding trends locating the turning points (blue square marks) in: synchronization (red line); syncopation (black line); Gold vertical solid line represents continuation phase onset.

Behavioral IRI

We estimated the MLR model's ability to predict IRI based on coordination mode and phase. A significant effect of each of the independent variables on the mean accuracy asynchrony index was found ($F_{1,11} = 86.1, P < 0.05$), with an R^2 of 0.23 in our estimated regression model. Moreover, there was a marginally significant main effect of phase on IRI ($F_{1,11} = 102.3, P = 0.05, \eta 2 = 0.27$).

As shown in Figure 21A, the average performance of trained participants was very consistent for all timing conditions, where IRI represents how evenly spaced taps are consistent. However, the stability of performance decreases as the timing complexity increases. For synchronized and syncopated pacing and continuation, the IRIs were 997.1 ± 43.2 (ms)(mean $\pm$ SD), 998.4 ± 45.8 (ms), 1000.8 ± 62.9 (ms), and 1016.3 ± 71.1 (ms), respectively. The only significant difference we observed was between the syncopated pacing and the syncopated continuation ($F_{1,11} = 6.43, P < 0.05, \eta 2 = 0.23$) conditions. As can be seen in Figure 21B, the IRI index in the

syncopated continuation condition was higher than in other conditions (consistent with Rahimpour et al.'s 2020 finding). Finally, we found an interaction between phase and coordination mode ($F_{3,11} = 9.41, P = 0.04, \eta 2 = 0.28$), which is also consistent with our previous findings (Rahimpour et al., 2020).

We used PGCM to estimate the fitted model of averaged pacing and continuation tapping trial cycles, as shown in Figures 21C. The top plot in this figure shows the temporal trends for the averaged tapping cycles corresponding to the two coordination modes. The trend for synchronization over time was consistent and close to an ideal IRI value (i.e., 1000 ms); however, abrupt changes were observed in the 10-17 second time range, particularly before the continuation onset time point. Similar to mean accuracy asynchrony, the temporal trends for the two coordination modes follow each other very closely at the beginning and at the end of the cycles. The bottom plot shows the second derivative of the trends, which specifies the turning point estimated by our interpolated model. As can be seen, the estimated turning point for synchronized and syncopated tapping occurred at 11 seconds (4 seconds before the phase transition time point) and at 12 seconds (3 seconds after phase transition). These observations are consistent with the findings (from the fNIRS alternating study) reported in chapter 2.

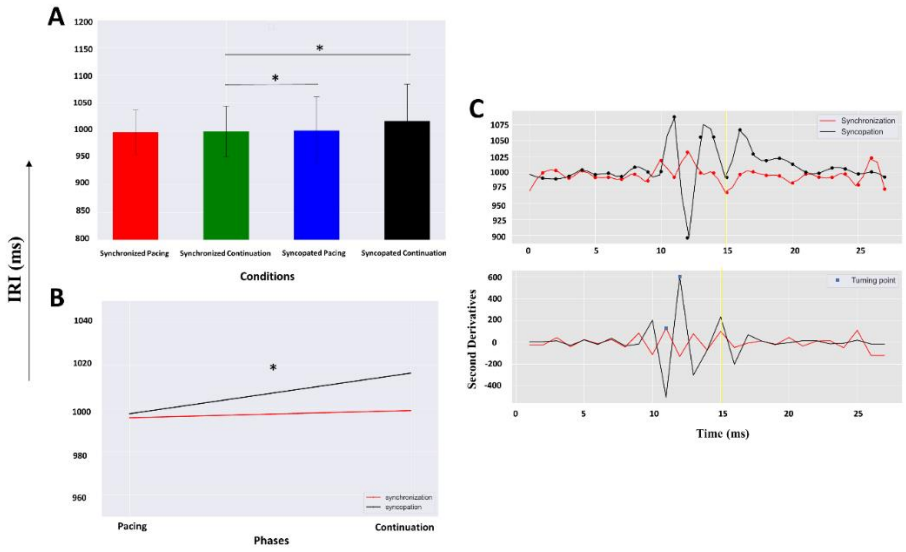

Figure 21. (A) IRIs of each timing condition (i.e., synchronized pacing, synchronized continuation, syncopated pacing, and syncopated continuation). Error bars show standard deviation (SD). Solid brackets indicate statistically significant comparisons between timing conditions. (B) IRI values from each timing condition: synchronization (red); syncopation (black); Error bar indicates standard error (SE). (C- Top) Estimated IRI trend during maintenance (pacing followed by continuation). (C-Bottom) Second derivatives of the corresponding trends locating the turning points (blue square marks) in: synchronization (red line); syncopation (black line); Gold vertical solid line represents continuation phase onset.

Neural results

As described in the Materials and Methods section, we measured stimulus-locked and response-locked ERPs for all timing conditions. In this study, we first aimed to use deep learning to extract neurophysiological features that predicted brain states. Because the significant contrasts of behavioral accuracy (i.e., mean accuracy asynchrony and IRI) were only observed for two timing phases and not for the two coordination modes, we aimed to classify pacing and continuation phases for each coordination mode (synchronization and syncopation). Finally, we estimated an MLR model using Pearson's r approach to establish the correlation between the extracted neurophysiological and behavioral indexes (i.e., mean asynchrony and IRI).

Feature Extraction and Classification

As described in the Materials and Methods section in this chapter, we used deep learning to investigate whether classification emerged within electrodes for stimulus- and response-locked ERPs. Deep learning predicts the presence of neurobiological markers to classify behavioral phases. Since the behavioral data revealed the performance differences modulated with pacing-continuation behavioral phases, this factor was considered in the deep learning step. Therefore, the study focused on the 2-class problem of pacing-continuation within two coordination dynamics—synchronization and syncopation—to train the deep learning architecture (EEGNet) on a training dataset. The trained model was then applied to the test/validation dataset in order to see how well it identified the two different timing conditions for each coordination mode. That is, for evaluating classification performance, we used the "10-fold cross validation" approach (see Materials and Methods for more details). We examined (4,2) features option. The chance level of our 2-class problem would be 50% classification accuracy. We thus calculated a threshold that indicated classification accuracies significantly above chance by assuming the classification error conformed to a binomial cumulative distribution.

Pacing-Continuation Classification

Synchronization Coordination Mode. The average accuracy of trial class prediction given stimulus-locked, single-trial EEG data was 70% (SD=28%), which was 20% (SD=17.2%) higher than the individual chance level ($t(11) = 16.3$; $p = 0.02$). The confusion matrix for the 2-class problem is shown in Figure 22A. Rows show real ("true") labels, while the columns show the classification labels, which were generated by the model on the basis of the single trial EEG data. The average prediction accuracy of 70% can be seen in the confusion matrix (see diagonal from top left to bottom right of the confusion matrix). Thus, performance was not only above chance, but correct predictions outnumbered incorrect predictions. In particular, synchronized continuation trials were incorrectly classified as synchronized pacing for only 26% of the cases. In contrast, synchronized continuation trials were correctly classified as such in 74% of cases. Generally, the confusion matrix shows that the deep learning approach employed here is able to classify trial class (experimental timing phase) based on single trial data.

Figure 22B presents separate visualization ("saliency") maps for each of the two classes of pacing and continuation. As can be seen in Figure 22B, the FC1 electrode strongly contributed to classification accuracy in the time window from 110 to 180 ms. Moreover, we observed contribution to classification for C4 and T8 in the time range from 110-140 and 190-260 ms, as well as for T7, C3, and Cz in the time range from 190 to 260 ms. Importantly, this was the case for both classes of pacing and continuation trials. The ERP plots showing activity at these electrodes can be seen in Figure 23. The identified time window overlaps with the auditory N1 and P2 peak latency component, which reflects auditory stimulus. Therefore, it appears that auditory attention contributes to the predictive power of stimulus-locked single trials from the synchronized form of the experiment. However, we did not observe meaningful classification of response-locked single trials of synchronization mode.

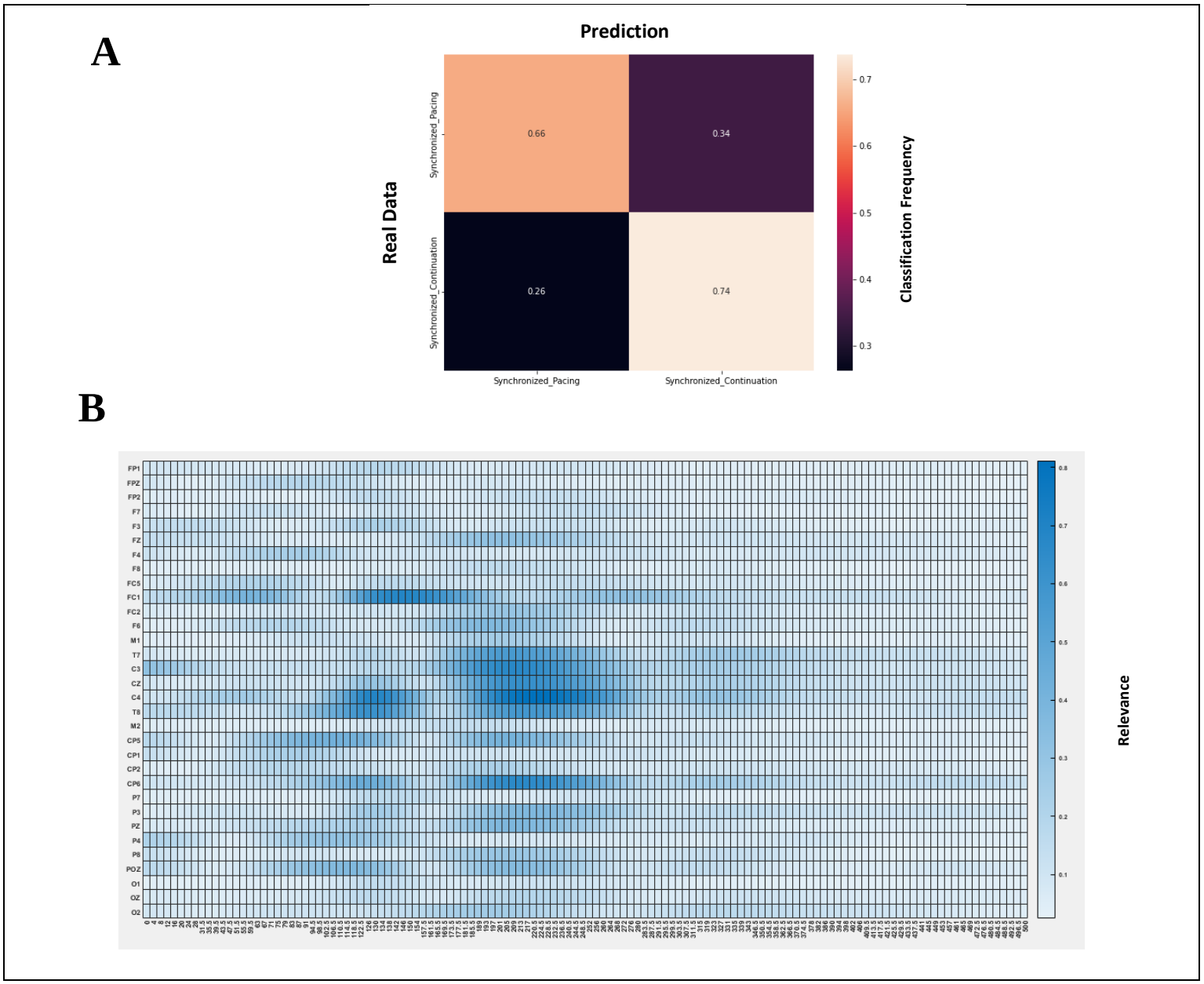

Figure 22. A) Confusion matrix showing the classification results for the stimulus-locked trials of the pacing (the same as continuation) in synchronization mode. Color shadings and number in the matrix denote the frequency at which the read data "true" label was classified into one of the two possible predicted classes. B) Visualization maps showing the relevance of all timepoints and electrodes for classification of two classes of pacing and continuation stimulus-locked trials in synchronization mode. Values close to 1 indicate that the specific feature at the specific timepoints contributes most to classification accuracy. The x-axis denotes the time in ms after auditory stimulus presentation. The y-axis indicates the different electrode sites.

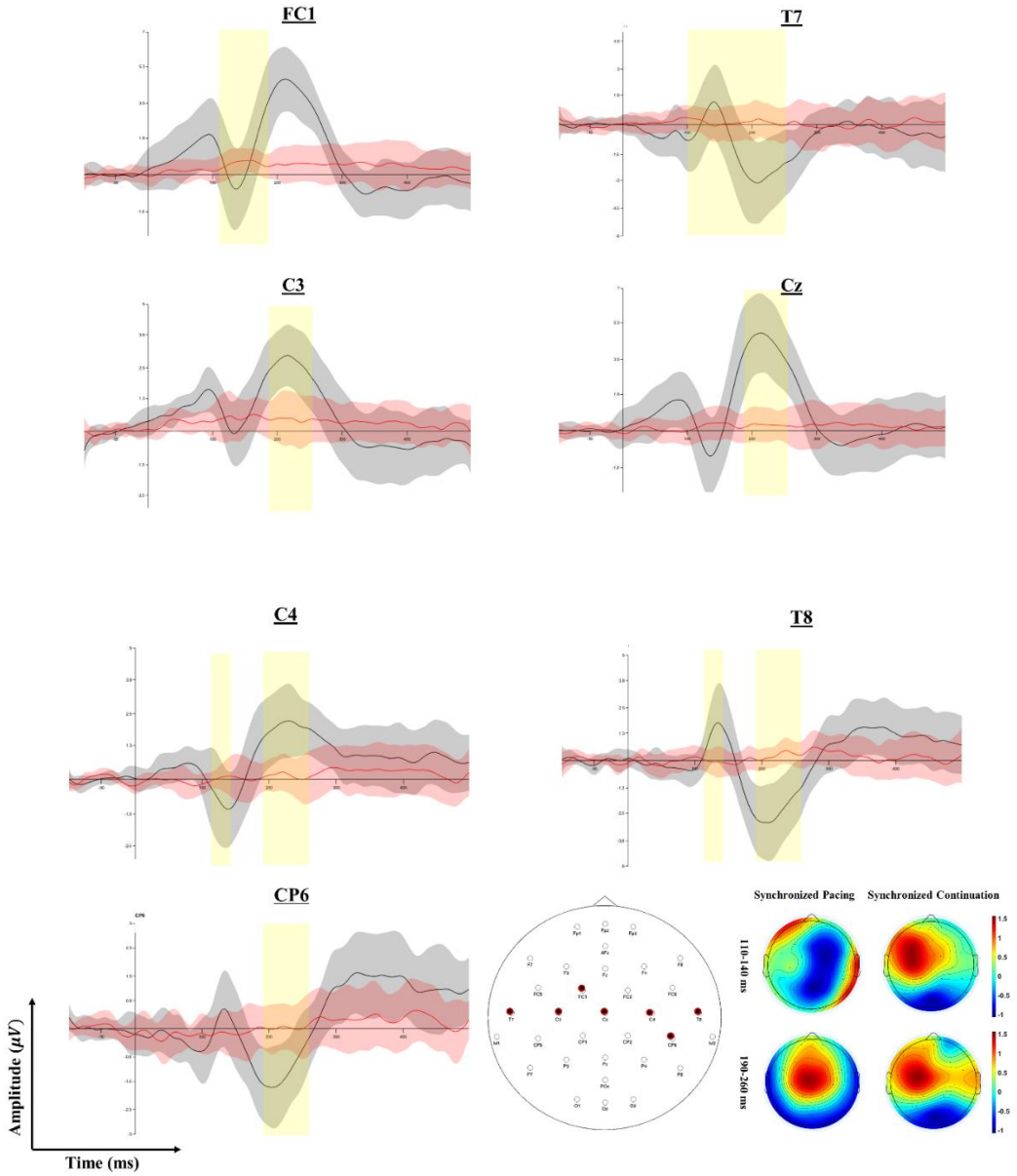

Figure 23. Stimulus-locked ERPs at the electrode sites contributing most to classification accuracy (for pacing vs. continuation) during synchronized tapping in the deep learning model. The x-axis indicates ms after auditory stimulus-locked presentation. The black and red curves indicate the averaged ERP values for pacing and continuation phases, respectively. The shading indicates the SE across the time. The y-axis indicates the voltage in μV (note that the scaling of the y-axis differs between the plots). The yellow shading shows the time interval that was found to contribute strongly to classification performance in the deep learning network. The scalp maps in bottom right side indicate the amplitude of electrode sites in extracted N1 peak latency (time range: 110-140 ms) and P2 peak latency (190-260 ms).

Syncopation Coordination Mode.

1) Stimulus-locked ERPs. The average accuracy of trial-level classification on the basis of the stimulus-locked single-trial EEG data was 70% (SD=26%) and thus 20% (SD=19.2%) higher than the individual chance level (t (11) =15.3; p=0.02). The confusion matrix for the 2-class (pacing -continuation) problem is shown in Figure 24A. Rows show real ("true") labels and columns show classification labels as predicted on the basis of the single trial EEG data. As can be seen in the confusion matrix, the average prediction accuracy was 70% (see diagonal from top left to bottom right in the confusion matrix). This was above chance and substantially larger than the percent of incorrect predictions. For example, syncopated continuation trials were only incorrectly classified as syncopated pacing in 25% of cases, meaning syncopated continuation trials were correctly classified as such in 75% of cases.

Figure 24B presents separate visualization ("saliency") maps for each of these two classes of pacing and continuation. As can be seen in Figure 24.B, C3, C4, T8, and CP6 electrodes strongly contributed to classification accuracy of timing phase in the time window from 115 to 135 and 190-250 ms. Electrode Pz also contributed to the classification accuracy in the time window 190 to 250 ms. Crucially, this was the case for both classes of pacing and continuation trials. The ERP plots showing activity at these electrodes are given in Figure 25. The identified time window overlaps with the auditory N1 and P2 ERP peak latency components, which reflects auditory processes. Therefore, auditory attention appears to be predictive of which phase of tapping a person is in given syncopated coordination mode.

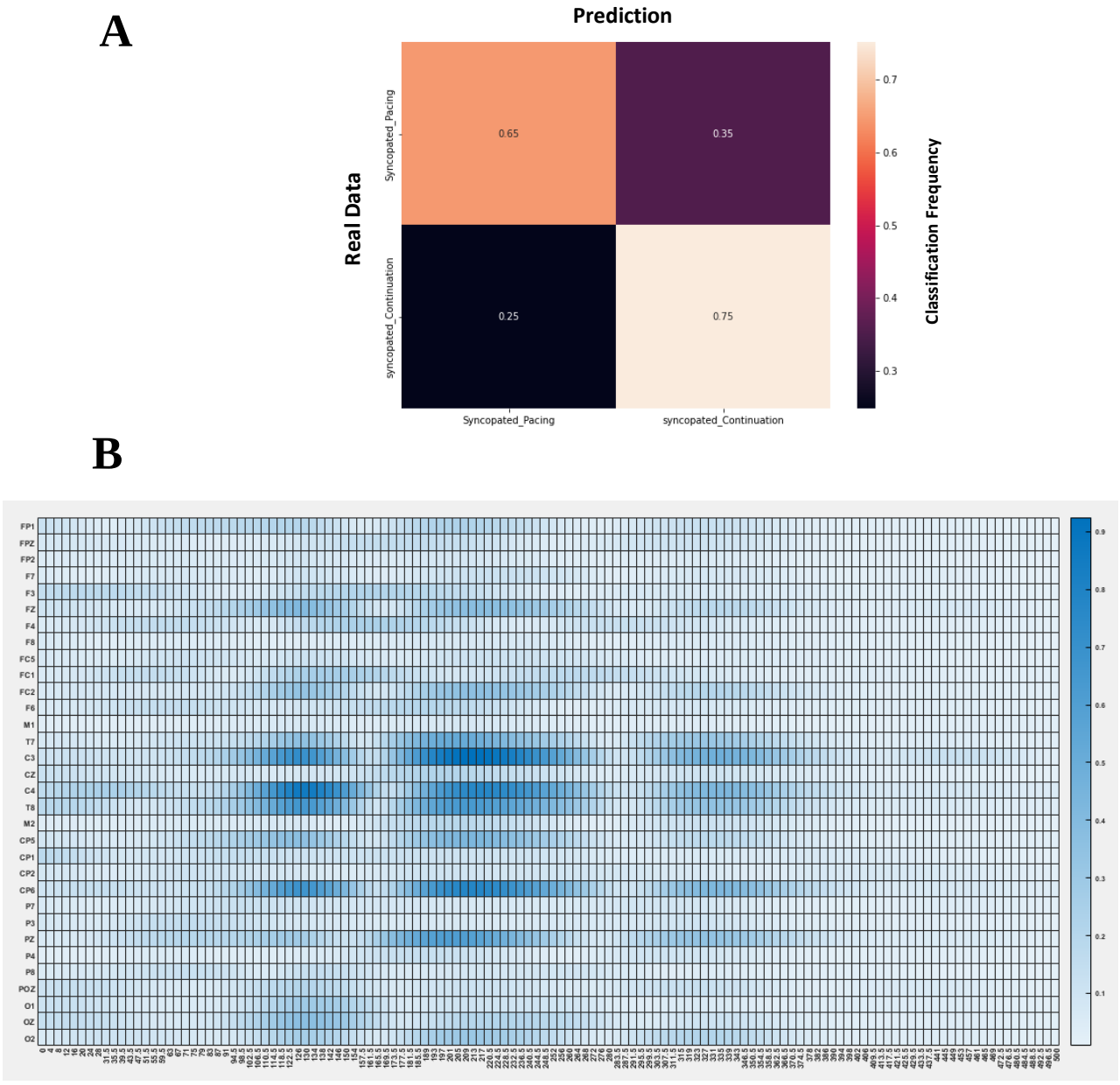

Figure 24. A) Confusion matrix showing the classification results for the pacing in the syncopation coordination mode. Color shadings and number in the matrix denote the frequency at which the read data "true" label was classified into one of the two possible predicted classes. B) Visualization maps showing the relevance of all timepoints and electrodes for classification between two classes of pacing trials and continuation stimulus-locked trials in syncopation mode. Values close to 1 indicate that the specific feature at the specific timepoints contributes most to classification accuracy. The x-axis denotes the time in ms after auditory stimulus presentation. The y-axis indicates the different electrode sites.

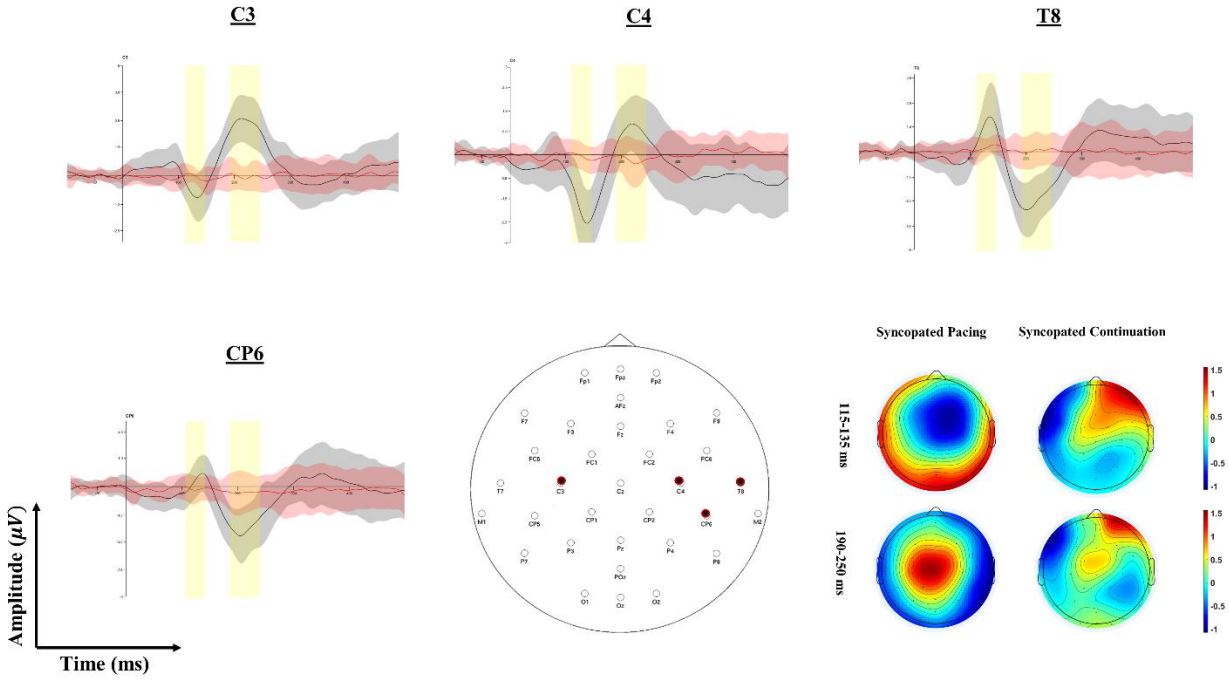

Figure 25. Stimulus-locked ERPs at the electrode sites contributing most to classification (pacing-continuation phases) accuracy of syncopation mode in the deep learning model. The x-axis the time in ms after auditory stimulus-locked presentation. The black and red curves indicate the averaged ERP values of pacing and continuation phases, respectively. The shading indicates the SE across the time. The y-axis indicates the voltage in μV (note that the scaling of the y-axis differs between the plots). The yellow shading shows the time interval that was found to contribute strongly to classification performance in the deep learning network. The scalp maps in bottom right side indicate the amplitude of electrode sites in extracted N1 (time range: 115-135 ms) and P2 peak latency component (190-260 ms).

2) Response-locked ERPs. The average accuracy of trial level classification prediction on the basis of the response-locked single-trial EEG data was 66% (SD=29.5%) and thus 16% (SD=23.2%) higher than the individual chance level (t (11) =18.7; p=0.046). The confusion matrix for the 2-class (pacing-continuation) problem is shown in Figure 26A. Rows show real ("true") label, the columns show the classification label, which was predicted on the basis of the single trial EEG data. As can be seen in the confusion matrix, the average prediction accuracy was 66% (see diagonal from top left to bottom right in the confusion matrix). Syncopated pacing trials were only incorrectly classified as syncopated continuation in 28% of cases. In contrast, syncopated pacing trials were correctly classified as such in 72% of cases. Generally, the confusion matrix shows that the deep learning approach employed here was able to classify trial class (i.e., phases) on the basis of single trial data.

Figure 26B presents separate visualization (“saliency”) maps for each of these two classes of pacing and continuation. As can be seen in Figure 27B, the strong contribution for classification accuracy can be observed in the following electrodes and time ranges: Fz: 80-130 ms; FC1: 60-100 ms; C3: 110-140 ms, 200-270 ms; C4: 90-140 ms, 200-250 ms; T8:100-130 ms, 210-250 ms; CP5:0-20 ms, 80-120 ms, 200-220 ms; CP6: 115-145 ms; 220-280 ms; Pz: 50-100 ms, 180-220 ms. Crucially, this was the case for both classes of pacing and continuation trials. The ERP plots showing activity at these electrodes are given in Figure 27. The identified time window overlaps with specified time range of motor components, which is known to reflect motor Processes. Therefore, motor response processes are predictive of response-locked timing phases in syncopation mode.

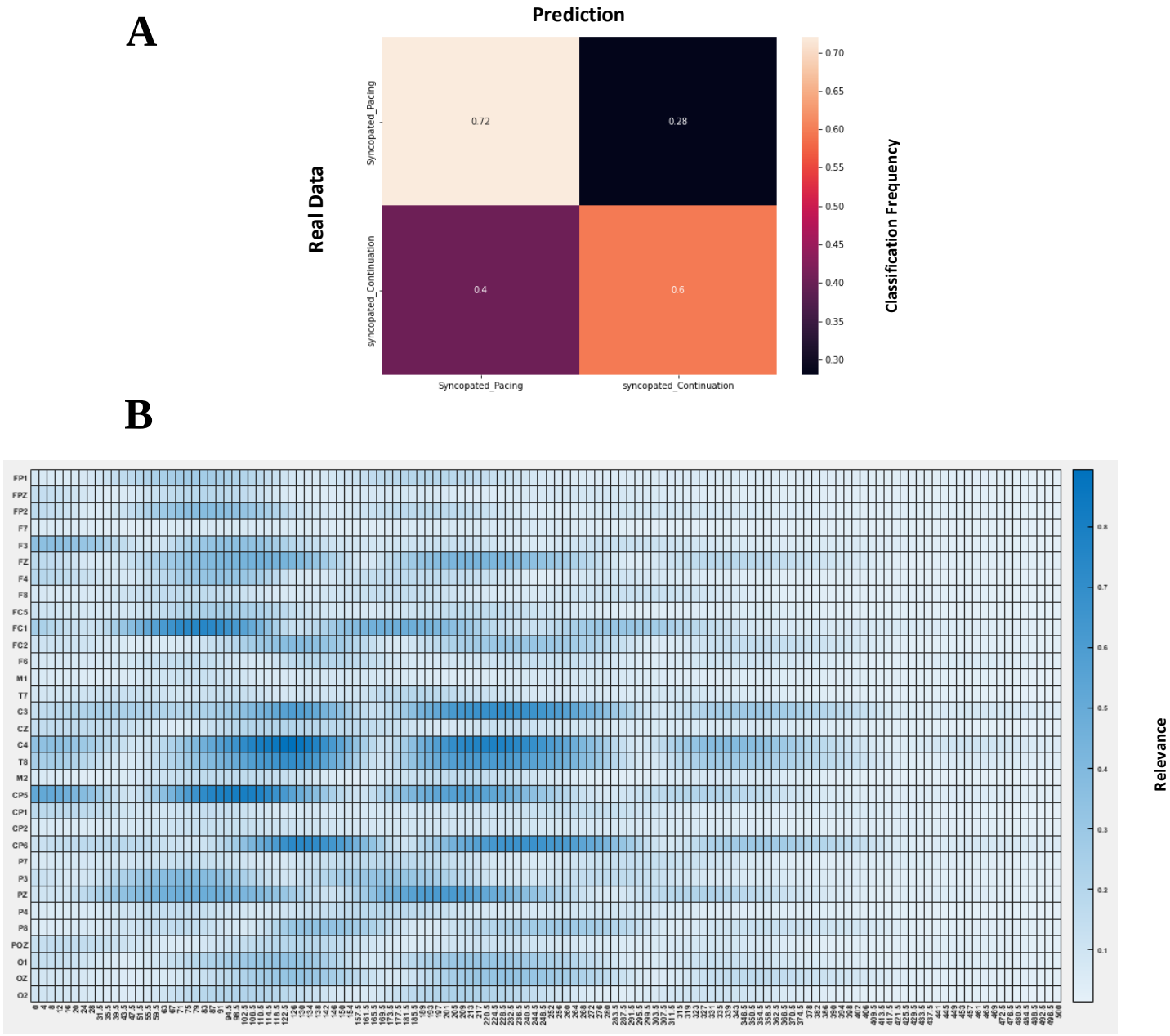

Figure 26. A) Confusion matrix showing the classification results for the response-locked trials of the pacing and continuation in syncopation mode. Color shadings and number in the matrix denote the frequency at which the read data "true" label was classified into one of the two possible predicted classes. B) Visualization maps showing the relevance of all timepoints and electrodes for classification between two classes of pacing trials and continuation tapping response-locked trials in syncopation mode. Values close to 1 indicate that the specific feature at the specific timepoints contributes most to classification accuracy. The x-axis denotes the time in ms after tapping response presentation. The y-axis indicates the different electrode sites

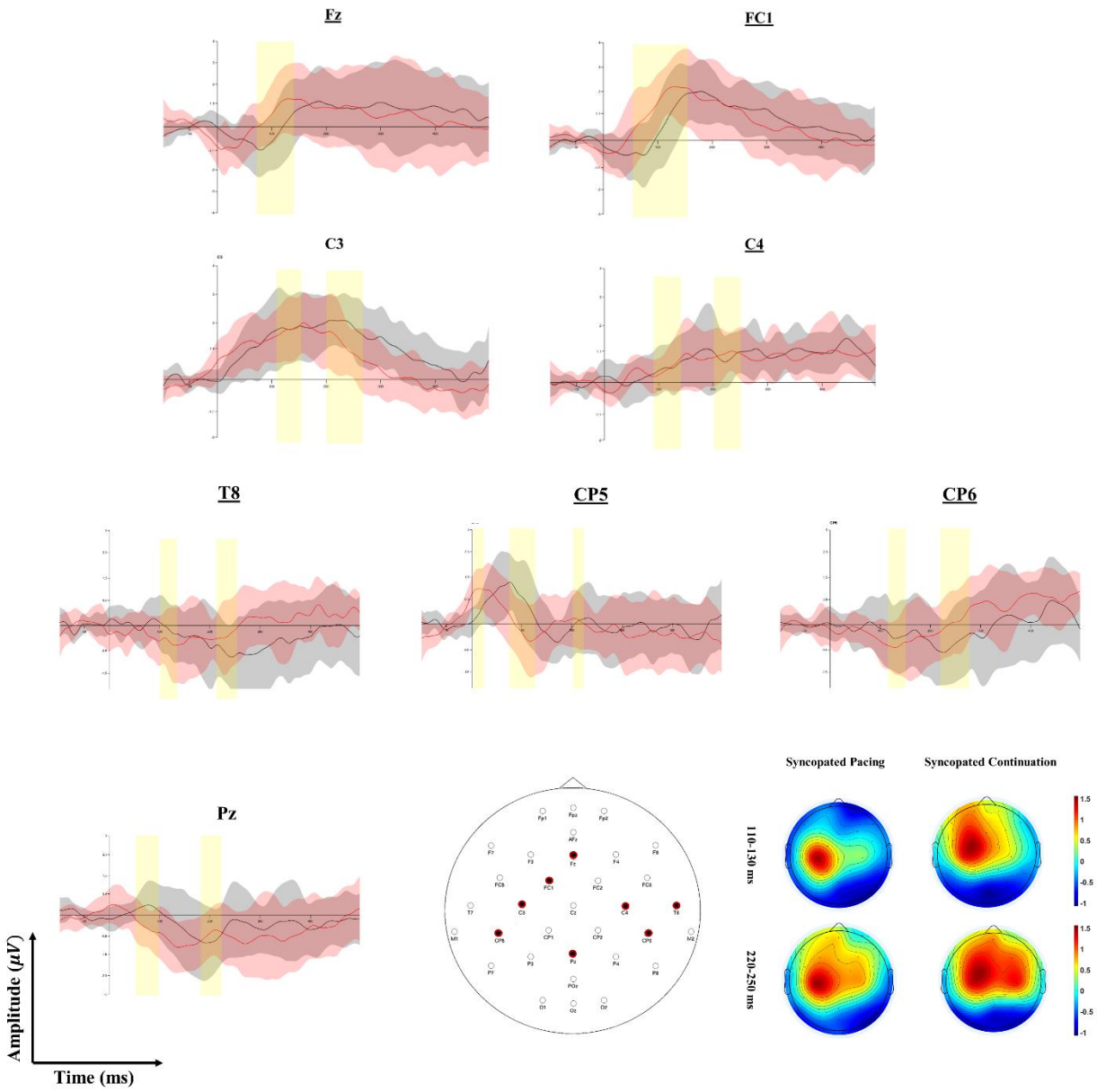

Figure 27. Response-locked ERPs at the electrode sites contributing most to classification accuracy (syncopated-pacing and syncopated continuation) in the deep learning model. The x-axis the time in ms after auditory tapping response-locked presentation. The black and red curves indicate the averaged ERP values of pacing and continuation phases, respectively. The shading indicates the SE across the time. The y-axis indicates the voltage in μV (note that the scaling of the y-axis differs between the plots. The yellow shading shows the time interval that was found to contribute strongly to classification performance in the deep learning network. The scalp maps in bottom right side indicate the amplitude of electrode sites in extracted motor components (time range: 110-130 ms and 220-250 ms).

It should be noted that the classification accuracy between synchronized and syncopated pacing was not above the change level (for stimulus locked single trial ERPs: %55; response-locked: 60%), also between synchronized continuation and syncopated continuation were not acceptable (for stimulus locked single trial ERPs: 52%; response-locked: 61%)

Relations Between Single Trial ERPs and Behavioral Measures

Based on the findings of single trial ERP classification, we predicted that individual differences in extracted cortical features (contributed auditory and motor components) would correlate with behavioral indices. Thus, separate MLR analyses were conducted to examine the relationship between individual differences in extracted single trial features and our behavioral accuracy measures (i.e., mean accuracy asynchrony and IRI). The behavioral mean accuracy asynchrony and IRI were the dependent variables in the regression model (N=12). The independent variables in the model are the extracted single-trial amplitudes in each electrode sites that contributed to the classification. We explored all possible correlations and plotted the ones that the relationship is statistically significant.

Mean Accuracy Asynchrony. The MLR analysis yielded a model with $r = 0.62, F\ (1,11) = 6.33, P = 0.03$ with the average stimulus-locked ERP emerging as the only significant unique predictor of mean accuracy asynchrony performance in the synchronization coordination mode averaging across phases. A scatterplot showing the negative correlation between the extracted auditory-locked ERP amplitude (included N1 peak latency: 180-220 ms) and mean accuracy asynchrony is shown in Figure 28. In support of our general hypothesis about the predictive power of single-trial ERPs, stronger neural activity in CP6 electrode site relates to lower mean accuracy asynchrony in the synchronized pacing condition.

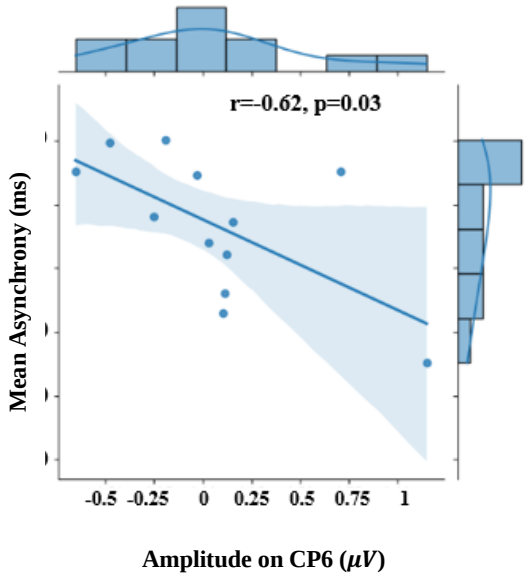

Figure 28. Scatterplots showing individual indices of extracted auditory locked single-trial neural features corresponding to mean accuracy asynchrony in the synchronized pacing condition. The plot illustrates that behavioral accuracy improves with increasing strength of amplitude of selective neural features in CP6.

We also found a correlation between the average response-locked ERP emerging as the predictor of mean accuracy asynchrony ($r = 0.62, F\ (1,11) = 5.2, P = 0.03$) in the syncopation mode. A scatterplot showing the positive correlation between the extracted tapping-locked ERP amplitude in FC1 electrode site extracted from deep learning method and mean accuracy asynchrony is shown in Figure 29. The greater neural activity at the FC1 electrode site relates to lower mean accuracy asynchrony in the syncopated pacing condition.

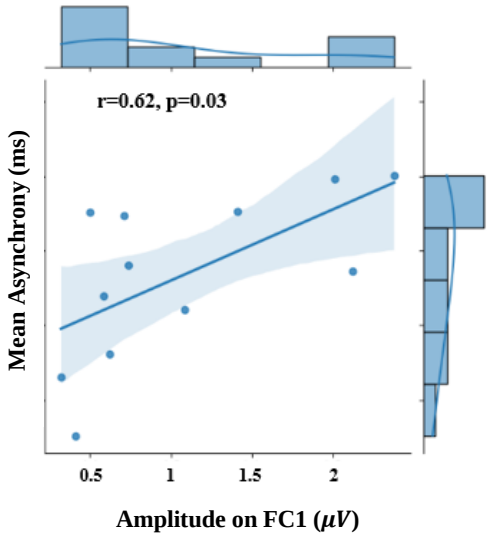

Figure 29. Scatterplots showing individual indices of extracted response tapping locked single-trial neural features corresponding to mean accuracy asynchrony in syncopated pacing condition. The plot illustrates that behavioral accuracy improves with increasing strength of amplitude of selective neural features in FC1.

In addition, a correlation was observed between averaged extracted single trial response-locked ERP emerging as the predictor of mean asynchrony ($r = 0.65, F\ (1,11) = 6.77, P = 0.02$) in syncopated continuation condition. A scatterplot showing the negative correlation between the extracted tapping-locked ERP amplitude at the Pz electrode site extracted from our deep learning model and mean accuracy asynchrony is shown in Figure 30. Thus, stronger neural activity at the Pz electrode site related to higher mean accuracy asynchrony in the syncopated continuation condition.

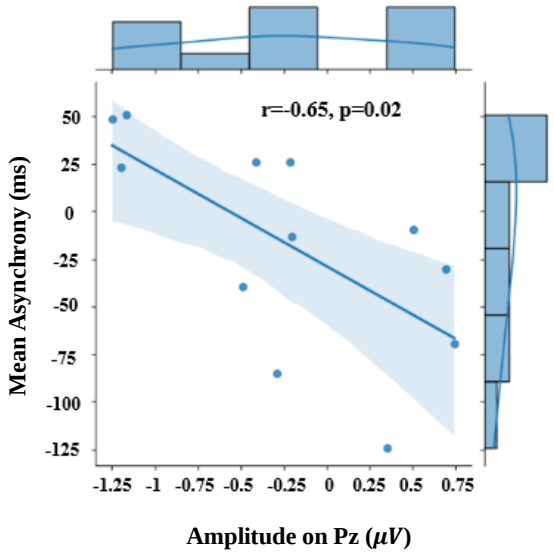

Figure 30. Scatterplots showing individual indices of extracted response tapping locked single-trial neural features corresponding to mean accuracy asynchrony in the syncopated continuation condition. The plot illustrates that behavioral accuracy improves with decreasing strength of amplitude of selective neural features in Pz.

IRI. We estimated our regression model in syncopation mode and found strong correlation $r = 0.72, F\ (1,11) = 9.05, P = 0.008$ with the average auditory locked ERP in Pz as another predictor of IRI performance. A scatterplot showing the strong positive correlation between the extracted auditory-locked ERP amplitude (included N1 peak latency: 180-220 ms) and IRI index is shown in Figure 31, indicating that stronger neural activity at the Pz electrode site relates to higher IRI in the syncopated pacing condition.

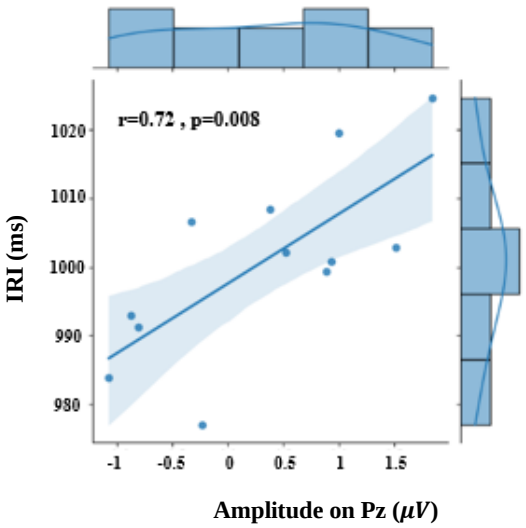

Figure 31. Scatterplots showing individual indices of extracted auditory locked single-trial neural features corresponding to IRI in syncopated pacing condition. The plot illustrates that behavioral accuracy improves with decreasing strength of amplitude of selective neural features in Pz.

Moreover, this analysis yielded a model with $r = 0.67, F\ (1,11) = 7.99, P = 0.01$ with the average selective response-locked ERP emerging as the significant predictor of IRI performance accuracy. A scatterplot indicating the negative correlation between the extracted ERP amplitude at the T8 electrode site and IRI accuracy is shown in Figure 32. Thus, stronger neural activity at the T8 electrode site relates to lower IRI in the syncopated pacing condition.

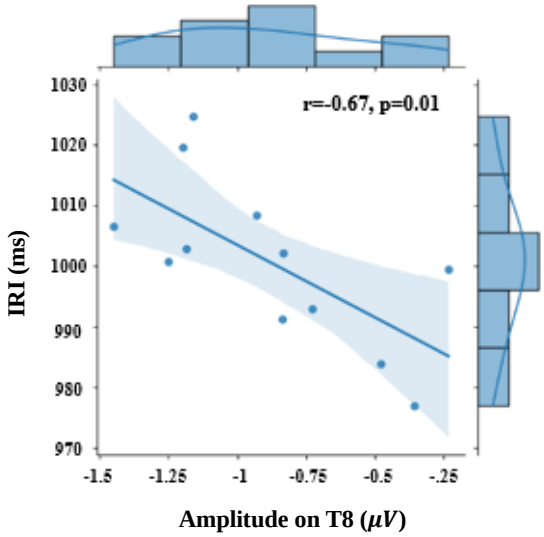

Figure 32. Scatterplots showing individual indices of extracted response tapping locked single-trial neural features corresponding to IRI in syncopated pacing condition. The plot illustrates that IRI behavioral accuracy may improves with decreasing strength of amplitude of selective neural features on T8.

Discussion

Here we investigated whether deep learning could identify neurophysiological features corresponding to finger tapping processes given systematic manipulation of tapping pattern (coordination mode) and phase in the continuation paradigm (pacing or continuation). Our findings go beyond conventional ERP component analyses to functionally relate EEG features to behavioral performance. We were able to achieve this at the time scale of single trials, indicating that neurophysiological processes correspond to a single behavior. These results demonstrate that deep learning can be used to classify classes of timing trials in an action-based timing task on a single trial level. The findings can then be used in a parametric correlational model to link to behavioral timing accuracy.

The central nervous system supports the dynamic behavior of the motor system for planning, controlling, and learning actions (Kawato, 1999; Wolpert et al., 1995), and listening to rhythmic sound sequences activates not only the auditory system but also the sensorimotor system (Fujioka et al., 2009). The findings we report here demonstrate how neurophysiological activity—arguably reflecting variable attentional, memory, motoric, and sensory demands—corresponds to performance on our finger tapping task, which in this case alternates in complexity from trial to trial.

Electrophysiological activity is differentially modulated by specific movement parameters (Jäncke et al., 1998; Thickbroom et al., 1998). Indeed, in the present study, each experimental condition activated a network compatible with the automatic, motor-related timing network, with additional contributions from frontal and central sites to motor coordination required by different levels of timing complexity. Consistent with our

previous study (Rahimpour et al., 2020), which reported that the increase of oxygenated hemoglobin (oxy-Hb) level, the amount of neurophysiological activity also corresponded to the degree of difficulty of the different timing behaviors.

The deep learning approach we implemented here revealed inherent differences between phases (pacing vs. continuation) by extracting meaningful contribution of ERP components and channels. This neural finding is consistent with the statistically significant contrast effects we observed in the behavioral results. In the stimulus-locked ERP waveforms, N1 and P2 peak latencies were significantly engaged in phase-contrast in both synchronization and syncopation patterns. These two components are generally associated in the extant literature with sensory and perceptual processes, including sensory gating, selective attention, and stimulus identification (Fogarty et al., 2020). We also observed the contribution of response-locked single trial features to sensorimotor electrode sites which associated with motor responses. These electrode sites have been associated with sensory, motor related, and attentional and working memory processes.

The finding shows that attentional, sensorimotor and working memory processes underlie the differences in timing sub-processes occurring during our finger tapping task. Results from deep learning further support the interpretation that attentional and working memory impacts on auditory-motor coupling contribute to rhythmic behavior.

This study provides insights into the neural basis of timing behavior by exploiting phases (pacing-continuation) of the continuation paradigm together with changes in coordination dynamics introduced by the alternating design used here. The deep learning results further show that neurophysiological correlates of attentional, memory processes and sensorimotor processes in central, frontal, parietal and temporal electrode sites exhibit distinct markers that can be used to guide classification of trial phase in the continuation paradigm. The results provide promising evidence for neurally-based predictions about memory, attentional, and sensorimotor processes in action-based behavior. Thus, deep learning may help elucidate our understanding of neural processes by guiding the generation of new hypotheses about timing behavior. This will represent an important step towards going beyond conventional ERP components and to functionally relate EEG features to behavioral timing performance.

However, there are several limitations to be addressed in future research. First, the results of other classifications (between coordination modes) were inconclusive. Therefore, increasing sample size to improve the quality of the data that serves as the basis for the deep learning approach may improve overall classification performance. Second, although using deep learning further validates our interpretation of some of our findings, particularly that attentional, working memory, and sensorimotor components are in play to different degrees to the different phases of the continuation paradigm, there are still some uncertainties in predicting behavioral accuracy based on single trial neurophysiological markers. Further research will be needed to further refine these deep-learning models. Third, more complex timing trials (Fitch & Rosenfeld, 2007) and alternating designs may not accurately reflect the underlying neural activity (Rahimpour et al., in press). Dynamic alternation between complex actions may stymie our ability to reliably investigate neural activity associated within and across the various subsystems involved in pacing and continuation phases of action-based timing behavior. Finally, we are mindful that our claims about the precise locations of the sources of activation using

the 10-20 system are limited. Thus, it is vital to better localize and validate localization of EEG sources through the use of other neuroimaging method with better spatial resolution (e.g., fNIRS). Indeed, this is the focus of the research detailed in Chapter 4.

Conclusion

The findings reported here based on implementation of deep learning point to neurophysiological predictors of different forms of action-based timing behavior. We have observed individual differences in neural activity that correlate with behavioral performance in action-based timing behavior. The results point to links between cortical and behavioral measures, and provide evidence that single trial brain activity has predictive relevance to our understanding of action-based timing behavior. The results show that specific neurophysiological features correspond to attentional, memory, and sensorimotor processes and thus may be used as distinct markers that help predict action-based timing accuracy.

References

Ashe, J., Lungu, O. V, Basford, A. T., & Lu, X. (2006). Cortical control of motor sequences. *Current Opinion in Neurobiology*, *16*(2), 213–221.

Bai, O., Mari, Z., Vorbach, S., & Hallett, M. (2005). Asymmetric spatiotemporal patterns of event-related desynchronization preceding voluntary sequential finger movements: a high-resolution EEG study. *Clinical Neurophysiology*, *116*(5), 1213–1221.

Balasubramaniam, R., Wing, A. M., & Daffertshofer, A. (2004). Keeping with the beat: Movement trajectories contribute to movement timing. *Experimental Brain Research*, *159*(1), 129–134. https://doi.org/10.1007/s00221-004-2066-z

Bavassi, L., Kamienkowski, J. E., Sigman, M., & Laje, R. (2017). Sensorimotor synchronization: neurophysiological markers of the asynchrony in a finger-tapping task. *Psychological Research*, *81*(1), 143–156.

Bell, A. J., & Sejnowski, T. J. (1995). An information-maximization approach to blind separation and blind deconvolution. *Neural Computation*, *7*(6), 1129–1159.

Boonstra, T. W., Daffertshofer, A., Peper, C. E., & Beek, P. J. (2006). Amplitude and phase dynamics associated with acoustically paced finger tapping. *Brain Research*, *1109*(1), 60–69.

Caldara, R., Deiber, M.-P., Andrey, C., Michel, C. M., Thut, G., & Hauert, C.-A. (2004). Actual and mental motor preparation and execution: a spatiotemporal ERP study. *Experimental Brain Research*, *159*(3), 389–399.

Chemin, B., Mouraux, A., & Nozaradan, S. (2014). Body movement selectively shapes the neural representation of musical rhythms. *Psychological Science*, *25*(12), 2147-2159.

Chen, J. L., Penhune, V. B., & Zatorre, R. J. (2008). Listening to musical rhythms recruits motor regions of the brain. *Cerebral Cortex*, *18*(12), 2844–2854.

Chen, J. L., Zatorre, R. J., & Penhune, V. B. (2006). Interactions between auditory and dorsal premotor cortex during synchronization to musical rhythms. *Neuroimage*, *32*(4), 1771–1781.

Chollet, F., DiPiero, V., Wise, R. J. S., Brooks, D. J., Dolan, R. J., & Frackowiak, R. S. J. (1991). The functional anatomy of motor recovery after stroke in humans: a study with positron emission tomography. *Annals of Neurology: Official Journal of the American Neurological Association and the Child Neurology Society*, *29*(1), 63–71.

Clark, C. R., Moores, K. A., Lewis, A., Weber, D. L., Fitzgibbon, S., Greenblatt, R., ... & Taylor, J. (2001). Cortical network dynamics during verbal working memory function. *International journal of psychophysiology*, *42*(2), 161-176.

Collective, B. S. M., & Shaw, D. (2012, February). Makey Makey: improvising tangible and nature-based user interfaces. In *Proceedings of the sixth international conference on tangible, embedded and embodied interaction* (pp. 367-370).

Comstock, D. C., & Balasubramaniam, R. (2018). Neural responses to perturbations in visual and auditory metronomes during sensorimotor synchronization. *Neuropsychologia*, *117*, 55–66.

Comstock, D. C., Hove, M. J., & Balasubramaniam, R. (2018). Sensorimotor synchronization with auditory and visual modalities: Behavioral and neural

differences. *Frontiers in Computational Neuroscience*, *12*, 53.
Davranche, K., Nazarian, B., Vidal, F., & Coull, J. (2011). Orienting attention in time activates left intraparietal sulcus for both perceptual and motor task goals. *Journal of Cognitive Neuroscience*, *23*(11), 3318–3330.
Delorme, A., & Makeig, S. (2004). EEGLAB: an open source toolbox for analysis of single-trial EEG dynamics including independent component analysis. *Journal of Neuroscience Methods*, *134*(1), 9–21.
De Pretto, M., Deiber, M.-P., & James, C. E. (2018). Steady-state evoked potentials distinguish brain mechanisms of self-paced versus synchronization finger tapping. *Human Movement Science*, *61*, 151–166.
der Merwe, A. (2009). A theoretical framework for the characterization of pathological speech sensorimotor control. Clinical management of sensorimotor speech disorders. Stuttgart, Germany: Thieme.
Dhamala, M., Pagnoni, G., Wiesenfeld, K., Zink, C. F., Martin, M., & Berns, G. S. (2003). Neural correlates of the complexity of rhythmic finger tapping. *Neuroimage*, *20*(2), 918–926.
Duffy, J. R. (2013). *Motor speech disorders-e-book: Substrates, differential diagnosis, and management*. Elsevier Health Sciences.
Ebrahimzadeh, E., Shams, M., Jounghani, A. R., Fayaz, F., Mirbagheri, M., Hakimi, N., ... & Soltanian-Zadeh, H. (2020). Localizing confined epileptic foci in patients with an unclear focus or presumed multifocality using a component-based EEG-fMRI method. *Cognitive Neurodynamics*, 1-16.
Ebrahimzadeh, E., Shams, M., Rahimpour Jounghani, A., Fayaz, F., Mirbagheri, M., Hakimi, N., ... & Soltanian-Zadeh, H. (2019). Epilepsy Presurgical Evaluation of Patients with Complex Source Localization by a Novel Component-Based EEG-fMRI Approach. *Iranian Journal of Radiology*, *16*(Special Issue).
Fitch, W. T., & Rosenfeld, A. J. (2007). Perception and production of syncopated rhythms. *Music Perception*, *25*(1), 43–58.
Fogarty, J. S., Barry, R. J., & Steiner, G. Z. (2020). Auditory stimulus-and response-locked ERP components and behavior. *Psychophysiology*.
Gore, J. C., Horovitz, S. G., Cannistraci, C. J., & Skudlarski, P. (2006). Integration of fMRI, NIROT and ERP for studies of human brain function. *Magnetic Resonance Imaging*, *24*(4), 507–513.
Grafton, S. T., Woods, R. P., Mazziotta, J. C., & Phelps, M. E. (1991). Somatotopic mapping of the primary motor cortex in humans: activation studies with cerebral blood flow and positron emission tomography. *Journal of Neurophysiology*, *66*(3), 735–743.
Grahn, J. A., & Brett, M. (2007). Rhythm and beat perception in motor areas of the brain. *Journal of Cognitive Neuroscience*, *19*(5), 893–906.
Grahn, J. A., & Rowe, J. B. (2009). Feeling the beat: premotor and striatal interactions in musicians and nonmusicians during beat perception. *Journal of Neuroscience*, *29*(23), 7540–7548.
Harrington, D. L., Haaland, K. Y., & Knight, R. T. (1998). Cortical networks underlying mechanisms of time perception. *Journal of Neuroscience*, *18*(3), 1085–1095.
Haufler, A. J., Spalding, T. W., Santa Maria, D. L., & Hatfield, B. D. (2000). Neuro-

cognitive activity during a self-paced visuospatial task: comparative EEG profiles in marksmen and novice shooters. *Biological Psychology*, *53*(2–3), 131–160.

Hove, M. J., Fairhurst, M. T., Kotz, S. A., & Keller, P. E. (2013). Synchronizing with auditory and visual rhythms: an fMRI assessment of modality differences and modality appropriateness. *Neuroimage*, *67*, 313–321.

Ivry, R. B., & Keele, S. W. (1989). Timing Functions of The Cerebellum. *Journal of Cognitive Neuroscience*, *1*(2), 136–152. https://doi.org/10.1162/jocn.1989.1.2.136

Ivry, R. B., & Spencer, R. M. C. (2004). The neural representation of time. *Current Opinion in Neurobiology*, *14*(2), 225–232.

Jäncke, L., Specht, K., Mirzazade, S., Loose, R., Himmelbach, M., Lutz, K., & Shah, N. J. (1998). A parametric analysis of therate effect'in the sensorimotor cortex: a functional magnetic resonance imaging analysis in human subjects. *Neuroscience Letters*, *252*(1), 37–40.

Jantzen, Kelly J, & Kelso, J. A. S. (2007). Neural coordination dynamics of human sensorimotor behavior: A Review. In *Handbook of brain connectivity* (pp. 421–461). Springer.

Jantzen, Kelly J, Steinberg, F. L., & Kelso, J. A. S. (2004). Brain networks underlying human timing behavior are influenced by prior context. *Proceedings of the National Academy of Sciences*, *101*(17), 6815–6820.

Kappenman, E. S., & Luck, S. J. (2010). The effects of electrode impedance on data quality and statistical significance in ERP recordings. *Psychophysiology*, *47*(5), 888–904.

Kaufer, D. I., & Lewis, D. A. (1999). Frontal lobe anatomy and cortical connectivity. *The Human Frontal Lobes*, 27–44.

Kawashima, R., Roland, P. E., & O'Sullivan, B. T. (1994). Activity in the human primary motor cortex related to ipsilateral hand movements. *Brain Research*, *663*(2), 251–256.

Kawashima, R., Yamada, K., Kinomura, S., Yamaguchi, T., Matsui, H., Yoshioka, S., & Fukuda, H. (1993). Regional cerebral blood flow changes of cortical motor areas and prefrontal areas in humans related to ipsilateral and contralateral hand movement. *Brain Research*, *623*(1), 33–40.

Kawato, M. (1999). Internal models for motor control and trajectory planning. *Current Opinion in Neurobiology*, *9*(6), 718–727.

Kerick, S. E., McDowell, K., Hung, T.-M., Santa Maria, D. L., Spalding, T. W., & Hatfield, B. D. (2001). The role of the left temporal region under the cognitive motor demands of shooting in skilled marksmen. *Biological Psychology*, *58*(3), 263–277.

Large, E. W., Herrera, J. A., & Velasco, M. J. (2015). Neural networks for beat perception in musical rhythm. *Frontiers in Systems Neuroscience*, *9*, 159.

Lewis, P. A., Wing, A. M., Pope, P. A., Praamstra, P., & Miall, R. C. (2004). Brain activity correlates differentially with increasing temporal complexity of rhythms during initialisation, synchronisation, and continuation phases of paced finger tapping. *Neuropsychologia*, *42*(10), 1301–1312.

Lopez-Calderon, J., & Luck, S. J. (2014). ERPLAB: an open-source toolbox for the analysis of event-related potentials. *Frontiers in Human Neuroscience*, *8*, 213.

Luck, S. J. (2014). *An introduction to the event-related potential technique*. MIT press.

Makeig, S., Makeig, S., Debener, S., Debener, S., Onton, J., Onton, J., … Delorme, A. (2004). Mining event-related brain dynamics. *Trends in Cognitive Sciences*, *8*(5), 204–210. https://doi.org/10.1016/j.tics.2004.03.008

Maris, E. (2012). Statistical testing in electrophysiological studies. *Psychophysiology*, *49*(4), 549–565.

Maris, E., & Oostenveld, R. (2007). Nonparametric statistical testing of EEG-and MEG-data. *Journal of Neuroscience Methods*, *164*(1), 177–190.

Mathias, B., Zamm, A., Gianferrara, P. G., Ross, B., & Palmer, C. (2020). Rhythm complexity modulates behavioral and neural dynamics during auditory–motor synchronization. *Journal of Cognitive Neuroscience*, *32*(10), 1864-1880.

Mayville, J. M., Bressler, S. L., Fuchs, A., & Kelso, J. A. S. (1999). Spatiotemporal reorganization of electrical activity in the human brain associated with a timing transition. *Experimental Brain Research*, *127*(4), 371–381.

Mayville, J. M., Jantzen, K. J., Fuchs, A., Steinberg, F. L., & Kelso, J. A. S. (2002). Cortical and subcortical networks underlying syncopated and synchronized coordination revealed using fMRI. *Human Brain Mapping*, *17*(4), 214–229.

Morris, G. W. T. B. A. P. I., Mastaglia, M. L. B. F. L., & Morris, I. (1998). Isometric force-related activity in sensorimotor cortex measured with functional MRI, 59–64.

Nachev, P., Kennard, C., & Husain, M. (2008). Functional role of the supplementary and pre-supplementary motor areas. *Nature Reviews Neuroscience*, *9*(11), 856–869.

Nobre, A. C. (2001). Orienting attention to instants in time. *Neuropsychologia*, *39*(12), 1317–1328.

Nozaradan, S., Peretz, I., & Keller, P. E. (2016). Individual differences in rhythmic cortical entrainment correlate with predictive behavior in sensorimotor synchronization. *Scientific Reports*, *6*, 20612.

Oostenveld, R., Fries, P., Maris, E., & Schoffelen, J.-M. (2011). FieldTrip: open source software for advanced analysis of MEG, EEG, and invasive electrophysiological data. *Computational Intelligence and Neuroscience*, *2011*.

Pabst, A., & Balasubramaniam, R. (2018). Trajectory formation during sensorimotor synchronization and syncopation to auditory and visual metronomes. *Experimental Brain Research*, *236*(11), 2847-2856.

Paek, A. Y., Agashe, H., & Contreras-Vidal, J. L. (2014). Decoding repetitive finger movements with brain activity acquired via non-invasive electroencephalography. *Frontiers in Neuroengineering*, *7*, 3.

Peper, C. E., Beek, P. J., & van Wieringen, P. C. W. (1995). Multifrequency coordination in bimanual tapping: Asymmetrical coupling and signs of supercriticality. *Journal of Experimental Psychology: Human Perception and Performance*, *21*(5), 1117.

Pernet, C. R., Latinus, M., Nichols, T. E., & Rousselet, G. A. (2015). Cluster-based computational methods for mass univariate analyses of event-related brain potentials/fields: A simulation study. *Journal of Neuroscience Methods*, *250*, 85–93.

Pfurtscheller, G., Woertz, M., Supp, G., & da Silva, F. H. L. (2003). Early onset of post-movement beta electroencephalogram synchronization in the supplementary motor area during self-paced finger movement in man. *Neuroscience Letters*, *339*(2), 111–114.

Rahimpour, A., Pollonini, L., Comstock, D., Balasubramaniam, R., & Bortfeld, H. (2020). Tracking Differential Activation of Primary and Supplementary Motor Cortex Across Timing Tasks: An fNIRS Validation Study. *Journal of Neuroscience Methods*, 108790.

Rao, S M, Harrington, D. L., Haaland, K. Y., Bobholz, J. A., Cox, R. W., & Binder, J. R. (1997). Distributed neural systems underlying the timing of movements. *The Journal of Neuroscience : The Official Journal of the Society for Neuroscience*, *17*(14), 5528–5535. Retrieved from http://www.ncbi.nlm.nih.gov/pubmed/9204934

Rao, Steven M, Binder, J. R., Bandettini, P. A., Hammeke, T. A., Yetkin, F. Z., Jesmanowicz, A., … others. (1993). Functional magnetic resonance imaging of complex human movements. *Neurology*, *43*(11), 2311.

Repp, B. H. (2005). Sensorimotor synchronization: A review of the tapping literature. *Psychonomic Bulletin and Review*. https://doi.org/10.3758/BF03206433

Rizzolatti, G., & Luppino, G. (2001). The cortical motor system. *Neuron*, *31*(6), 889–901.

Sakai, K., Hikosaka, O., Miyauchi, S., Takino, R., Tamada, T., Iwata, N. K., & Nielsen, M. (1999). Neural representation of a rhythm depends on its interval ratio. *Journal of Neuroscience*, *19*(22), 10074–10081.

Sassenhagen, J., & Draschkow, D. (2019). Cluster-based permutation tests of MEG/EEG data do not establish significance of effect latency or location. *Psychophysiology*, *56*(6), e13335.

Sergent, J. (1993). Mapping the musician brain. *Human Brain Mapping*, *1*(1), 20–38. https://doi.org/10.1002/hbm.460010104

Serrien, D. J. (2008). The neural dynamics of timed motor tasks: Evidence from a synchronization--continuation paradigm. *European Journal of Neuroscience*, *27*(6), 1553–1560.

Smit, D. J. A., Linkenkaer-Hansen, K., & de Geus, E. J. C. (2013). Long-range temporal correlations in resting-state alpha oscillations predict human timing-error dynamics. *Journal of Neuroscience*, *33*(27), 11212–11220.

Smith, E. E., & Jonides, J. (1998). Neuroimaging analyses of human working memory. *Proceedings of the National Academy of Sciences*, *95*(20), 12061–12068.

Spencer, N. J., Bywater, R. A. R., Holman, M. E., & Taylor, G. S. (1998). Inhibitory neurotransmission in the circular muscle layer of mouse colon. *Journal of the Autonomic Nervous System*, *70*(1–2), 10–14.

Studenka, B. E., Zelaznik, H. N., & Balasubramaniam, R. (2012). The distinction between tapping and circle drawing with and without tactile feedback: An examination of the sources of timing variance. *Quarterly Journal of Experimental Psychology*, *65*(6), 1086–1100. https://doi.org/10.1080/17470218.2011.640404

Tanji, J. (2001). Sequential organization of multiple movements: involvement of cortical motor areas. *Annual Review of Neuroscience*, *24*(1), 631–651.

Wallenstein, G. V, Kelso, J. A. S., & Bressler, S. L. (1995). Phase transitions in spatiotemporal patterns of brain activity and behavior. *Physica D: Nonlinear Phenomena*, *84*(3–4), 626–634.

Wing, A. M. (2002). Voluntary timing and brain function: an information processing approach. *Brain and Cognition*, *48*(1), 7–30.

Wing, A. M., & Kristofferson, A. B. (1973). Response delays and the timing of discrete motor responses. *Perception & Psychophysics*, *14*(1), 5–12. https://doi.org/10.3758/BF03198607

Witt, S. T., Laird, A. R., & Meyerand, M. E. (2008). Functional neuroimaging correlates of finger-tapping task variations: an ALE meta-analysis. *Neuroimage*, *42*(1), 343–356.

Wolpert, D. M., & Ghahramani, Z. (2000). Computational principles of movement neuroscience. *Nature Neuroscience*, *3*(11), 1212–1217.

Wolpert, D. M., Ghahramani, Z., & Jordan, M. I. (1995). An internal model for sensorimotor integration. *Science*, *269*(5232), 1880–1882.

Yoshii, F., Ginsberg, M. D., Kelley, R. E., Chang, J. Y., Barker, W. W., Ingenito, G., … Boothe, T. E. (1989). Asymmetric somatosensory activation with right-vs left-hand stimulation: a positron emission tomographic study. *Brain Research*, *483*(2), 355–360.

Zhu, F. F., Maxwell, J. P., Hu, Y., Zhang, Z. G., Lam, W. K., Poolton, J. M., & Masters, R. S. W. (2010). EEG activity during the verbal-cognitive stage of motor skill acquisition. *Biological Psychology*, *84*(2), 221–227.

Ziemann, U., & Hallett, M. (2001). Hemispheric asymmetry of ipsilateral motor cortex activation during unimanual motor tasks: further evidence for motor dominance. *Clinical Neurophysiology*, *112*(1), 107–113.

Chapter 4
Using EEG and fNIRS to Explore Cortical Source Localization

Abstract

This research aims to substantiate claims about the ability of both EEG and fNIRS systems to localize sources of timing-based action behavior in the brain. We compared both behavioral and neural findings using the alternating-design tapping task described in C2 based on data collected across two testing sessions. FNIRS data were collected in the first session and EEG data in the second. The behavioral task was identical across the two sessions. Overall, we found that experience with the finger tapping task played an important role in the accuracy of participants' behavioral performance from the first to the second session. This experience likewise impacted patterns of brain activation across the two sessions. We observed training effects on mean accuracy asynchrony and IRI across the four timing conditions (synchronized pacing, synchronized continuation, syncopated pacing, syncopated continuation). This improvement in performance from the first imaging session to the second resulted in differential activation patterns from one session to the next.

Keywords: Source Localization, DIPFIT, ICA, EEG, fNIRS, IRI, Asynchrony

Introduction

Source localization of the electroencephalography (EEG) signal is a way to estimate identification of the brain regions that underlie the EEG signal. Localizing sources is increasingly relevant in neuroscience research and in clinical applications that use EEG (Cui et al., 2011). As an increasing number of studies employ cortical source localization to identify where in the brain responses collected with EEG originate, it is crucial to validate the accuracy of the methodology. For example, ERPs are derived from the EEG recording of transient brain responses to cognitive stimuli; ERPs are averages of specific segments of the EEG recordings taken during repeated presentations of specific events. The temporal and frequency content of the signal during these repeated events can be characterized in terms of specific patterns common across the same event. These *components* are the specific smaller waveforms that make up the more complex ERP waveform. In recent years, the specific components that correspond to different perceptual and cognitive processes have been well delineated (Woodman, 2010). However, precise localization of the predominant source of these electrical events in the brain based on the data recorded from the scalp using EEG has continued to be a challenge.

Over the past three decades, several current density estimation techniques have been developed to address the *neuroelectromagnetic inverse problem* (Baillet, 2001; Bast et al., 2004; Koles, 1998), a term that refers to the challenge of identifying the origins (sources) of neural activation as recorded by the electrodes placed at various points on the scalp. Researchers now implement a wide range of techniques in an effort to localize the cortical sources of the EEG signal. A common toolbox and graphic user interface, EEGLAB, running under the cross-platform MATLAB environment, is widely used for processing EEG data. A specific function of EEGLAB is to facilitate applying and evaluating the independent component analysis (ICA) of EEG data. ICA algorithms have proven capable of isolating both neurally generated and artefactual EEG sources. Researchers have pursued several approaches, including the finite element method (Jatoi et al., 2014), skull modeling (Montes-Restrepo et al., 2014), low-resolution electromagnetic tomographic analysis (LORETA), minimum norm, recursive multiple signal classification (MUSIC), and focal underdetermined system solution (FOCUSS) (Song et al., 2015), to name just a handful. The most widely used and successful modeling techniques include LORETA, Local Autoregressive Average (LAURA) (Michel et al., 2004), and DIPFIT (Iversen & Makeig, 2014). DIPFIT is the model that our research lab uses, and is the most recommended EEGLAB plug-in for localizing equivalent dipole locations of independent component-guided scalp maps, and the DIPFIT plug-in is now regularly applied to the source localization issue (Makeig et al., 2004).

In the DIPFIT approach, ICA (Makeig et al., 2004) isolates both artifactual and neurally generated EEG sources (Jung et al., 2000; Makeig et al., 1999). This method was first applied to EEG by Makeig et al. (1996) and has been widely used in the research community ever since, most often to remove noise artifacts (Jung et al., 2000; Jung et al., 1999; Makeig et al., 1996). Its relevance to source localization became apparent when it was found capable of separating brain sources whose activity patterns were distinctly

linked to behavioral phenomena. The DIPFIT approach of EEG source localization combines ICA, time/frequency analysis, and trial-by-trial visualization (Makeig et al., 2004).

The goal of the current project is to explore the validity of the DIPFIT source localization program for EEG using fNIRS. We compared source localization outcomes using DIPFIT to the more spatially accurate fNIRS data that were collected during each participant's performance of the same finger-tapping task. Our motivation for making this comparison is that fNIRS has certain advantages over other neuroimaging methods. In particular, it has a higher temporal resolution than fMRI and positron emission tomography (PET) and better spatial resolution than EEG. Moreover, other recording techniques are highly affected by head movements, while fNIRS is less so, making it especially useful with difficult-to-test populations such as infants and young children. Our group has broad methodological expertise in fNIRS research (Bortfeld et al., 2007, 2009; Jahani et al., 2015; Rahimpour et al., 2017, 2018), and we are keen to delineate the neural mechanisms that underlie different perceptual and cognitive processes. Doing so well depends on precisely localizing the cortical sources of brain-based signals. Although fMRI is the gold standard for localization, given its high spatial resolution, we need a device that allows participants to be in the same EEG experimental paradigm. For this purpose, fNIRS has the highest spatial resolution while maintaining other aspects of the participant's experience in the EEG environment.

Here we examine an approach to localizing the sources of neural activation—DIPFIT—by monitoring and tracking trial-to-trial variation in neural data collected via EEG, and compare that with data collected via fNIRS from the same participants using the same task. NIR topography has been applied to evaluate, for example, the within-subject reproducibility of sensorimotor-activation NIRS signals in healthy adults (Cui et al., 2011; Kameyama et al., 2006; Okamoto et al., 2004; Strangman et al., 2002). Thus, fNIRS is an appropriate substitute for fMRI for localizing cortically-based brain activity related to cognitive tasks (Cui et al., 2011). Therefore, we compared fNIRS data collected as described in Chapter 2 to predictions generated by the DIPFIT source localization approach as applied to the data collected as described in Chapter 3.

Brain Activity

Finger tapping tasks generally recruit primary cortices (S1, M1), SMA, PMC, inferior parietal cortex, basal ganglia, and cerebellum (Witt et al., 2008). However, different task-specific parameters may modulate the specific neural mechanisms that are engaged in any particular task. The dual coordination mode, continuation paradigm used in the current studies helps isolate similarities and differences in the neural circuits engaged by paced and continuation (i.e., self-paced) tapping of varying levels of difficult (synchronization/syncopation). Much progress has been made in studying the neural correlates of various processes relevant to sensorimotor synchronization. For example, simple synchronized finger tapping engages the cortical network that includes somatosensory and motor areas, while continuation tapping relies more on preferential areas due to its load on working memory (More complex sensorimotor synchronization tasks result in greater activation in related motor areas, including pre-SMA, PMC, and the cerebellum, as well as in stronger coupling to the auditory area (Repp et al., 2013). Sensorimotor cortices, SMA, and the anterior portion of the cerebellum are commonly

activated during both paced and continuation tapping (Witt et al., 2008). Moreover, earlier studies have shown that motor areas are recruited to a greater extent in continuation than in paced tapping (Rahimpour et al., 2020).

Researchers have been used several approaches to find neurologically based activity of finger tapping. Based on frequency domain analyses, Boonstra et al (2006) found that, while the evoked response in the slower cortical oscillations (i.e., in the theta and alpha bands) during paced tapping reflected auditory processing, the induced responses (i.e., modulations in phase and amplitude) in the beta band were associated with the motor act of tapping and were phase phased-locked with the tap onsets. The amplitude of the event-related changes in the beta band also decreased with increasing movement rate (Boonstra et al., 2006). Serrien (2008) found somewhat higher tapping variability, as well as more functional connectivity in the beta band in the mesial-central area (covering areas such as PMC and SMA), in continuation than synchronization tapping. Significant activity in the prefrontal-parietal-temporal network (consisting of dorsal and ventral prefrontal cortex, middle temporal gyrus, and bilateral prefrontal lobes) was present only during continuation tapping, not in paced tapping. Activity in these areas is typically associated with various working memory manipulations, and the observed activity was attributed to the increased demand on working memory given the temporal representation of the auditory stimuli when the pacing signal was switched off (Serrien, 2008). Although SMA is primarily involved in motor planning, its activity can also reflect an active supervisory role of motor processing supported by activity in M1 (Kasess et al., 2008).

Our aim here is to compare the EEG and fNIRS data to identify the unique strengths of each. To do so, we tracked brain activation in participants while they completed the tapping task that alternated that complexity of the tapping pattern with participants either synchronizing or syncopating their finger tapping responses by first pacing and then continuing the tapping pattern in the absence of auditory cue. We hypothesized that (1) the finger-tapping task would recruit primary S1 and M1, SMA, PMC, and inferior parietal cortex (Witt et al., 2008). We also hypothesized that localization findings would be comparable across EEG and fNIRS at a general level, (2) fNIRS would play the ground truth role to establish more precise spatial localization, and (3) EEG would reveal more nuanced information about the training effect of timing-based neural activation across the four tapping conditions. We predicted that brain activity would likewise relate to the temporal complexity of specific finger tapping patterns.

Materials and Methods

Participants

First, sixteen healthy adults were recruited for the study. Four of them were removed due to lack of concentration (results that were missing tap responses for more than half of the session) during the study, bad channel quality (due to having thick hair or a head circumference that was too large for our probe), or due to light saturation from the testing environment. This resulted in a participant pool of twelve healthy right-handed adult volunteers (mean age 27.3, range 19-41) at the University of California, Merced

who successfully participated in both the fNIRS and EEG data collection in two separate sessions. FNIRS data were collected during the first session and EEG data during the second. Each participant completed the two sessions on the same day. No participants reported any neurological or skeletomuscular disorders or injuries at the time of the experiment. The study's protocol was approved by the Institutional Review Board (IRB) for research ethics and human subjects. All participants gave informed consent after the experimental procedures were explained to them.

Experiment

The alternating experimental design for each testing session was within-participant. Participants were asked to perform two distinct tapping patterns in relation to a regularly spaced auditory tone, continuing each tapping pattern for a fixed amount of time after the tone stopped. Thus, the design was 2 (synchronous/asynchronous tapping) x 2 (pacing to tone/continuation without tone) x 2 (session1/session2). Seated participants performed repetitive right (dominant) finger movements in the presence of an auditory metronome that produced a 1 kHz tone for 20 ms every 1000 ms (1 Hz). There were ten trials in each condition, with each trial involving 27 cycles of responses.

Task

We collected data from the same participants on EEG followed by fNIRS on a single day using the same experimental protocol. Tapping was performed with the index finger of the right hand on a metal plate attached to a MakeyMakey input device that records tapping by sending a small electrical signal to an output lead that the subject holds on their left hand. An input lead for the MakeyMakey was then attached to a metal plate that the subject tapped. When the subject touched the metal plate, it completed a circuit in the MakeyMakey, which sends the signal to the computer to indicate a tap (Collective & Shaw, 2012). Subjects performed the task while seated in a comfortable chair (See more details in Materials and Methods-Chapter 3).

Behavioral Analysis

The time of each behavioral response was defined as the point of tapping the finger on MakeyMakey plate. The time of each response was corrected by 25 ms to account for the temporal delay of the MakeyMakey device. Two relative measures of performance were calculated. Mean accuracy asynchrony was defined as the time difference between each behavioral response and the preceding stimulus onset; inter-response interval (IRI) was defined as the time between consecutive behavioral responses.

EEG Approach

Preprocessing

EEG was continuously recorded with an ANT-Neuro 32 electrode cap with electrodes placed according to the 10–20 International electrode system and recorded at 1024 Hz. The EEG data were processed with EEGLAB (Delorme & Makeig, 2004). ERP data were preprocessed by first down sampling to 512 Hz, then applying a high pass filter with 6db cutoff at .1 Hz, followed by a low-pass filter with a 6db cutoff at 56.25 Hz to eliminate 60 Hz line noise. Data were then examined, and any bad sections were removed by hand. Any bad channels were detected and removed using the probability measure

within the ASR plugin for EEGLAB that compares channels with their surrounding channels (Mullen et al., 2015). ICA was performed using the infomax algorithm within EEGLAB (Bell & Sejnowski, 1989). Following ICA, the component data were examined, and components related to eyeblinks and eye movement were rejected to clean the data of further artifacts (Jung et al., 2000). Data were epoched using ERPLAB centered around the onset of the perturbed stimulus and centered on the participants taps that corresponded to the perturbed stimuli. Each epoch was from −0.1 s of the event onset to 0.5 s past the onset. In addition to removing blinking and eye movement components, any epoch that had an eye blink during the stimulus onset was removed.

ICA-DIPFIT Source Localization

ICA is a linear data decomposition method which separates multichannel data into the different constituent components. Each component contains a time course of neural activity in every trial and a single scalp map, indicating the strength of the volume conducted component activity at each scalp electrode. A linear ICA decomposition is one whose component activities are mostly temporally independent (Lee et al., 2000), and therefore also mostly temporally "distinct". Every EEG electrode montage acts as a set of spatial filters cortical field dynamics. ICA performs further linear spatial filtering on the recorded data to cancel the effects of summing the volume-conducted cortical source activities in each recording channel and identifies sources by finding distinctive sources of information in the data. If the activity time courses of different EEG components are relatively independent of one another, their local field activities must be primarily decoupled physiologically. Thus, ICA should separate EEG (or equally MEG) data into physiologically and functionally distinct sources under favorable circumstances. Results of actual data decomposition demonstrates that ICA, applied to sufficiently large and clean high-density EEG datasets, can separate the large or minor activities, scalp maps, and scalp data contributions of dozens of maximally independent information sources whose scalp maps fit near-perfectly the dipolar projections of cortical EEG sources (Vorobyov & Cichocki, 2002; Hyvärinen & Oja, 2000; Makeig et al., 1999).

ICA separates EEG sources with tangential and radial orientations (Oostendorp & Oosterom, 1996). This method decomposes the data into sources with independent time courses and dipolar scalp maps. Disregarding head geometry or electrode locations, the ICA approach strongly suggests that the index of the recovered component is a physiologically separate process. Previous studies revealed standard EEG processes with distinct spatial and event-related dynamic characteristics that account for most non-artifactual EEG (Makeig et al., 2004). Not surprisingly, these component clusters are similar in many ways to traditionally recognized types of EEG activity, although with better spatial definition and signal-to-noise ratio relative to the single scalp electrode data (Jung et al., 2000).

The most recommended plug-in in EEGLAB for localizing equivalent dipole locations of independent component-guided scalp maps is the DIPFIT plug-in, which is now being applied to as a source localization approach. Therefore, we used ICA in DIPFIT to localize neural activation across four timing conditions. As specified earlier, data were examined and any bad channels were detected and removed using the probability measure within the ASR plugin for EEGLAB that compares channels with their surrounding channels. The data were then re-referenced to the linked mastoids. ICA

was then performed using the infomax algorithm within EEGLAB. Dipole source localization was performed using the Dipfit2 plugin that performs source localization by fitting an equivalent current dipole model using a non-linear optimization technique using a 4-shell spherical model (Kavanagh et al., 1978).

fNIRS Approach

Functional near-infrared spectroscopy (fNIRS) provides an alternative to fMRI for assessing superficial cortical hemodynamics. The NIRS method is based on near-infrared light absorption changes that depend on concentration changes of the chromophores $[Oxy - Hb]$ and $[deOxy - Hb]$ in the brain. We used 55-channel two-wavelength NIRS systems with a sampling rate of 3.785 Hz (NIRScout, NIRx, Glen Head, NY) (Pollonini et al., 2014) with sixteen light-incident and twenty detector fibers. The depth of the measuring point depends on the distance between the transmitters and the receivers; it is reported that the NIRS signal reflects the absorption at a depth of 1.2–2 cm from the scalp when the inter-probe distance is 2.7 cm (Kobayashi et al., 2006; Raichle, 1994). As the human cerebral cortex usually lies about 1.0–2.0 cm deep from the scalp, the suitable inter-probe distance should be about 2.5–3.0 cm to measure the activities of the cerebral surface. According to the above discussions, the inter-probe distance is decided to be 3.0 cm in our study. The light sources were continuous laser diodes with wavelengths of 760 and 850 nm. The optodes were positioned according to the 10-20 system for standard electrode positions.

The mean of the fNIRS signal during the test condition relative to the mean of the fNIRS signal during the pre-baseline condition was estimated using a regression model and computed using an autoregressive model, pre-whitened iterative reweighted least squares (AR-IRLS) algorithm that is robust to artifacts introduced by subject motion and serial correlations introduced by systemic physiology (Barker et al. 2013). Thus, we used a hemodynamic response function (HRF) that had an elongated return to baseline after the termination of the test condition (Hoppes et al., 2018; Lin et al., 2017).

We applied mixed effect analysis to estimate the regression model at the group level. The relative signal change was inspected on a per subject basis, in which the results were used for a second, group-level analysis. Group level analysis was performed via a linear mixed effects model that included random intercept terms for each subject to model within-subject correlations (Abdelnour & Huppert, 2009). The group level model was estimated per channel using the built-in MATLAB 2022a package for estimating linear mixed effects models (Mathworks, Natick, MA, USA). The fNIRS measurement positions were registered to an anatomical atlas brain (Colin27) (Holmes et al., 1998) using a custom registration algorithm based on the international 10–20 coordinate system (Tsuzuki & Dan, 2014). For each channel, estimates of the regression coefficients, β, for [HbO] and [Hb], as well as the standard error, were computed for each subject group, and each trial. T-tests were used to determine if the regression coefficient differed from 0, using the false discovery rate method to adjust the p value (pFDR < 0.05).

NIRS data are typically analyzed in a model that calculates mean hemoglobin concentrations across designated periods. Analyses focusing on the multichannel NIRS data are expected to clarify the spatial pattern of brain activation, which we then compare to the EEG findings generated via the ICA analysis.

Region of Interest

We aim to examine the spatial source localization of neurophysiological activity and hemodynamic responses in specified regions of interest (ROI). To this end, we aimed to investigate those regions identified as engaged to different degrees in Session 1. For spatial localization visualization, we map the channels onto a brain template. Figure 33A depicts channel positions relative to common scalp landmarks. Red numbers represent 10 –20 scalp landmarks. Yellow lines connect light sources and detectors which represent data channels. Figure 33B shows the sensitivity map for our probe design as derived from photon migration simulations of the probe on a 3D head model.

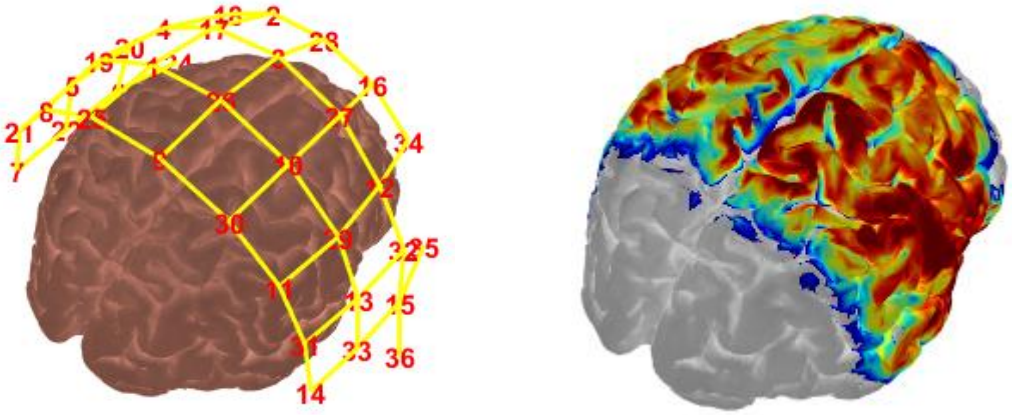

Figure 33. Channel placement and sensitivity. (A) Depiction of temporal head channel positioning relative to common scalp landmarks. Red numbers represent 10 –20 scalp landmarks. Yellow lines connecting light sources and detectors represent data channels. (B) Sensitivity map (mm^{-1}) derived from photon migration simulations of probe in a 3D head model. This figure is adapted from Chapter 2.

Behavioral Results

Mean Accuracy Asynchrony

Our estimated multiple regression model was calculated to predict mean accuracy asynchrony based on coordination and phase across the two separate sessions. We observed main effects of phase ($F_{1,11} = -261.3, P < 0.001, \eta 2 = 0.43$), coordination mode ($F_{1,11} = 8.03, P < 0.001, \eta 2 = 0.23$) and study session ($F_{1,11} = 215, P < 0.001, \eta 2 = 0.37$) on mean accuracy asynchrony. Therefore, all three independent variables—coordination mode, maintenance phase, and study session—significantly impacted mean asynchrony. Moreover, a significant phase × study session interaction ($F_{1,24} = 5.48, P < 0.01, \eta 2 = 0.2$) was observed. A significant contrast effect was also observed between two sessions ($F_{1,11} = 20.4, P = 0.001, \eta 2 = 0.24$) due to the practice effect. We also observed significant difference between synchronization and syncopation modes ($F_{1,11} = 5.4, P = 0.001, \eta 2 = 0.14$). A three-way interaction effect

between phase, coordination mode and study session was also observed ($F_{2,22} = 5.48, P = 0.001, \eta 2 = 0.2$).

Session 1

In order to calculate the accuracy of synchronized and syncopated paced tapping, the average mean accuracy asynchronies (with SD) were measured as 22.27 ± 100.56 (ms) (mean$\pm$SD) and 3.16 ± 123.45 (ms), respectively (see Figure 34). Moreover, the mean accuracy asynchrony for continuation phase with no metronome present was estimated at 58.44 ± 196.1 (ms) for synchronized tapping and 66.6 ± 205.88 (ms) for syncopated tapping coordination modes. This indicates more variability for continuation than pacing in both coordination modes in the first session.

By using post hoc tests, we observed significant differences of mean accuracy asynchrony between pacing and continuation in synchronization mode ($F_{1,11} = 6.14, P = 0.001, \eta 2 = 0.27$) and between phases in syncopation ($F_{1,24} = 11.9, P = 0.001, \eta 2 = 0.31$).

Session 2

For participants in the second session, for synchronized and syncopated pacing and continuation, the mean accuracy asynchronies were -46.48 ± 102.3 (ms)(mean $\pm$ SD), -49.31 ± 120.5 (ms), 27.33 ± 197.68 (ms), and 3.45 ± 212.75 (ms), respectively, as illustrated in Figure 34. Results revealed that the pacing phase resulted in more stable tapping compared to the continuation phase. Also, we observed negative average accuracy asynchrony in the pacing phase for both coordination modes in session 2. Significant differences between pacing and continuation were observed for synchronized ($F_{1,11} = 15.23, P < 0.001, \eta 2 = 0.33$) and syncopated ($F_{1,11} = 11.6, P = 0.001, \eta 2 = 0.27$) coordination modes. Moreover, a significant difference in mean accuracy asynchrony between synchronization and syncopation in the continuation phase was also observed ($F_{1,11} = 5.17, P < 0.001, \eta 2 = 0.22$).

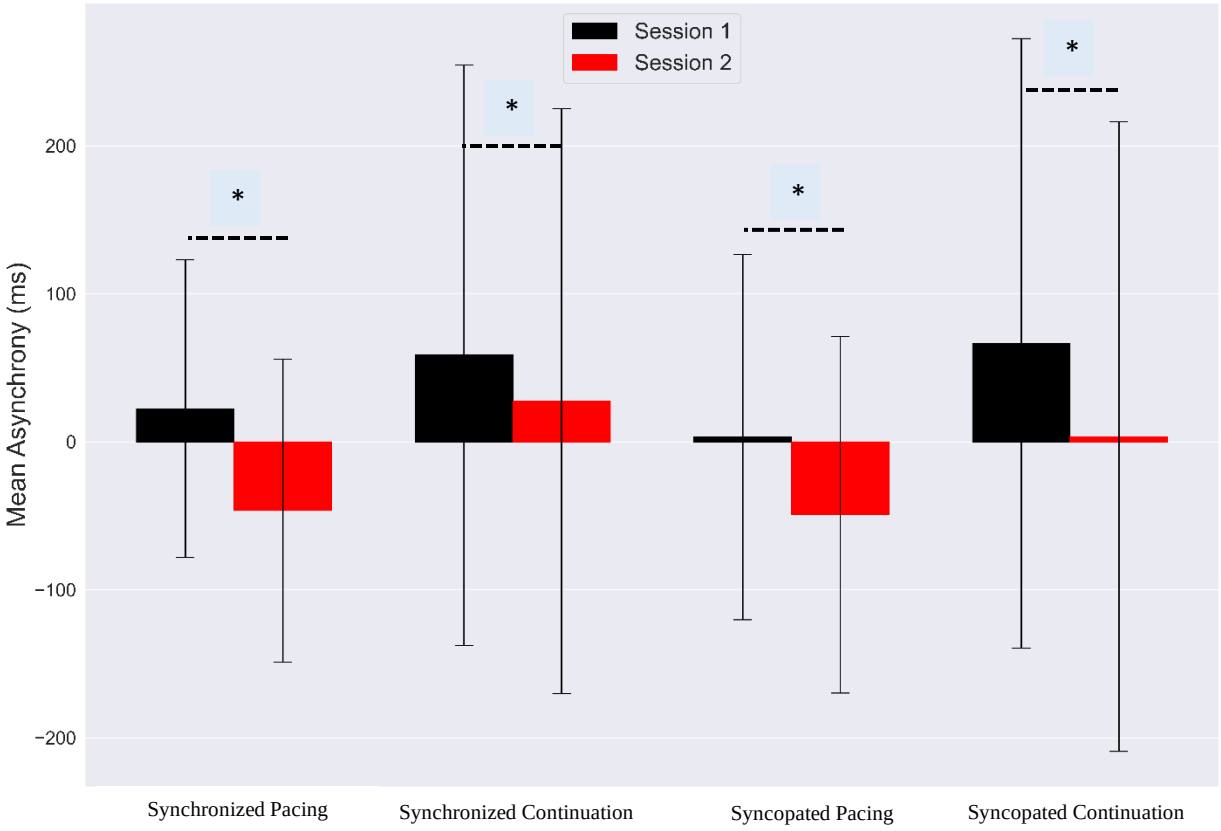

Figure 34. Mean asynchronies of each timing condition (i.e., synchronized pacing, synchronized continuation, syncopated pacing, and syncopated continuation) in session 1 (black) and session 2 (red). Error bars show standard deviation (SD). Dashed brackets indicate statistically significant comparisons between two study sessions.

As shown in Figure 34, the contrast effects between two study sessions were observed in all timing conditions: synchronized pacing ($F_{1,11} = 12.15, P = 0.001, \eta 2 = 0.32$); synchronized continuation ($F_{1,11} = 6.08, P = 0.001, \eta 2 = 0.23$); syncopated pacing ($F_{1,11} = 11.06, P = 0.001, \eta 2 = 0.21$); and syncopated continuation ($F_{1,11} = 12.38, P < 0.001, \eta 2 = 0.29$). These contrasts clearly demonstrate the impact of practice from one session to the next on timing behavior in all conditions.

IRI

Our MLR was modeled to predict IRI based on coordination and phase in two separate sessions. There were main effects of phase ($F_{1,11} = 196.85, P < 0.001, \eta 2 = 0.41$), coordination mode ($F_{1,11} = 111.9, P < 0.001, \eta 2 = 0.26$) and study session ($F_{1,11} = 19, P < 0.001, \eta 2 = 0.32$) on IRI. Moreover, a significant phase × study session interaction ($F_{1,11} = 25.56, P < 0.01, \eta 2 = 0.28$) was observed. A three-way interaction between phase, coordination mode, and study session has also been observed ($F_{2,22} = 21, P = 0.001, \eta 2 = 0.21$). A contrast effect between two sessions has also been observed ($F_{1,11} = 6.3, P = 0.001, \eta 2 = 0.14$) due to the practice effect. We also

observed a significant effect between synchronization and syncopation modes ($F_{1,11} = 12.13, P = 0.001, \eta 2 = 0.29$).

Session 1

To calculate the accuracy of synchronized and syncopated paced tapping, the average IRI (with SD) was measured, $987.26 \pm 53.2\ (ms)$ (mean$\pm$SD) and 1001.66 ± 56.36 (ms), respectively (see Figure 36). Moreover, the average IRI for continuation (with no metronome present) was estimated at 1013.37 ± 61.7 (ms) for synchronized tapping and 1030.75 ± 70.5 (ms) for syncopated tapping coordination modes.

By using post hoc tests, we observed significant differences between pacing and continuation in synchronization mode ($F_{1,11} = 11.22, P = 0.001, \eta 2 = 0.22$) and between phases in syncopation ($F_{1,11} = 14.39, P = 0.001, \eta 2 = 0.36$). We also observed a significant difference between synchronization and syncopation modes in pacing ($F_{1,11} = 6.33, P = 0.001, \eta 2 = 0.12$), and continuation ($F_{1,11} = 8.35, P = 0.001, \eta 2 = 0.19$) phases.

Session 2

For participants in the second session, across synchronized and syncopated pacing and continuation, the mean accuracy asynchronies were 996.5 ± 43.08 (ms)(mean $\pm$ SD) for synchronized pacing, 997.7 ± 47.62 (ms) for syncopated pacing, 997.13 ± 67.53 (ms) for synchronized continuation, and 1021.78 ± 75.72 (ms) for syncopated continuation, respectively, as illustrated in Figure 35. These results show that synchronization resulted in more accurate tapping compared to syncopation. Moreover, significant differences were observed between pacing and continuation for syncopation ($F_{1,11} = 13.97, P < 0.001, \eta 2 = 0.4$), and a significant difference between synchronization and syncopation in continuation phase has also been observed ($F_{1,11} = 14.09, P < 0.001, \eta 2 = 0.32$).

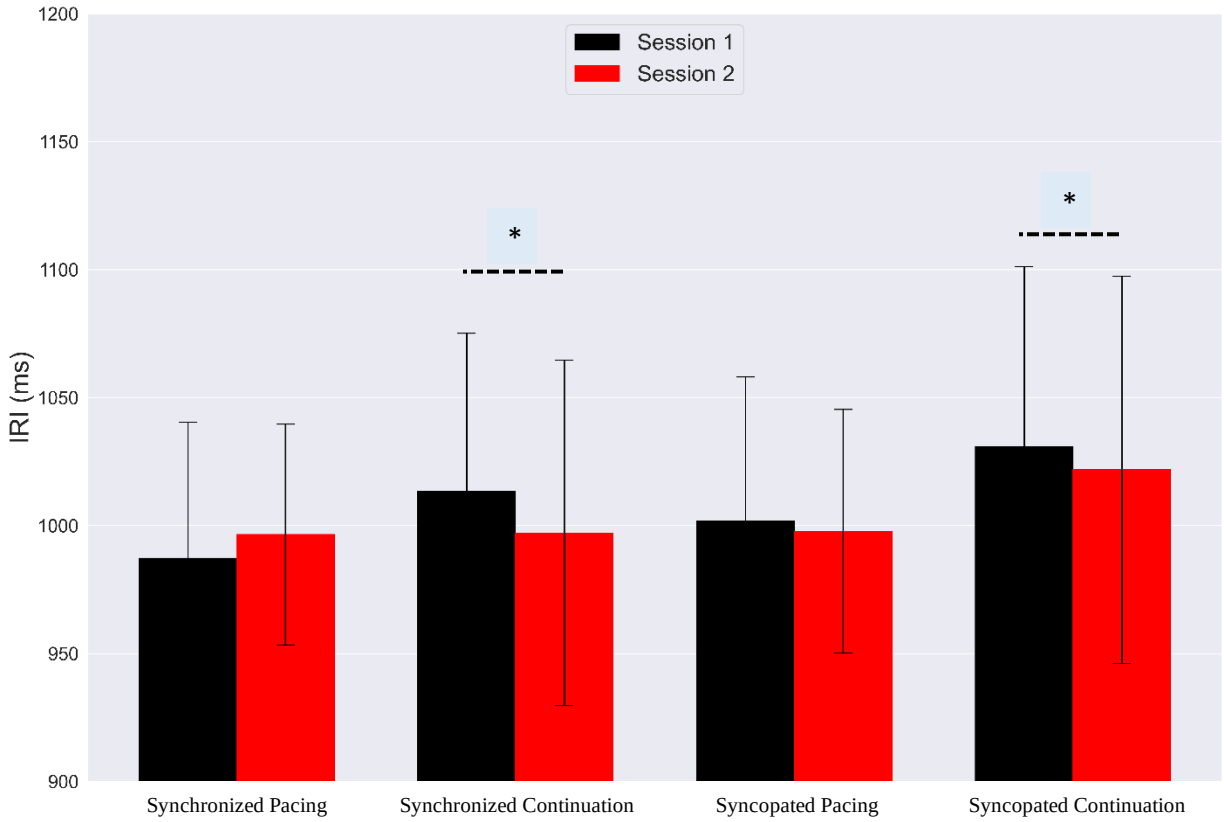

Figure 35. Averaged IRIs with SDs for each condition (i.e., synchronized pacing, synchronized continuation, syncopated pacing, and syncopated continuation) for block (black) and alternating designs (red). Dashed brackets indicate statistically significant comparisons between the two study sessions.

As shown in Figure 35, the contrast effects between two study sessions were observed for the continuation phase for synchronization ($F_{1,11} = 8.62, P = 0.001, \eta 2 = 0.3$) and syncopation ($F_{1,11} = 4.57, P < 0.02, \eta 2 = 0.19$). These contrasts demonstrate the training effects (in Session 2) impacting IRI timing behavior for continuation phase tapping.

Brain Activation Comparison

We estimated activated areas based on MNI coordinates and extracted Brodmann areas using the atlas viewer for fNIRS channel maps; Besides, DIPFIT2 plugin in EEGLAB was used to covert Talairach to MNI coordinates. We predefined 10 clusters for k-means clustering method for EEG source localization and then report the ones that are located inside Brodmann areas.

We report the results of our comparison of electrophysiological activity and hemodynamic responses for each timing condition given an alternating design using fNIRS (Session 1) and EEG (Session 2). We then explore the conditions that have spatial similarities within specified ROI (see section Materials and Methods-Region of Interest).

Based on the generated sensitivity maps, the fNIRS average channel maps for each timing condition are shown. Finally, we compare the hemodynamic results with neurally-based source localization within specified ROIs as obtained using DIPFIT, showing temporal ERPs, equivalent dipole clusters, and scalp maps.

Synchronized Pacing

Regions of significant $[Oxy - Hb]$ activated channels for the synchronized pacing condition are shown in Figure 36A and 37A. This figure identifies the only activated regions, which are primarily between FC3 and FC5 in the left STG area [MNI coordinates (-48, 13, 17), Brodmann area 44L] ($t_{FC3-FC5} = 7.06, q < 0.01$). However, the left hemisphere independent component (IC) cluster was a group of 10 ICs (mean=0.88, SD=0.47) from 12 subjects in auditory-locked ERP. The centroid was at MNI coordinates (-44, -23, 20) corresponding to left primary sensorimotor cortex (S1/M1) in Brodmann area 1L. See Figure 36B for the cluster components of equivalent dipoles as well as associated auditory-locked ERP plot and mean IC scalp map. The auditory locked P1, N1, and P2 components can be observed in the corresponding ERP waveshape.

Furthermore, the left hemisphere IC cluster was a group of 6 ICs (mean=-0.38, SD=0.87) from 12 subjects in response-locked ERP activity. The centroid was at MNI coordinates (-6, 2, 50) corresponding to left SMA in Brodmann area 6L. Figure 37B also shows the cluster components and mean equivalent dipoles as well as associated response-locked ERP plot and mean IC scalp map.

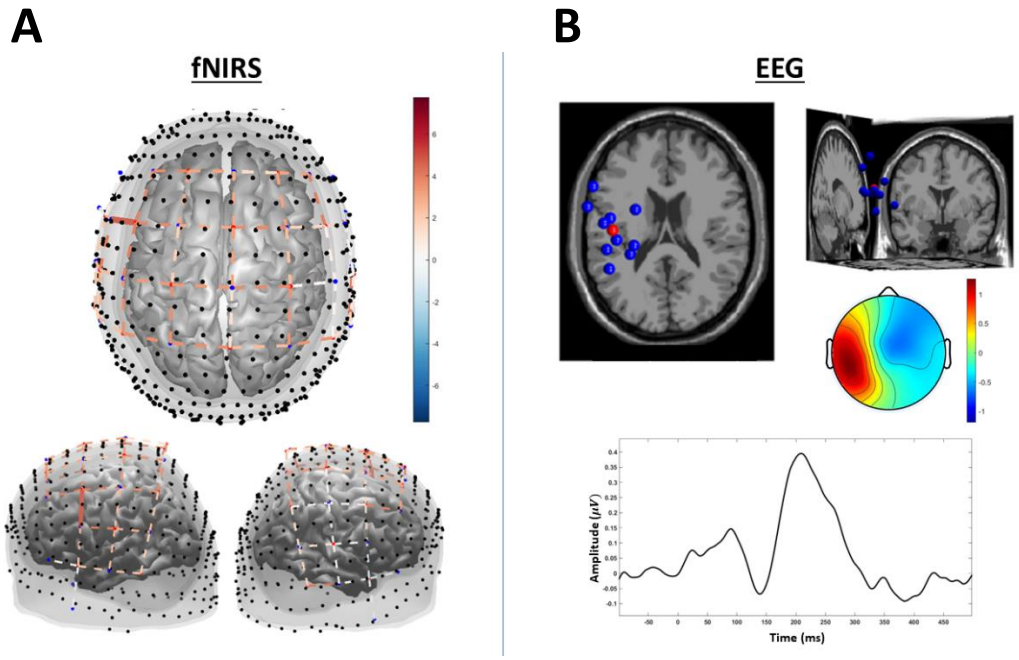

Figure 36. (A) Channel maps of the main effect (q<0.5) of synchronized pacing condition on [Oxy-Hb] hemodynamic activation obtained by synchronized pacing condition. (B) Top: Cluster component equivalent dipoles generated by stimulus-locked ERPs in blue and dipole centroid in red. Bottom: The averaged of IC components and cluster mean IC scalp map. Color bars in A and B represent the t-value and amplitude range, respectively.

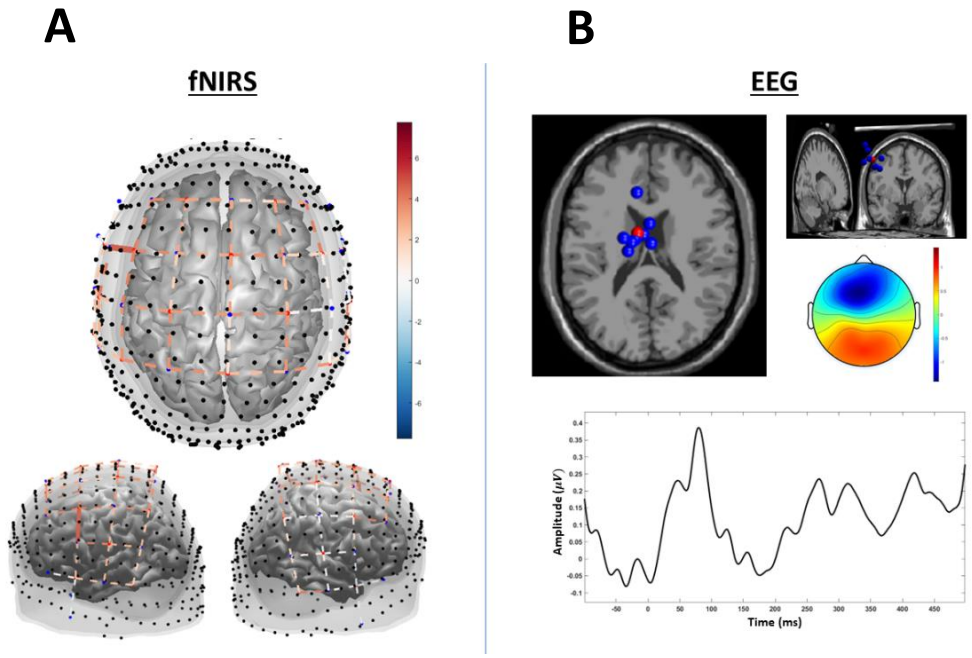

Figure 37. (A) Channel maps of the main effect (q<0.5) of synchronized pacing condition on [Oxy-Hb] hemodynamic activation obtained by synchronized pacing condition. (B) Top: Cluster component equivalent dipoles generated by response-locked ERPs in blue and dipole centroid in red. Bottom: The averaged of IC components and cluster mean IC scalp map. Color bars in A and B represent the t-value range and amplitude, respectively.

Synchronized Continuation

Regions of significant $[Oxy - Hb]$ activated channel for the synchronized continuation condition is shown in Figure 38A and 39A and reported in Table 4. The figures and table identify the activated regions in SMA/preSMA, left medal frontal gyrus, left premotor cortex (PLC), left STG, pre-SMA, left transverse temporal gyrus (TTG), and left STG. The fNIRS results for synchronized continuation also show broad activation in sensorimotor areas compared to the corresponding pacing phase.

However, the central hemisphere cluster was the groups of 18 ICs included 1-2 ICs per subject (mean=0.02, SD=0.4) from 12 subjects in auditory-locked EEG. The cluster centroids were at (MNI: -1, -17, 50) corresponding to premotor cortex and SMA, in Brodmann area 6. See Figure 38B for the cluster component and centroid equivalent dipole positions and mean IC scalp maps. Moreover, greater numbers of associated ICs within the cluster were observed in auditory locked continuation comparing to pacing phase although significantly less amplitude level ($F(1,11) = 2.6, q < 0.05$).

The central hemisphere cluster was the groups of 11 ICs included one ICs per subject (mean=0.04, SD=0.24) from 12 subjects in synchronized continuation response-locked ERPs. The cluster centroids were at (MNI: 8, -8, 67) corresponding to premotor

cortex and SMA, in Brodmann area 6. Figure 39B represents the cluster component and centroid equivalent dipole positions and mean IC scalp maps. Response-locked synchronized continuation showed spatially close activated area to centralized response-locked synchronized pacing (figure 37B). However, more associated ICs within the cluster were observed in response locked continuation comparing to pacing although significantly less averaged amplitude level ($F(1,11) = 1.9, q < 0.05$).

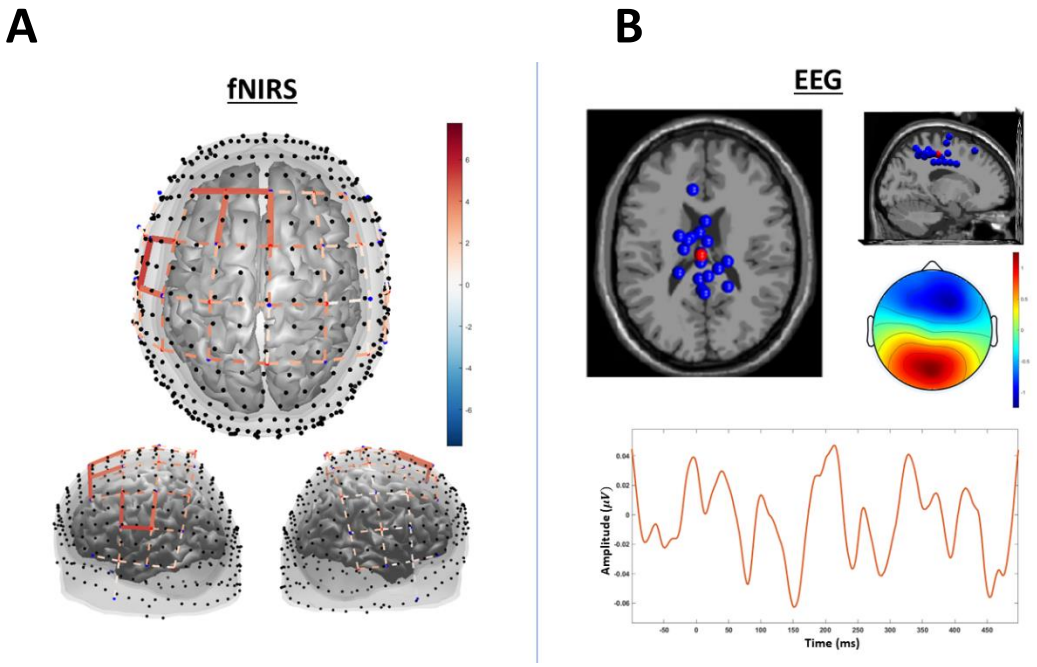

Figure 38. (A) Channel maps of the main effect (q<0.5) of synchronized continuation condition on [Oxy-Hb] hemodynamic activation obtained by synchronized pacing condition. (B) Top: Cluster component equivalent dipoles generated by stimulus-locked ERPs in blue and dipole centroid in red. Bottom: The averaged of IC components and cluster mean IC scalp map. Color bars in A and B represent the amplitude and t-value range, respectively.

A B

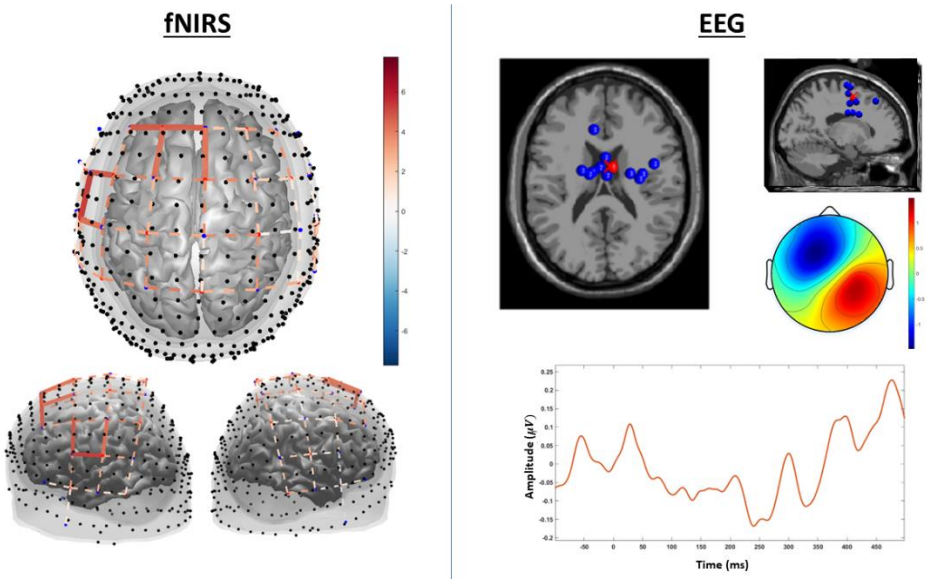

Figure 39. (A) Channel maps of the main effect (q<0.5) of synchronized continuation condition on [Oxy-Hb] hemodynamic activation obtained by synchronized pacing condition. (B) Top: Cluster component equivalent dipoles generated by response-locked ERPs in blue and dipole centroid in red. Bottom: The averaged of IC components and cluster mean IC scalp map. Color bars in A and B represent the t-value range and amplitude, respectively.

Table 4. Brain regions showing oxy-Hb hemodynamic significant effects in syncopated continuation condition in fNIRS alternating designs

Channel	X	Y	Z	Brodmann	t-value	p-value	Region
Cz-Fz	1	-1	52	6	5.8	0.03	SMA/preSMA
Fz-F1	-1	26	46	8	6	0.02	L-Medial Frontal
FC1-F1	-5	39	20	22	5.9	0.02	L-Premotor
FC3-FC5	-48	13	17	22	6.3	0.01	L-STG
F1-F3	-25	10	46	6&8	6.1	0.02	L-preSMA
FC5-C5	-52	-20	7	41&42	7.43	0.01	L-TTG
C3-C5	-57	-20	1	22	5.3	0.05	LSTG

Syncopated Pacing

Figures 40A depicts the activated channel maps of $[Oxy - Hb]$ in the syncopated pacing condition. Table 5 also represent the activated channels with the estimated coordinates (MNIs) and Brodmann area information. As shown, broad areas of the brain including MTG, STG, PTG, ATG, S1/M1, PMC, SMA/pre-SMA are associated with syncopated pacing measuring hemodynamic response. Our observation of bilateral activation is consistent with findings from our previous study (Rahimpour et al., 2020).

Moreover, the central and right hemisphere clusters of auditory-locked neural activity were the group of 19 ICs (mean=0.25, SD=0.21) and 4 ICs (mean=-0.1, SD=0.26), respectively. This centralized cluster included 1-2 ICs per subject from 12 subjects. The central and right cluster centroids were at (MNI: 5, -18, 61) corresponding to SMA and premotor cortex area, in Brodmann area 6 and at right STG area (MNI: 54, -8, -10) in Brodmann 22, respectively. See Figure 40B for the cluster component and centroid equivalent dipole positions and mean IC scalp maps. P1-N1 and P2 components are observed in auditory locked ERPs. However, no cluster of dipoles was observed in response-locked ERPs in the syncopated pacing condition.

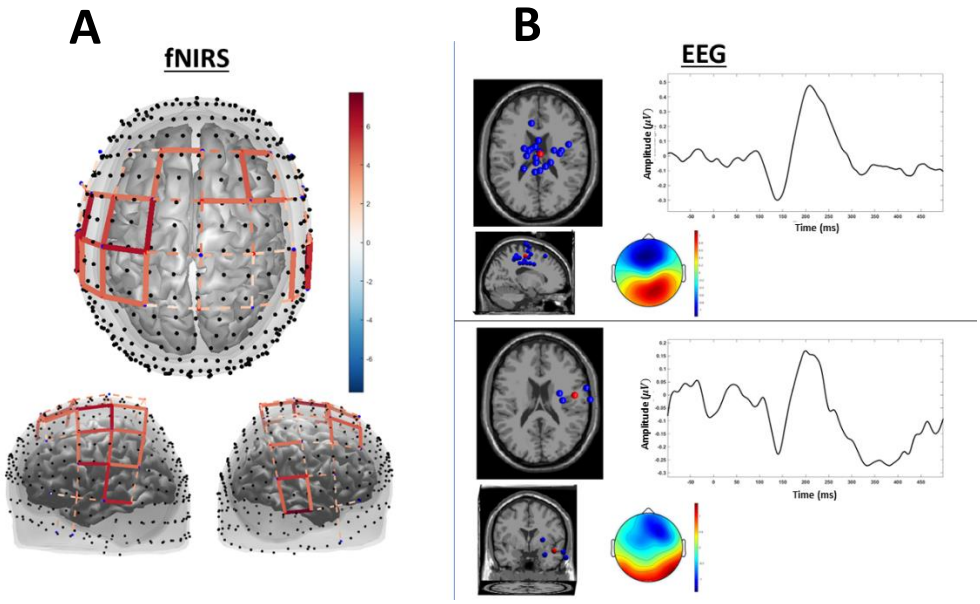

Figure 40. (A) Channel maps of the main effect (q<0.5) on [Oxy-Hb] hemodynamic activation obtained by syncopated pacing condition. (B) Top: Cluster component equivalent dipoles generated by stimulus-locked ERPs in blue and dipole centroid in red. Bottom: The averaged of IC components and cluster mean IC scalp map. Color bars in A and B represent the t-value and amplitude range, respectively.

Table 5. Brain regions showing oxy-Hb hemodynamic significant effects in syncopated pacing condition in fNIRS alternating designs

Channel	X	Y	Z	Brodmann	t-value	p-value	Region
T8-TP8	60	-27	-9	21	7.4	0.01	R-MTG
TP8-CP6	51	-33	34	40	6.1	0.03	R-SMG
CP6-C6	50	-21	7	41	6.2	0.03	R-PTG
C6-T8	50	-23	-9	21&41	6.1	0.03	R-ATG
CP4-C4	41	-32	46	2	5.9	0.04	R-S1/M1
FC2-FC4	28	-1	51	6	5.7	0.04	R-PMC
F2-FC2	25	13	48	6&8	6.1	0.03	R-SMA/preSMA
F2-F4	21	25	43	8	5.3	0.05	R-SMA
Fz-F1	-13	27	51	8	5.2	0.05	L-SMA
F1-FC1	-20	-4	51	6&8	5.3	0.05	L-SMA/preSMA
FC1-C1	-32	-10	50	4&6	7.3	0.01	L-PMC/SMA
C1-CP1	-14	-33	48	5	5.1	0.05	L-S1
FC1-FC3	-28	-2	52	6	5	0.05	L-PMC/SMA
C1-C3	-22	-25	48	4	6.9	0.01	L-S1/M1
CP1-CP3	-40	-27	47	2	5.3	0.05	Primary Sensory
FC3-C3	-36	-10	46	4	6.2	0.02	L-PMC
C3-CP3	-53	-32	33	40	5.7	0.04	L-SMG
C3-C5	-46	-26	50	2&42	5.8	0.04	Somatosensory
C5-CP5	-53	-32	33	40	5.3	0.05	L-Supramarginal
C5-T7	-52	-19	7	41&42	7	0.01	L-PTG
T7-TP7	-59	-25	-13	21	7.1	0.01	L-MTG

Syncopated Continuation

Figure 41A represents the activated channels of $[Oxy - Hb]$ in the syncopated continuation condition. Estimated coordinates for activated channels is also shown in Table 6. As shown, broad areas of the brain are associated with syncopated continuation as measured by hemodynamic response (cortical areas: MTG, opercular, SMA/preSMA, PMC, PTG, STG, IFG and temporal pole). Our observation is consistent with our previous study (Rahimpour et al., 2020).

Although no cluster of dipoles was observed in auditory-locked neurophysiological activity for the syncopated continuation condition, we observed a left hemisphere cluster of the group of 8 ICs (mean=0.15, SD=0.34) from 12 subjects in response-locked ERPs. The cluster centroids were at (MNI: -5, -13, 51) corresponding to left SMA and PMC area, in Brodmann area 6. See Figure 41B for the cluster component and centroid equivalent dipole positions and mean IC scalp maps.

A **B**

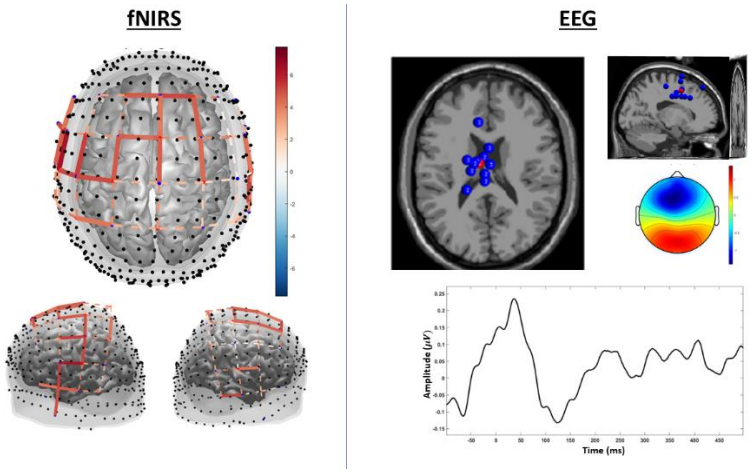

Figure 41. (A) Channel maps of the main effect (q<0.5) of syncopated continuation condition on [Oxy-Hb] hemodynamic activation obtained by synchronized pacing condition. (B) Top: Cluster component equivalent dipoles generated by response-locked ERPs in blue and dipole centroid in red. Bottom: The averaged of IC components and cluster mean IC scalp map. Color bars in A and B represent the t-value range and amplitude, respectively.

Table 6. Brain regions showing oxy-Hb hemodynamic significant effects in syncopated continuation condition in fNIRS alternating designs

Channel	X	Y	Z	Brodmann	t-value	p-value	Region
T8-TP8	60	-27	-9	21	6.4	0.03	R-MTG
C6-FC6	49	12	17	44	6.1	0.02	R-Opercular
F2-FC2	25	13	48	6&8	6.3	0.02	R-SMA/preSMA
FC2-C2	28	-1	51	6	6.3	0.02	R-PMC/SMA
Fz-F2	22	26	45	8	6.4	0.02	R-preSMA
Fz-FCz	4	26	45	8	6	0.03	preSMA
Cz-FCz	-6	-21	70	6	6.1	0.03	PMC/SMA
Fz-F1	-13	27	51	8	5.9	0.04	L-SMA
FC1-FCz	-15	-21	70	6	6	0.03	L-PMC
FC1-C1	-32	-10	50	4&6	6.2	0.03	L-PMC/SMA
C1-C3	-22	-25	48	4	6.4	0.02	L-S1/M1
CP1-CP3	-40	-27	47	2	5.1	0.05	Primary Sensory
FC3-C3	-36	-10	46	4	6.8	0.01	L-PMC
C3-C5	-46	-26	50	2&42	6.4	0.02	Somatosensory
FC5-C5	-55	-19	4	41&42	7.2	0.01	L-PTG
T7-FT7	-49	-2	-11	22	6.2	0.03	L-STG
FC5-FT7	-48	13	17	44	6.4	0.03	L-Opercular
F7-FT7	-40	31	-13	47	6.2	0.02	L-IFG
FT7-FT9	-43	13	-30	38	6.5	0.02	L-Temporal pole

Discussion

A large body of research has advanced our knowledge about how temporal mechanisms control behavior, and focus has shifted to whether and how timing is represented in the central nervous system. Studies of finger tapping provide information about the mental timing system that is not confounded with more complex motor actions or feedback mechanisms (Ivry & Keele, 1989; Sergent, 1993; Wing & Kristofferson, 1973). In the finger-tapping task used here, individuals tapped their index finger either in or out of synchrony (i.e., synchronization vs. syncopation) given auditory cues presented at a constant interval. Further knowledge is gained by having participants continue their tapping despite cessation of the auditory cue (i.e., continuation). In the case of continuation, performance depends on a mental representation of the interval duration and thus reveals essential information about internal timing mechanisms. Finger tapping tasks have revealed a lot about internal timing mechanisms (Balasubramaniam et al., 2004; Cluff et al., 2010; Ross & Balasubramaniam, 2014; Studenka et al., 2012). We used a modified finger tapping task (two timing conditions: synchronization-continuation/syncopation-continuation) as a stimulus to examine the activations of cortical areas. We found that the finger-tapping task recruited primary sensorimotor cortices (S1 and M1), supplementary motor area (SMA), premotor cortex (PMC), and inferior parietal cortex (Witt et al., 2008). We also compared the two imaging modalities to determine whether EEG and fNIRS can localize cortical activation resulting from this task equally well. An additional aim was to characterize the responses obtained using the different modalities to identify the unique strengths of each for providing spatial and temporal information about brain activity.

While our goal was to explore ICA-DIPFIT source localization and compare it to localization observed via fNIRS, we instead observed a training effect, such that performance was much more accurate during the EEG data collection than during the fNIRS data collection. We were able to demonstrate that cortical areas are recruited in finger-tapping in direct relation to the complexity of the timing behavior being performed. Moreover, we found that both neuroimaging methods recruited sensorimotor areas and observed some activation clusters in frontal, parietal, and temporal areas depending on the degree of the training effect, which varied across behavioral timing conditions. However, given the training effect observed from the first to second imaging session, we are not able to make any claims about the spatial localization accuracy of the source modeling approach tested here.

One problem for DIPFIT analysis is that the number of clusters are pre-defined and, consequently, we are limited to the number of ICs assigned to the pre-defined cluster. Future work should explore standardized low-resolution electromagnetic tomographic analysis (sLORETA) since in this way we are able to feed extracted channels and timepoints to the model (see Chapter 3), which would generate more robust and reliable source localization findings. Another limitation was that we did not quantitatively compare the spatial accuracy across the two imaging modalities, and thus must provide qualitative descriptions based on estimated cortical coordinates extracted from the EEG and fNIRS findings. This is an open question for future studies. Lastly, an important limitation was that all participants participated first in the fNIRS session and then in the EEG session, producing practice effects specific to the EEG data. This was

because participants did not want to have to wash their hair in the middle of the day (to remove EEG gel) between the two testing sessions. We thus observed training effects in both our behavioral and neural results in Session 2, which was always the EEG session. For future work, we strongly recommend doing multimodal EEG-fNIRS data collection simultaneously, or at least recommend counterbalancing the order of fNIRS and EEG sessions in order to control for training effects specific to one or the other imaging modality.

Conclusion

This research provides initial insight into the ability of fNIRS system to validate the results obtained from ICA-DIPFIT source localization of timing-based action. We investigated and compared behavioral and brain-based findings obtained during performance of a systematically varied tapping task by using two neuroimaging methods, fNIRS and EEG, across two testing sessions. We found that finger-tapping experience plays an important role in behavioral performance, as well as in both hemodynamic and neural activation. The two imaging modalities showed distinct patterns of cortical activation due to the training effects we have described. We observed the training effect on behavior too: on mean accuracy asynchrony across all four timing conditions. However, training impact IRI only for the continuation phase of the two modes of tapping. Mean accuracy asynchrony provided a more detailed view of the training effects in action-based timing behavior. Our findings show that training leads to improved performance on the complex behaviors and increasingly automated performance on the less complex ones. These effects manifested in different brain-based patterns of activation across the two imaging modalities as well.

References

Abdelnour, A. F., & Huppert, T. (2009). Real-time imaging of human brain function by near-infrared spectroscopy using an adaptive general linear model. *Neuroimage*, *46*(1), 133–143.

Baillet, S. (2001). *Electromagnetic Brain Mapping*. *February 2013*. https://doi.org/10.1109/79.962275

Balasubramaniam, R., Wing, A. M., & Daffertshofer, A. (2004). Keeping with the beat: Movement trajectories contribute to movement timing. *Experimental Brain Research*, *159*(1), 129–134. https://doi.org/10.1007/s00221-004-2066-z

Bast, T., Oezkan, O., Rona, S., Stippich, C., Seitz, A., Rupp, A., Fauser, S., Zentner, J., Rating, D., & Scherg, M. (2004). EEG and MEG source analysis of single and averaged interictal spikes reveals intrinsic epileptogenicity in focal cortical dysplasia. *Epilepsia*, *45*(6), 621–631. https://doi.org/10.1111/j.0013-9580.2004.56503.x

Bell, A. J., & Sejnowski, T. J. (1989). *An information-maximisation approach to blind separation and blind deconvolution*. *1034*(February 1995), 1004–1034.

Boonstra, T. W., Daffertshofer, A., Peper, C. E., & Beek, P. J. (2006). Amplitude and phase dynamics associated with acoustically paced finger tapping. *Brain Research*, *1109*(1), 60–69.

Boonstra, T. W., Daffertshofer, A., Peper, C. E., & Beek, P. J. (2006). *Amplitude and phase dynamics associated with acoustically paced finger tapping*. *09*. https://doi.org/10.1016/j.brainres.2006.06.039

Bortfeld, H., Fava, E., & Boas, D. A. (2009). Identifying cortical lateralization of speech processing in infants using near-infrared spectroscopy. *Developmental Neuropsychology*, *34*(1), 52–65.

Bortfeld, H., Wruck, E., & Boas, D. A. (2007). Assessing infants' cortical response to speech using near-infrared spectroscopy. *NeuroImage*, *34*(1), 407–415. https://doi.org/10.1016/j.neuroimage.2006.08.010

Cluff, T., Gharib, T., & Balasubramaniam, R. (2010). Attentional influences on the performance of secondary physical tasks during posture control. *Experimental Brain Research*, *203*(4), 647–658. https://doi.org/10.1007/s00221-010-2274-7

Collective, B. M., & Shaw, D. (2012). Makey Makey: improvising tangible and nature-based user interfaces. *Proceedings of the Sixth International Conference on Tangible, Embedded and Embodied Interaction*, 367–370.

Cui, X., Bray, S., Bryant, D. M., Glover, G. H., & Reiss, A. L. (2011). A quantitative comparison of NIRS and fMRI across multiple cognitive tasks. *NeuroImage*, *54*(4), 2808–2821. https://doi.org/10.1016/j.neuroimage.2010.10.069

Cutini, S., Scarpa, F., Scatturin, P., Acqua, R. D., & Zorzi, M. (2014). *Number – Space Interactions in the Human Parietal Cortex : Enlightening the SNARC Effect with Functional Near-Infrared Spectroscopy*. *February*, 444–451. https://doi.org/10.1093/cercor/bhs321

Deligniéres, D., Torre, K., & Lemoine, L. (2009). Long-range correlation in synchronization and syncopation tapping: A linear phase correction model. *PLoS ONE*, *4*(11). https://doi.org/10.1371/journal.pone.0007822

Delorme, A., & Makeig, S. (2004). *EEGLAB : an open source toolbox for analysis of single-trial EEG dynamics including independent component analysis*.

Holmes, C. J., Hoge, R., Collins, L., Woods, R., Toga, A. W., & Evans, A. C. (1998). Enhancement of MR images using registration for signal averaging. *Journal of computer assisted tomography*, *22*(2), 324-333.

Hoppes, C. W., Sparto, P. J., Whitney, S. L., Furman, J. M., & Huppert, T. J. (2018). *Functional near-infrared spectroscopy during optic flow with and without fixation*. 1–14.

Hoshi, Y. (2003). Functional near-infrared optical imaging: Utility and limitations in human brain mapping. *Psychophysiology*, *40*(4), 511–520. https://doi.org/10.1111/1469-8986.00053

Hoshi, Y., & Tamura, M. (1997). Near-infrared optical detection of sequential brain activation in the prefrontal cortex during mental tasks. *NeuroImage*, *5*(4 I), 292–297. https://doi.org/10.1006/nimg.1997.0270

Hyvärinen, A., & Oja, E. (2000). *Independent Component Analysis : Algorithms and Applications*. *1*(1).

Iversen, J. R., & Makeig, S. (2014). MEG/EEG data analysis using EEGLAB. *Magnetoencephalography*, *199–212*.

Ivry, R. B., & Keele, S. W. (1989). Timing Functions of The Cerebellum. *Journal of Cognitive Neuroscience*, *1*(2), 136–152. https://doi.org/10.1162/jocn.1989.1.2.136

Jahani, S., Berivanlou, N. H., Rahimpour, A., & Setarehdan, S. K. (2015). *Attention level quantification during a modified stroop color word experiment : An fNIRS based study*. *November*, 25–27.

Jantzen, K. J., Steinberg, F. L., & Kelso, J. A. S. (2004). Brain networks underlying human timing behavior are influenced by prior context. *Proceedings of the National Academy of Sciences*, *101*(17), 6815–6820. https://doi.org/10.1073/pnas.0401300101

Jatoi, M. A., Kamel, N., Malik, A. S., & Faye, I. (2014). EEG based brain source localization comparison of sLORETA and eLORETA. *Australasian Physical and Engineering Sciences in Medicine*, *37*(4), 713–721. https://doi.org/10.1007/s13246-014-0308-3

Jung, T. P., Makeig, S., Westerfield, M., Townsend, J., Courchesne, E., & Sejnowski, T. J. (2000). Removal of eye activity artifacts from visual event-related potentials in normal and clinical subjects. *Clinical Neurophysiology*, *111*(10), 1745–1758. https://doi.org/10.1016/S1388-2457(00)00386-2

Jung, W. Y., Pacia, S. V, & Devinsky, R. (1999). Neocortical temporal lobe epilepsy: intracranial EEG features and surgical outcome. *Journal of Clinical Neurophysiology : Official Publication of the American Electroencephalographic Society*, *16*(5), 419–425. https://doi.org/10.1097/00004691-199909000-00003

Kameyama, M., Fukuda, M., Yamagishi, Y., Sato, T., Uehara, T., Ito, M., Suto, T., & Mikuni, M. (2006). Frontal lobe function in bipolar disorder: A multichannel near-infrared spectroscopy study. *NeuroImage*, *29*(1), 172–184. https://doi.org/10.1016/j.neuroimage.2005.07.025

Kasess, C. H., Windischberger, C., Cunnington, R., Lanzenberger, R., Pezawas, L., & Moser, E. (2008). *The suppressive influence of SMA on M1 in motor imagery revealed by fMRI and dynamic causal modeling*. 1–10. https://doi.org/10.1016/j.neuroimage.2007.11.040

Kavanagh, R. N., Darcey, T. M., Lehmann, D., & Fender, D. H. (1978). *Evaluation of Methods for Three-Dimensional Localization of Electrical Sources in the*. *5*, 421–429.

Kobayashi, E., Bagshaw, A. P., Grova, C., Dubeau, F., & Gotman, J. (2006). Negative BOLD responses to epileptic spikes. *Human Brain Mapping*, *27*(6), 488–497. https://doi.org/10.1002/hbm.20193

Koles, Z. J. (1998). *Trends in EEG source localization*. *106*, 127–137.

Kuboyama, N., Nabetani, T., Shibuya, K.-I., Machida, K., & Ogaki, T. (2004). The effect of maximal finger tapping on cerebral activation. *Journal of Physiological Anthropology and Applied Human Science*, *23*(4), 105–110. https://doi.org/JST.JSTAGE/jpa/23.105 [pii]

Lee, T.-W., Lewicki, M. S., & Sejnowski, T. J. (2000). ICA mixture models for unsupervised classification of non-Gaussian classes and automatic context switching in blind signal separation. *IEEE Transactions on Pattern Analysis and Machine Intelligence*, *22*(10), 1078–1089.

Lin, C. C., Barker, J. W., Sparto, P. J., Furman, J. M., & Huppert, T. J. (2017). Functional near-infrared spectroscopy (fNIRS) brain imaging of multi-sensory integration during computerized dynamic posturography in middle-aged and older adults. *Experimental Brain Research*, *0*(0), 0. https://doi.org/10.1007/s00221-017-4893-8

Makeig, S., J. Bell., A., Jung, T.-P., & Sejnowski, T. J. (1996). Independent Component Analysis of Electroencephalographic Data. *Advances in Neural Information Processing Systems*, *8*, 145–151. https://doi.org/10.1109/ICOSP.2002.1180091

Makeig, S., Makeig, S., Debener, S., Debener, S., Onton, J., Onton, J., Delorme, A., & Delorme, A. (2004). Mining event-related brain dynamics. *Trends in Cognitive Sciences*, *8*(5), 204–210. https://doi.org/10.1016/j.tics.2004.03.008

Makeig, S., Westerfield, M., Townsend, J., Jung, T. P., Courchesne, E., & Sejnowski, T. J. (1999). Functionally independent components of early event-related potentials in a visual spatial attention task. *Philosophical Transactions of the Royal Society of London. Series B, Biological Sciences*, *354*, 1135–1144. https://doi.org/10.1098/rstb.1999.0469

Michel, C. M., Murray, M. M., Lantz, G., Gonzalez, S., Spinelli, L., & Grave De Peralta, R. (2004). EEG source imaging. In *Clinical Neurophysiology* (Vol. 115, Issue 10, pp. 2195–2222). https://doi.org/10.1016/j.clinph.2004.06.001

Montes-Restrepo, V., Van Mierlo, P., Strobbe, G., Staelens, S., Vandenberghe, S., & Hallez, H. (2014). Influence of skull modeling approaches on EEG source localization. *Brain Topography*, *27*(1), 95–111. https://doi.org/10.1007/s10548-013-0313-y

Mullen, T. R., Kothe, C. A., Chi, Y. M., Ojeda, A., Kerth, T., Makeig, S., ... & Cauwenberghs, G. (2015). Real-time neuroimaging and cognitive monitoring using wearable dry EEG. *IEEE Transactions on Biomedical Engineering*, *62*(11), 2553-2567.

Okamoto, M., Dan, H., Shimizu, K., Takeo, K., Amita, T., Oda, I., ... & Dan, I. (2004). Multimodal assessment of cortical activation during apple peeling by NIRS and fMRI. *Neuroimage*, *21*(4), 1275-1288.

Oostendorp, T. F., & Oosterom, A. Van. (1996). *The Surface Laplacian of the Potential : Theory and Ap*. *43*(4), 394–405.

Pollonini, L., Olds, C., Abaya, H., Bortfeld, H., Beauchamp, M. S., & Oghalai, J. S. (2014). Auditory cortex activation to natural speech and simulated cochlear implant speech measured with functional near-infrared spectroscopy. *Hearing Research*, *309*, 84–93. https://doi.org/10.1016/j.heares.2013.11.007

Rahimpour, A., Dadashi, A., Soltanian-zadeh, H., Member, S., & Setarehdan, S. K. (2017). *CLASSIFICATION OF FNIRS BASED BRAIN HEMODYNAMIC RESPONSE TO*. *Ipria*, 113–117.

Rahimpour, A., Noubari, H. A., & Kazemian, M. (2018). A case-study of NIRS application for infant cerebral hemodynamic monitoring: A report of data analysis for feature extraction and infant classification into healthy and unhealthy. *Informatics in Medicine Unlocked*, *11*, 44–50. https://doi.org/10.1016/J.IMU.2018.04.001

Rahimpour, A., Pollonini, L., Comstock, D., Balasubramaniam, R., & Bortfeld, H. (2020). Tracking Differential Activation of Primary and Supplementary Motor Cortex Across Timing Tasks: An fNIRS Validation Study. *Journal of Neuroscience Methods*, 108790.

Raichle, M. E. (1994). Images of the mind: Studies with modern imaging techniques. *Annual review of psychology*, *45*, 333.

Rao, S. M., Harrington, D. L., Haaland, K. Y., Bobholz, J. A., Cox, R. W., & Binder, J. R. (1997). Distributed neural systems underlying the timing of movements. *The Journal of Neuroscience : The Official Journal of the Society for Neuroscience*, *17*(14), 5528–5535.

Repp, B. H. (2005). Sensorimotor synchronization: A review of the tapping literature. In *Psychonomic Bulletin and Review* (Vol. 12, Issue 6, pp. 969–992). https://doi.org/10.3758/BF03206433

Repp, B. H., & Su, Y. H. (2013). Sensorimotor synchronization: A review of recent research (2006-2012). *Psychonomic Bulletin and Review*, *20*(3), 403–452. https://doi.org/10.3758/s13423-012-0371-2

Ross, J. M., & Balasubramaniam, R. (2014). Physical and neural entrainment to rhythm: human sensorimotor coordination across tasks and effector systems. *Frontiers in Human Neuroscience*, *8*. https://doi.org/10.3389/fnhum.2014.00576

Sato, T., Ito, M., Suto, T., Kameyama, M., Suda, M., Yamagishi, Y., Ohshima, A., Uehara, T., Fukuda, M., & Mikuni, M. (2007). Time courses of brain activation and their implications for function: A multichannel near-infrared spectroscopy study during finger tapping. *Neuroscience Research*, *58*(3), 297–304. https://doi.org/10.1016/j.neures.2007.03.014

Sergent, J. (1993). Mapping the musician brain. *Human Brain Mapping*, *1*(1), 20–38. https://doi.org/10.1002/hbm.460010104

Serrien, D. J. (2008). *The neural dynamics of timed motor tasks : evidence from a synchronization – continuation paradigm*. *27*(December 2007), 1553–1560. https://doi.org/10.1111/j.1460-9568.2008.06110.x

Song, J., Davey, C., Poulsen, C., Luu, P., Turovets, S., Anderson, E., Li, K., & Tucker, D. (2015). EEG source localization: Sensor density and head surface coverage. *Journal of Neuroscience Methods*, *256*, 9–21. https://doi.org/10.1016/j.jneumeth.2015.08.015

Strangman, G., Culver, J. P., Thompson, J. H., & Boas, D. A. (2002). A quantitative comparison of simultaneous BOLD fMRI and NIRS recordings during functional brain activation. *Neuroimage*, *17*(2), 719-731.

Studenka, B. E., Zelaznik, H. N., & Balasubramaniam, R. (2012). The distinction between tapping and circle drawing with and without tactile feedback: An examination of the sources of timing variance. *Quarterly Journal of Experimental Psychology*, *65*(6), 1086–1100. https://doi.org/10.1080/17470218.2011.640404

Tsuzuki, D., & Dan, I. (2014). Spatial registration for functional near-infrared spectroscopy: From channel position on the scalp to cortical location in individual and group analyses. *NeuroImage*, *85*, 92–103. https://doi.org/10.1016/J.NEUROIMAGE.2013.07.025

Vorobyov, S., & Cichocki, A. (2002). *Blind noise reduction for multisensory signals using ICA and subspace filtering , with application to EEG analysis*. *303*, 293–303. https://doi.org/10.1007/s00422-001-0298-6

Wing, A. M., & Kristofferson, A. B. (1973). Response delays and the timing of discrete motor responses. *Perception & Psychophysics*, *14*(1), 5–12. https://doi.org/10.3758/BF03198607

Witt, S. T., Laird, A. R., & Meyerand, M. E. (2008). Functional neuroimaging correlates of finger-tapping task variations: an ALE meta-analysis. *Neuroimage*, *42*(1), 343-356.

Woodman, G. F. (2010). A brief introduction to the use of event-related potentials in studies of perception and attention. *Attention, Perception, & Psychophysics*, *72*(8), 2031-2046.

Chapter 5

Summary

Findings from the experiments reported here provide insight into the influence of contextual action-based timing on behavior and brain (both hemodynamic and neural). The aim of these studies was to characterize how behavioral performance under different levels of difficulty corresponds to brain-based neurophysiological activity. More specifically, the work investigated how action-based timing is influenced by maintenance and coordination dynamics and how different context-dependent parameters modulate both behavioral and brain-based responses.

Procedures used to elicit both behavioral and neurophysiological data to address particular cognitive questions can impact the nature of the data collected. With that in mind, Chapter 2 interrogated the dynamic nature of rhythmic entrainment as reflected in both behavioral and brain responses given different rhythmic patterns of motor coordination as introduced via the pacing-continuation task. Specifically, data collected using the same paradigm in which responses were compared across a rhythmically blocked versus a rhythmically alternating study design highlighted the dynamic nature of action-based timing behavior. Results revealed that there are better and worse timing conditions for rhythmic entrainment to occur, and that the differences between them can be relatively subtle.

Overall, the behavioral results point to the substantial influence of study design on complex timing behavior. Results show that the complexity and difficulty of the design likewise impacts the degree and breadth of neural activation elicited. The significantly higher levels of activity we observed in fNIRS data across all four tapping conditions in the block design may reflect development of an internal representation of the timing patterns (i.e., entrainment), something that was not possible for participants in the alternating design. Thus, our findings demonstrate the critical impact of a study's design on the degree of rhythmic entrainment that can be achieved given different forms of coordination dynamics. Likewise, neural correlates of timing behavior reflect context-dependent parameters.

Our results provide insight into the influence of the broader experimental context on timing behavior and the underlying neural activity that supports it, an interpretation consistent with several previous findings (Jantzen et al., 2004, 2007; Rahimpour et al., 2020). Thus, representation of timing information is formed in a context-dependent manner, with the introduction of different cognitive states or expectations, as well as difficulty levels, impacting behavioral performance and the corresponding neural engagement supporting it. Here we have observed that it takes time to develop an internal timing representation and thus entrain motorically to complex rhythmic stimuli.

We then used EEG to investigate moment-to-moment neurological activity during the alternating design task, relating findings to those on participants' behavioral performance. Chapter 3 exploited the pacing-continuation forms of coordination dynamics given alternating patterns of synchronized and syncopated tapped to further elucidate the neural basis of timing behavior. Task-induced neural activation manifested as auditory- and motor-evoked potentials over a broad area of central, temporal and frontal electrode sites, corresponding to those regions in the cortex.

Moreover, we found that individual differences in rhythmic entrainment as reflected in the cortex predicted behavior in context-based timing behavior using a deep learning approach. Our study highlighted the strong coupling of behavioral performance accuracy and single-trial neurophysiological activity. These results revealed a direct link between our cortical and behavioral measures, thus providing evidence that single trial brain activity has predictive relevance to action-based timing behavior. Thus, this is an initial demonstration that neurophysiological correlates of sensorimotor processes exhibit distinct markers that can be used to predict different degrees of action-based timing accuracy.

The research reported in Chapter 4 provides insight into the ability of fNIRS to validate the results obtained using an EEG ICA-DIPFIT source localization approach as applied to the same timing behavior. We compared both behavioral and brain-based findings using the two neuroimaging modalities (fNIRS and EEG), with data collected across two identical testing sessions with the same participants completing both on the same day. Not surprisingly, we found that experience with the action-based timing behavior significantly impacted participants' behavioral performance accuracy from one session to the next, as well as their brain-based responsivity while completing the task. Importantly, both neuroimaging modalities showed the impact of different cognitive states/expectations and levels of difficulty for the participants, as manifested in cortical activation differences given prior experience or no such experience. We observed a training effect on mean accuracy asynchrony across all timing conditions, with some nuanced differences between the two measures of accuracy we employed. The findings support our conclusion that training significantly improves performance of more complex timing behaviors, as well as helps "automate" less complex behaviors, and that such differences are manifested both behaviorally and in the brain.

Developmental Implication

The role of time/timing is relevant to a wide range of different cognitive skills and deficiencies. In this study, we scrutinized the role of timing in perception and action in adults. Time/timing representations arise from sensorimotor coding and are apparent in different actions, reflecting different coordination dynamics depending on contextual factors. This point of view was supported by the philosopher Guyau (1890) and was further described by Piaget (1946) in his description of sensorimotor development. More recently, the protracted nature of sensorimotor development has been validated by researchers working with children (e.g. Droit, 1995; Droit-Volet & Rattat, 1999; Rattat & Droit Volet, 2002; McCormack & Hoerl, 2017), as well as those working with adults (Cassenti, 2011; Fujioka et al., 2012; Kononowicz & Van Rijn, 2015; Manning & Schutz, 2013; Morillon et al., 2014). Interestingly, Monier et al (2019) found that the beneficial effects of action on timing are greater in young children than adults. For example, synchronized action during learning systematically helped timing performance for younger children in particular. This finding highlights the degree to which action itself shapes the cognitive representation of interval duration, helping children construct an independent and flexible representation of time. With development, this produces the strongly coupled sensorimotor coding for action and time observed in adults across a wide range of tasks and conditions.

Here we have characterized the neural bases of voluntary movement for finger tapping in adults. In contrast to adults, imaging studies show that children have relatively greater activation in left SM1 and extending into bilateral SMA, reflecting compensation for an underdeveloped motor system and relatively reduced experience in the execution of voluntary movement (Turesky et al., 2018).

In contrast, fMRI findings from the same task with adults reveal stronger recruitment of the basal ganglia, reflecting a developmental shift to more subcortical processing in adulthood. Interestingly, both pre-SMA/SMA and basal ganglia are associated with initiation of movement and motor control, respectively, particularly with complex movements. This suggests a different role in children and adults, as development of motor control of voluntary movement proceeds across the lifespan (Turesky et al., 2018).

In comparisons of child and adult performance on the continuation paradigm, both show activation in the primary motor cortex, premotor cortex, and cerebellum. However, overall patterns of activation were different, with adults demonstrating much more deactivation, particularly in the occipital and frontal cortices. Additional differences involved added recruitment of motor and premotor areas in children compared with adults, and increased activity in the cerebellum in children as well. These findings demonstrate that performance of the continuation paradigm is less efficient and automatic in children, who need to recruit the cerebellum more extensively to maintain rhythmic tapping. Moreover, children performed less accurately than adults, despite this additional cerebellar activation (De Guio et al., 2012).

Another contribution of our study is in providing links between specific cognitive processes and the neural structures supporting action-based timing behavior. While we focused on adult data, developmental data provide an important foundation for understanding clinically relevant aspects of motor development, relevant to children with motor disorders. The implication can be extended to the development of clinical assessment procedures for children as well (Lundy-Ekman et al., 1991). More specifically, action-based tasks can reveal atypically poor performance in children that may be improved by additional timing training.

Another developmental domain in which timing deficits have been shown to be critical is in the language domain. For example, atypicalities in temporal aspects of audio-motor skills may be a key contributing factor of language and literacy difficulties in dyslexic children (Miendlarzewska & Trost, 2014). In these studies, such children show timing difficulties in the domain of language, music perception and cognition, as well as motor control. Indeed, musical training leads to positive outcomes for both phonological and spelling skills in previously underperforming children (Flaugnacco et al., 2015). This and other research in this domain can help us understand what relationships, if any, exist between musical training and improvement of language and literacy skills. More generally, the development of timing in childhood may well contribute to learning across the lifespan (Overy, 2003).

Limitations and Future Works

Due to the inherent complexity of dynamic timing behavior, we encountered several limitations specific to our research methodology, which form the basis for suggestions of future work. First, it is vital to scrutinize parametric-based impacts on timing behavior. For example, findings from Chapter 2 merit exploring whether an increase in the overall length of trials in the alternating design context would lead to sufficient entrainment to produce comparable levels of hemodynamic activity to those observed in our original (Rahimpour et al., 2020) blocked study design.

Second, sample size is a crucial factor in data-driven approaches. Given constraints on our participant numbers in Chapter 3, the results of classifications between coordination modes were inconclusive. Therefore, increasing sample size as a means of providing more training data for the novel deep learning approach we introduced, a move that may improve overall classification accuracy. As it is, there are still some uncertainties about whether we can predict behavioral accuracy based on single trial neurophysiological markers. Thus, further research will be needed to further refine these deep-learning models.

Regarding Chapter 4, more exploration is needed to find the best way to estimate EEG source localization. One problem of the approach used in the current study (i.e., DIPFIT analysis) is that the number of clusters are pre-defined and, consequently, we were limited to the number of independent components assigned to the pre-defined clusters. We recommend exploring standardized low-resolution electromagnetic tomographic analysis (sLORETA) as a way of feeding extracted channels and timepoints to the model, which may result in the generation of more robust and reliable source localization. Another limitation was that we were unable to quantitatively compare spatial accuracy across the two neuroimaging modalities, fNIRS and EEG. Rather, our observations about comparability are qualitative descriptions based on estimated cortical coordinates extracted the two sets of findings. How to make such a comparison remains an open question for future studies. Finally, a critical limitation to our localization comparisons was that all participants participated first in the fNIRS session and then in the EEG session, producing practice effects specific to the EEG data. For future work, we strongly recommend doing multimodal EEG-fNIRS data collection simultaneously, or at least recommend counterbalancing the order of fNIRS and EEG sessions in order to control for training effects specific to one or the other imaging modality.

References

Académie de Droit International de la Ha. (1995). *Cours général de droit international public* (Vol. 248). Martinus Nijhoff Publishers.

Cassenti, D. N. (2011). The intrinsic link between motor behavior and temporal cognition. *New Ideas in Psychology*, *29*(2), 72-79.

De Guio, F., Jacobson, S. W., Molteno, C. D., Jacobson, J. L., & Meintjes, E. M. (2012). Functional magnetic resonance imaging study comparing rhythmic finger tapping in children and adults. *Pediatric neurology*, *46*(2), 94-100.

Droit-Volet, S., & Rattat, A. C. (1999). Are time and action dissociated in young children's time estimation?. *Cognitive Development*, *14*(4), 573-595.

Flaugnacco, E., Lopez, L., Terribili, C., Montico, M., Zoia, S., & Schön, D. (2015). Music training increases phonological awareness and reading skills in developmental dyslexia: A randomized control trial. *PloS one*, *10*(9), e0138715.

Fujioka, T., Trainor, L. J., Large, E. W., & Ross, B. (2012). Internalized timing of isochronous sounds is represented in neuromagnetic beta oscillations. *Journal of Neuroscience*, *32*(5), 1791-1802.

Guyau, M. (1890). L'Art au Point de vue Sociologique. Éducation et Hérédité. *Mind*, *15*(58).

Jantzen, K. J., Oullier, O., Marshall, M. L., Steinberg, F. L., & Kelso, J. A. S. (2007). A parametric fMRI investigation of context effects in sensorimotor timing and coordination. *Neuropsychologia*, *45*(4), 673–684.

Jantzen, K. J., Steinberg, F. L., & Kelso, J. A. S. (2004). Brain networks underlying human timing behavior are influenced by prior context. *Proceedings of the National Academy of Sciences*, *101*(17), 6815–6820.

Kononowicz, T. W., & van Rijn, H. (2015). Single trial beta oscillations index time estimation. *Neuropsychologia*, *75*, 381-389.

Lundy-Ekman, L., Ivry, R., Keele, S., & Woollacott, M. (1991). Timing and force control deficits in clumsy children. *Journal of cognitive Neuroscience*, *3*(4), 367-376.

Manning, F., & Schutz, M. (2013). "Moving to the beat" improves timing perception. *Psychonomic bulletin & review*, *20*(6), 1133-1139.

McCormack, T., & Hoerl, C. (2017). The development of temporal concepts: Learning to locate events in time. *Timing & Time Perception*, *5*(3-4), 297-327.

Miendlarzewska, E. A., & Trost, W. J. (2014). How musical training affects cognitive development: rhythm, reward and other modulating variables. *Frontiers in neuroscience*, 279.

Monier, F., Droit-Volet, S., & Coull, J. T. (2019). The beneficial effect of synchronized action on motor and perceptual timing in children. *Developmental Science*, *22*(6), e12821.

Morillon, B., Schroeder, C. E., & Wyart, V. (2014). Motor contributions to the temporal precision of auditory attention. *Nature communications*, *5*(1), 1-9.

Overy, K. (2003). Dyslexia and music: From timing deficits to musical intervention. *Annals of the New York academy of sciences*, *999*(1), 497-505.

Piaget, J. (1946). Classes, Relations et Nombres (Book Review). *Revue de Métaphysique et de Morale*, *51*, 94.

Rahimpour, A., Pollonini, L., Comstock, D., Balasubramaniam, R., & Bortfeld, H. (2020). Tracking Differential Activation of Primary and Supplementary Motor Cortex Across Timing Tasks: An fNIRS Validation Study. *Journal of Neuroscience Methods*, 108790.

Rattat, A. C., & Droit-Volet, S. (2002). Le transfert d'un apprentissage de durée d'action chez le jeune enfant: l'effet facilitateur de la variété des actions?. *Enfance*, *54*(2), 141-153.

Turesky, T. K., Olulade, O. A., Luetje, M. M., & Eden, G. F. (2018). An fMRI study of finger tapping in children and adults. *Human brain mapping*, *39*(8), 3203-3215.